NOTICE

The quality of this microform is heavily dependent upon the quality of the original thesis submitted for microfilming. Every effort has been made to ensure the highest quality of reproduction possible.

If pages are missing, contact the university which granted the degree.

Some pages may have indistinct print especially if the original pages were typed with a poor typewriter ribbon or if the university sent us an inferior photocopy.

AVIS

La qualité de cette microforme dépend grandement de la qualité de la thèse soumise au microfilmage. Nous avons tout fait pour assurer une qualité supérieure de reproduction.

S'il manque des pages, veuillez communiquer avec l'université qui a conféré le grade.

La qualité d'impression de certaines pages peut laisser à désirer, surtout si les pages originales ont été dactylographiées à l'aide d'un ruban usé ou si l'université nous a fait parvenir une photocopie de qualité inférieure.

SERIES SOLUTION FOR A CYLINDRICAL COMPOSITE SHELL SUBJECT TO AXISYMMETRIC LOADINGS

by

D. W. LINDSTROM

A Thesis

presented to the University of Ottawa

July, 1990

in partial fulfillment of the

requirements for the degree of

DOCTOR of PHILOSOPHY

in

MECHANICAL ENGINEERING

Ottawa-Carleton Institute for

Mechanical and Aeronautical Engineering

ISBN 0-315-60559-6

UNIVERSITÉ D'OTTAWA
UNIVERSITY OF OTTAWA

PREVIEW

The use of a multi–term power series expansion for the deformations of a thick–walled orthotropic cylindrical shell subject to axisymmetric loading is detailed in this thesis. Three cases are considered – the infinite cylinder, the semi–infinite cylinder hinged at the origin, and the semi–infinite cylinder rigidly held at the origin.

A method of experimentally verifying the thick–walled theory is also presented, as well as the development of a filament winding apparatus, a pressurization facility, and a specimen manufacturing and test procedure.

ACKNOWLEDGEMENTS

The author wishes to acknowledge the excellent cooperation he received from all members of the Mechanical Engineering Department of the University of Ottawa.

The members of the department's machine shop facilities must be highly praised for their suggestions and patience in making much of the machinery, mentioned herein, operational.

It is the author wishes to pay particular thanks to Professor M. Munro who provided countless thoughtful suggestions and ideas throughout this work. The interest, patience, encouragement, and dedication offered by Dr. Munro are highly valued.

Particular thanks are also due to the members of the author's advisory committee Dr. S. Mirza, Dr. D.J. Gorman, and Dr. D. Redekop. Special thanks is given to Dr. J. Gardner in his advice on the contents of this thesis.

The author also thanks the Department of National Defence and the National Research Council for funding to make this work possible.

A special appreciation must be expressed to Mrs. S. Grab, who's tremendous efforts were directed at putting this manuscript into its present form.

The author

ABSTRACT

The elasticity equations have been solved to an arbitrary degree of precision for a thick-walled orthotropic cylinder, subject to axisymmetric loading. The theory is directly applicable to a layered composite material where each layer is orthotropic in character. The solution proceeds by representing the deformations of the cylinder wall as a power series in a non-dimensional radial parameter. By introducing a generalized stress resultant and a generalized stiffness for the material, a series of coupled second order differential equations in the coefficients of the deformation series results. These have been solved using a generalized eigenvalue technique for an infinitely long cylinder, a simply held cylinder, and a rigidly clamped cylinder.

The solution has been shown to reduce to standard shell solutions for thin cylinders. A thick-walled filament wound test specimen is also detailed that when fabricated and pressurized, would experimentally verify the refined theory developed.

LIST OF SYMBOLS

$\underline{\alpha}$ solution vector for displacement coefficients

$\underline{\alpha}_H$ homogeneous part of $\underline{\alpha}$

$\underline{\alpha}_P$ particular part of $\underline{\alpha}$

$\underline{\beta}^{(j)}$ displacement coefficients

$\beta_{ro}^{(j)}$ radial displacement coefficient at origin

β eigenvalue for isotropic cylinder

γ_{ij} engineering shear strains

ε_{ij} normal strains

λ shell thickness parameter

λ_i eigenvalues for deformation equations

ξ radial distance from cylinder midplane

$\underline{\phi}^{(j)}$ displacement coefficients – cylinder axes centered

Γ complementary energy

σ_{ij} stress

τ_{ij} shear stress

ν_{ij} Poisson's ratio

$\underline{\Phi}$ solution vector for displacement coefficients – cylinder axes centered

τ torque applied to cylinder

θ angular position

$\underline{\underline{A}}^{(n)}$ generalized stiffness

$\underline{\underline{C}}$ stiffness matrix

D flexural rigidity

E_{ij} elastic moduli

f_{rj} radial loading coefficients

F_z axial force applied to cylinder

h cylinder wall thickness

K_i complex eigenvalues

$\underline{\underline{N}}^{(n)}$ generalized stress resultant

P_{in} internal pressure

P_{out} external pressure

q non–dimensional radial distance

$\underline{\underline{Q}}$ reduced stiffness

$\underline{\underline{R}}$ Reuter's matrix

r radial position

r_i inner radius of cylinder

r_o outer radius of cylinder

r_c mid–plane radius of cylinder

$\underline{\underline{S}}$ compliance matrix

$\underline{\underline{T}}$ rotational transformation matrix

U strain energy

$\underline{u}$ displacement vector

u_{ro} radial displacement at origin

W work done by external forces

ω fiber orientation

$\underline{X}_i$ eigenvectors

z axial coordinate

TABLE OF CONTENTS

TABLE OF CONTENTS [continued]

TABLE OF CONTENTS [continued]

TABLE OF CONTENTS [continued]

TABLE OF CONTENTS [continued]

LIST OF FIGURES

LIST OF FIGURES [continued]

LIST OF TABLES

Chapter 1

INTRODUCTION

1.1 Fiber Composite Materials

A composite material is a combination of "two or more constituents having a potentially new range of performance characteristics" [1]. For the purposes of this study, a fiber composite material consists of reinforcing fibers such as graphite, glass, or kevlar embedded in a matrix such as polyester resin, epoxy resin, etc.

The matrix material is usually isotropic in character. That is, its mechanical properties (or electrical or chemical) are not dependent upon the orientation of the material. The reinforcing fibers may be isotropic (such as E–glass) or non–isotropic (such as graphite).

Generally speaking, fiber reinforced composite materials have become widely used in the aerospace, automotive, sports, chemical, and petroleum industries. The unique ability of material property tailoring by the appropriate selection of matrix and fibers offers this material distinct advantages over conventional non-reinforced materials.

For weight critical applications, such as required by the aerospace and aircraft industries, the high specific strength and modulus of these materials offer a significant advantage. For the chemical and petroleum industries, the high corrosion resistance is significant, even though the maximum service temperatures are lower than conventional metals.

The materials as a rule are highly non-isotropic in character; this must be taken into account when designing with these materials.

Materials in the most general sense are anisotropic, where material properties vary with orientation, and no plane of material symmetry for the properties exists. If one plane of symmetry exists, the material is monoclinic. If two orthogonal planes of symmetry exist, the material is called orthotropic. Such a material for example, is a uni-directional composite material (see Figure 1-1). A material that possesses a single plane where the properties are invariant to a rotation in that plane is call transversely isotropic. If any rotation in any orientation produces no change in the material properties, the material is said to be isotropic.

Composite materials are often layered; each individual layer is called a lamina, and the stack is called a laminate.

The terms isotropic, transversely isotropic, specially orthotropic, and generally orthotropic refer also to the mechanical stress-strain response of a lamina on a macroscopic scale. On a microscopic scale, the individual fibers and matrix filled interstices would dominate the stress and strain states. On a macroscopic scale, these local variations blend to form a quasi-homogeneous material.

For the purposes of this discussion, composite materials are assumed to obey linear elastic stress–strain relationships; that is, stress is proportional to strain.

For an isotropic material (ignoring thermal and residual stress effects) [2],

$$\begin{Bmatrix} \sigma_{11} \\ \sigma_{22} \\ \sigma_{33} \\ \tau_{23} \\ \tau_{31} \\ \tau_{12} \end{Bmatrix} = \begin{Bmatrix} C_{11} & C_{12} & C_{12} & 0 & 0 & 0 \\ C_{12} & C_{11} & C_{12} & 0 & 0 & 0 \\ C_{12} & C_{12} & C_{11} & 0 & 0 & 0 \\ 0 & 0 & 0 & \frac{C_{11}-C_{12}}{2} & 0 & 0 \\ 0 & 0 & 0 & 0 & \frac{C_{11}-C_{12}}{2} & 0 \\ 0 & 0 & 0 & 0 & 0 & \frac{C_{11}-C_{12}}{2} \end{Bmatrix} \begin{Bmatrix} \varepsilon_{11} \\ \varepsilon_{22} \\ \varepsilon_{33} \\ \gamma_{23} \\ \gamma_{31} \\ \gamma_{12} \end{Bmatrix}$$

where σ_{11}, σ_{22}, σ_{33}, τ_{23}, τ_{31}, and τ_{12} are defined in Figure 1–2.

Two elastic constants are all that is necessary to completely describe the stress–strain behavior.

For a transversely isotropic material, five independent constants are required [2], i.e.

$$\begin{Bmatrix} \sigma_{11} \\ \sigma_{22} \\ \sigma_{33} \\ \tau_{23} \\ \tau_{31} \\ \tau_{12} \end{Bmatrix} = \begin{Bmatrix} C_{11} & C_{12} & C_{13} & 0 & 0 & 0 \\ C_{12} & C_{11} & C_{13} & 0 & 0 & 0 \\ C_{13} & C_{13} & C_{33} & 0 & 0 & 0 \\ 0 & 0 & 0 & C_{44} & 0 & 0 \\ 0 & 0 & 0 & 0 & C_{44} & 0 \\ 0 & 0 & 0 & 0 & 0 & \frac{C_{11}-C_{12}}{2} \end{Bmatrix} \begin{Bmatrix} \varepsilon_{11} \\ \varepsilon_{22} \\ \varepsilon_{33} \\ \gamma_{23} \\ \gamma_{31} \\ \gamma_{12} \end{Bmatrix}$$

Nine constants are needed for an orthotropic material [2],

$$\begin{Bmatrix} \sigma_{11} \\ \sigma_{22} \\ \sigma_{33} \\ \tau_{23} \\ \tau_{31} \\ \tau_{12} \end{Bmatrix} = \begin{Bmatrix} C_{11} & C_{12} & C_{13} & 0 & 0 & 0 \\ C_{12} & C_{22} & C_{23} & 0 & 0 & 0 \\ C_{13} & C_{23} & C_{33} & 0 & 0 & 0 \\ 0 & 0 & 0 & C_{44} & 0 & 0 \\ 0 & 0 & 0 & 0 & C_{55} & 0 \\ 0 & 0 & 0 & 0 & 0 & C_{66} \end{Bmatrix} \begin{Bmatrix} \varepsilon_{11} \\ \varepsilon_{22} \\ \varepsilon_{33} \\ \gamma_{23} \\ \gamma_{31} \\ \gamma_{12} \end{Bmatrix}$$

For a monoclinic material, thirteen constants are required to define the mechanical properties.

$$\begin{Bmatrix} \sigma_{11} \\ \sigma_{22} \\ \sigma_{33} \\ \tau_{23} \\ \tau_{31} \\ \tau_{12} \end{Bmatrix} = \begin{Bmatrix} C_{11} & C_{12} & C_{13} & 0 & 0 & C_{16} \\ C_{12} & C_{22} & C_{23} & 0 & 0 & C_{26} \\ C_{13} & C_{23} & C_{33} & 0 & 0 & C_{36} \\ 0 & 0 & 0 & C_{44} & C_{45} & 0 \\ 0 & 0 & 0 & C_{45} & C_{55} & 0 \\ C_{16} & C_{26} & C_{36} & 0 & 0 & C_{66} \end{Bmatrix} \begin{Bmatrix} \varepsilon_{11} \\ \varepsilon_{22} \\ \varepsilon_{33} \\ \gamma_{23} \\ \gamma_{31} \\ \gamma_{12} \end{Bmatrix}$$

If the material is orthotropic and viewed from a coordinate system that is not in line with the principle material directions, only nine constants are needed to define the lamina mechanical properties. Each element of the stiffness matrix above has a term however, which can be calculated from the nine constants. For the case of an anisotropic material, twenty one individual material properties are required. The stresses are related to the strains by

$$\begin{Bmatrix} \sigma_{11} \\ \sigma_{22} \\ \sigma_{33} \\ \tau_{23} \\ \tau_{31} \\ \tau_{12} \end{Bmatrix} = \begin{Bmatrix} C_{11} & C_{12} & C_{13} & C_{14} & C_{15} & C_{16} \\ C_{12} & C_{22} & C_{23} & C_{24} & C_{25} & C_{26} \\ C_{13} & C_{23} & C_{33} & C_{34} & C_{35} & C_{36} \\ C_{14} & C_{24} & C_{34} & C_{44} & C_{45} & C_{46} \\ C_{15} & C_{25} & C_{35} & C_{45} & C_{55} & C_{56} \\ C_{16} & C_{26} & C_{36} & C_{46} & C_{56} & C_{66} \end{Bmatrix} \begin{Bmatrix} \varepsilon_{11} \\ \varepsilon_{22} \\ \varepsilon_{33} \\ \gamma_{23} \\ \gamma_{31} \\ \gamma_{12} \end{Bmatrix}$$

1.2 Composite Pressure Vessels

In the manufacture of fiber composite pipe or pressure vessels, thin fiber composite laminae are stacked upon one another to form a laminate. The properties of the laminate are governed by material selection and laminae construction, orientation and stacking.

The end uses of fiber composite pressure vessels fall into three relatively distinct markets (industrial, military, and the aerospace/aeronautical) each governed by their own design and qualification procedures. For instance, standard industrial vessels require a design (or burst) pressure of at least six times the maximum anticipated operating pressure to allow for fatigue situations and less stringent quality control procedures [3]. Vessels for the military and aerospace sectors are generally manufactured from higher quality materials with tighter manufacturing control and are allowed a safety factor of two or three depending upon the situation. As summarized in Table 1-1, end uses can be categorized according to service pressures as well as target markets.

Low pressure service (up to 3.5 MPa) is common in the chemical process industries where the corrosion resistant properties of polyesters are combined with the low cost of the E-glass fibers to produce pressure vessels with economic advantages over their metal counterparts. Advanced composites such as Kevlar 49, carbon, and S-2 glass fibers combined with an epoxy matrix see service in the low pressure military and aeronautical sectors as storage containers for rocket fuel and oxidants. The increased cost of these materials and the higher level of technical expertise required for their effective use has limited the penetration of these composites into the industrial sector.

Increasing service pressures sees the elimination of the polyester resin family in favor of epoxy resins. E-glass as a structural fiber is also replaced by the more advanced fibers in all market sectors.

The composite pressure vessel industry in the high pressure regions is dominated by two design approaches. Load sharing thick metal casings (liners) have been overwrapped with a structural composite to improve vessel weight efficiencies* for such applications as compressed air storage, fire extinguisher storage, and helium storage for propulsion on NASA'S manned maneuvering unit. Vessel shapes are cylindrical and spherical [4].

Thin metal liners, used only to prevent gas permeation through the pressure vessel wall, are a competing design because of their increased weight efficiency over their thick-liner counterparts.

1.3 Problem Definition

Composite vessels for service above 70 MPa are only now reaching market acceptance and then only for the military and aerospace sectors. Typically, helium would be stored in these vessels for the pneumatic activation of cylinders on spacecraft or for rocket motor pressurants on air launched missiles [5]. Cylindrical vessels of a hybrid construction are currently available with a burst pressure of 300 MPa. Spherical vessels are being developed with burst pressures above 400 MPa [6].

---

*

$$\text{weight efficiency} = \frac{\text{burst pressure x enclosed volume}}{\text{weight}}$$

A convenient parameter for weighting the relative advantages of a given vessel design is, again, the weight efficiency of the vessel. A sampling of available data in the literature reveals an interesting situation. The range of scatter in the efficiency for thin-walled vessels is tremendous (Table 1-2), possibly accounted for by material variations and variations in the mode of failure.

A number of studies have been undertaken to date on ultra-high pressure vessels. The earliest attempt utilizing S-901 glass wound on a spheroidal mandrel tried unsuccessfully to obtain better material efficiency through fiber prestressing [7]. Studies have also produced cylindrical vessels from a hybrid material construction with burst pressures of 300 MPa but again with low weight efficiencies [5]. Figure 1-3 graphically illustrates the pressure-efficiency data contained in Table 1-2. Three families are presented:

(a) actual vessel efficiency (including liner weight),
(b) efficiency of the composite wall, and
(c) theoretically expected efficiencies for the composite wall for a spherical transversely isotropic vessel.

As the wall is thickened and the burst pressure increases, a marked fall in attained vessel efficiency is seen, with the majority of vessels attaining about 25% of the ideal efficiency at the higher pressures. It has been suggested that serious material shortcomings at the high transverse compressive stress levels experienced by these vessels were the reason for the low efficiencies [5].

Studies at the Sandia National Laboratories produced vessels of exceptional laminate quality from Kevlar 49/epoxy, which achieved efficiencies near that theoretically predicted for a single material vessel. A single small diameter roving bundle was used in the manufacture of these vessels [6].

It is postulated at this point that achieving the high structural efficiencies in thick-walled composite vessels has not been possible because of:

(1) imprecise control of fiber placement during manufacture resulting in misaligned laminae in the structure;
(2) approximate methods of design using simplified stress analysis and inadequate failure theories giving a false impression of what is achievable in a thick-walled vessel; and
(3) poor transverse compressive properties of the fiber composite material as a result of material selection and manufacturing techniques resulting in premature failure of the vessel walls.

1.4 Thesis Overview

Introduction

The research presented in this thesis addressed all three of the above postulates. A highly accurate computer controlled filament winder was designed, constructed, and used in the fabrication of material specimens and E/XA-S carbon fiber and Kevlar 49 pressure vessels. The third item was also evaluated by fabricating flat composite specimens and testing them in the transverse compressive mode - a stress state occurring in a thick-walled fiber composite pressure vessel. The above research was necessary for the problem as defined, but was only a minor aspect. In addition, they formed part of a classified contract for the Department of National Defence, for which permission has been given for the released data.

The main emphasis for the thesis is the first aspect of the second postulate, i.e. providing an improved method of stress analysis for thick–walled pressure vessels manufactured from a composite material. This is detailed in the following section.

Stress Analysis of Vessels and Tubes

Three basic approaches have been used in the analysis of composite pressure vessels, namely, netting analysis, linear anisotropic elasticity theory, and finite element analysis. Netting analysis treats the vessel as a netted structure of fibers, ignoring the matrix effects. As such, it is really only valid in cases where the matrix is totally disintegrated before fiber breakage occurs. Netting analysis is no longer considered an appropriate model for composite materials and has not received much attention for a number of years.

Most continuum analyses have assumed linear elastic material properties for the material. Solutions for the deformations or strains are usually numerical although analytical solutions are available for a layered quasi–isotropic sphere [8, 9, 10] and a single layer composite cylinder of infinite length [11, 12]. Most studies have limited themselves to either spherical or cylindrical shells. The subject material of the following chapter will be the review of elastic cylinder analysis.

Finite element analysis has been used to study stresses in tubes [6, 13, 14]. By modelling a tube or vessel as a connected collection of minute elastic blocks, the structures have been modelled with excellent accuracy being achieved in the calculation of the stresses and strains in the material. The technique is most important when the geometries being considered are not as simple as the sphere or cylinder.

The tubular specimen has been used to establish the fundamental properties of the composite material [15, 16, 17, 18, 19]. The impetus is to use a long, thin tube so that end effects would not be evident at the mid– span of the specimen. The problem is to develop a specimen end attachment method that does not introduce large end effects to cause specimen failure near the attachment grips.

The standard approach for this specimen [20, 21] is to anchor the ends of the tubular specimen in a solid grip attachment. The end effect problems are overcome somewhat by a simple thickening of the tube in the region of the end attachment [22].

Finite element analysis [20, 22] and finite difference techniques [23] have been used to model typical grip configurations for tubular specimens indicating possibly useful specimen designs.

The object of the present study is two fold. A thick shell theory for orthotropic materials will be developed. This theory is shown to predict the state of stress in a very thick–walled cylinder to any desired degree of accuracy. As such it extends the simple thin–walled theory to its logical completion, and provides a comparison solution for finite element studies. It is useful in its present form however only for axisymmetric loading situations.

Secondly, a thick–walled tubular specimen design has been developed and experimentally tested using high quality manufacturing techniques for the precise control of fiber placement and composite volume fraction. Lack of time has prevented the completion of the experimental study, however, details of it will be included in the thesis of Mr. Tenace of this department.

Service Pressure MPa (psi)	Industrial Market	Military Market	Aerospace/Aeronautical Market	Remaining Challenges
Low 0 – 3.5 (0 – 500)	E glass/polyester – compressor tanks – chemical storage/ processing – filtration tanks		S glass, Kevlar, Carbon/Epoxy – rocket fuel/oxidizer storage	manufacturing economics
Moderate 3.5 – 14 (500 – 2000)	E glass, S glass/epoxy – chemical storage/ processing – salt water desalina-tion		S glass,Kevlar, Carbon/Epoxy – rocket fuel/oxidizer storage – nitrogen storage for space-craft	manufacturing economics
High 14 – 70 (2000 – 10000)	S glass,Kevlar/epoxy – compressed natural gas – compressed air back pack	S glass, Kevlar, Carbon/epoxy – rocket launching tubes	Kevlar/epoxy – compressed air (Boeing 747) – compressed helium (shuttle) – air tanks/space suits – hydrogen storage (Venus probe)	– liner buckling – liner weight – manufacturing variability
Ultra-High 70 + (10000 +)	Metals – high pressure processing – material research – detonation tanks	S glass/Kevlar/ Carbon Hybrids – compressed helium/missile systems	S glass,Kevlar, Carbon hybrids – compressed helium/spacecraft	– composite material properties – liner problems

Table 1–1 Composite Pressure Vessel End Uses [78]

Vessel Description				Burst Pressure MPa	Overall Efficiency m x 10^3	Composite Efficiency m x 10^3	Liner Thickness Wall Thickness	Comments	
Composite	Liner	Size (cm)	Shape						
Kevlar 49	rubber	10.1	cyl	18.0	N/A	38.6	N/A		24
Kevlar 49	rubber	20.3	cyl	14.2	N/A	36.3	N/A		24
Kevlar 49	Al	20.3	cyl	15.0	N/A	39.6	N/A		24
Kevlar 49	Al	20.3	sphere	28.7	N/A	34.0	.256		24
Kevlar 49	Al	20.3	sphere	39.0	N/A	42.2	.497		24
Kevlar 49	rubber	20.3	sphere	35.4	N/A	41.4	N/A		24
Carbon	Ti	10.1	sphere	39.4	21.6	39.6	N/A		24
Carbon	Ti	10.1	cyl	47.4	24.6	41.4	N/A		24
Kevlar 49	Ti	31.8	sphere	46.5	19.4	31.2	.140		25
Kevlar 49	Inconel	63.5	sphere	34.1	16.2	30.7	.102		25
Kevlar 49	Ti	63.5	sphere	45.5	19.2	31.0	.135		25
Carbon	Al	10	cyl	22.5	13.8	N/A	N/A		26
Carbon	Ti	10	cyl	34.3	15.1	N/A	N/A		26
Carbon	rubber	10	cyl	25.7	N/A	35.6	N/A		26
S2,K49,Carbon	Al	10	cyl	330	8.76	N/A	.042	estimated from data	5
S2,K49,Carbon	Al	10	cyl	304	7.98	N/A	.041	estimated from data	5
Kevlar 49	Al	10	sphere	312	9.40	N/A	N/A		27
S901 Glass	S.S	10	isotens	165	6.35	N/A	N/A	estimated from data	7
Kevlar 49	S.S	61	sphere	30.7	20.0	43.9	.154	estimated from data	28
Kevlar 49	Al	94	sphere	20.3	12.6	25.9	.310	estimated from data	28
S2 glass	Al		cyl	46.5	8.81	N/A	N/A	estimated from data	28
Kevlar 49	Al		cyl	88.2	17.4	N/A	N/A	estimated from data	28
E glass	Steel	50	cyl	20.7	3.30	N/A	N/A	design estimate	29
E glass	Steel	50	cyl	20.7	3.30	N/A	N/A	design estimate	29
Kevlar 49	Copper	10.1	sphere	430	16.2	20.9	.055		6
Kevlar 49	Copper	5.0	cyl	400	11.8	19.1	N/A		6

Table 1–2 Composite Pressure Vessel Properties [78]

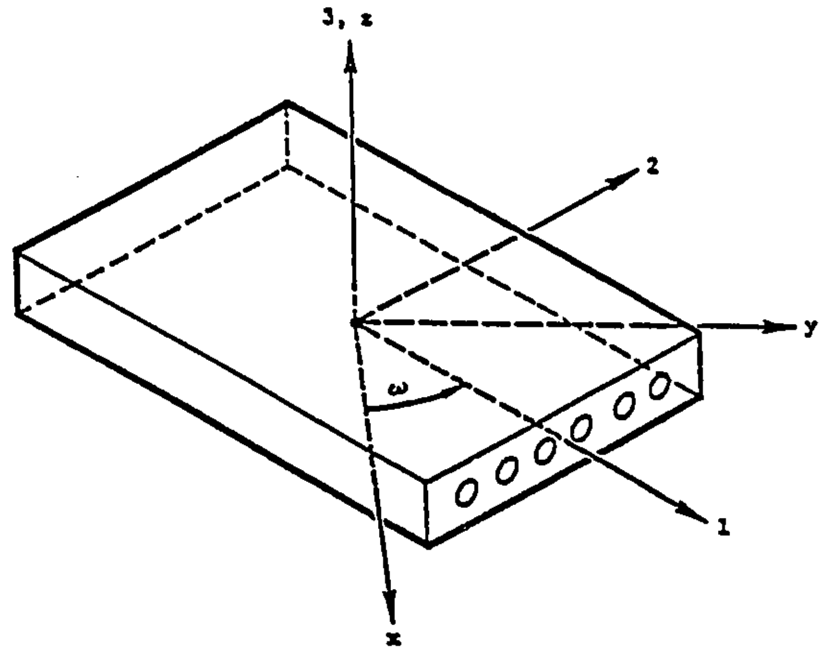

Figure 1–1 Fiber Reinforced Composite Material

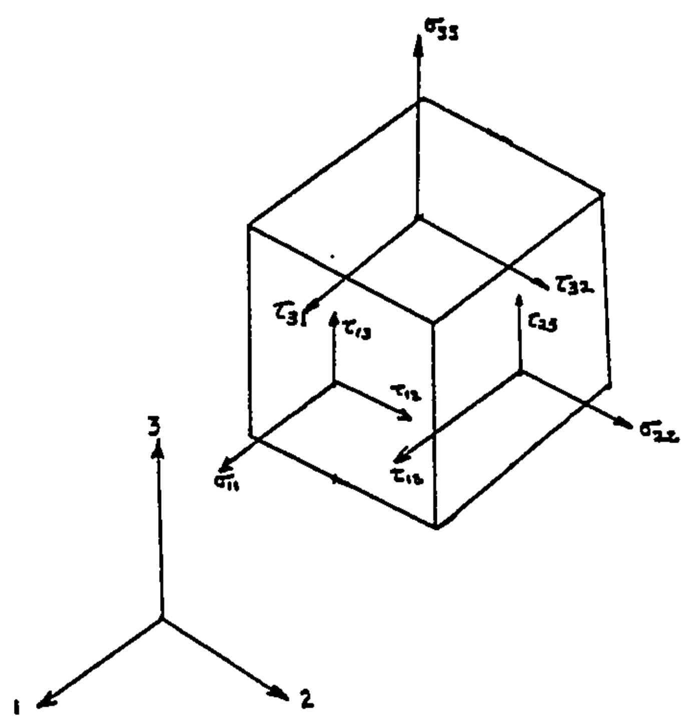

Figure 1–2 Stresses and Strains in Fiber Composite Material

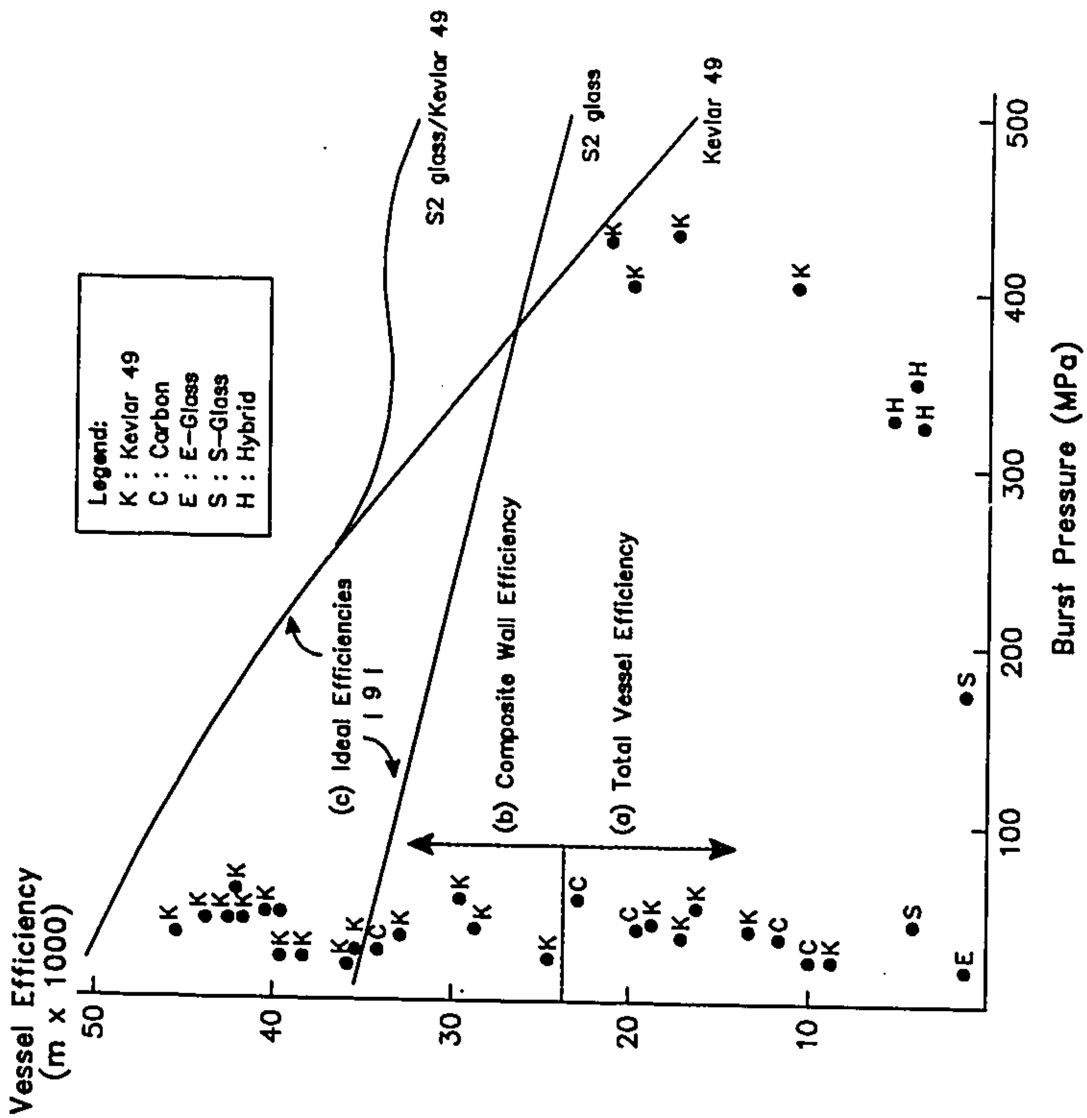

Figure 1-3 Vessel Efficiency Versus Burst Pressure [78]

Chapter 2

REVIEW OF CYLINDRICAL SHELL THEORIES BASED UPON SERIES EXPANSIONS

2.1 Introduction

The basic equations of linear elasticity, namely the equilibrium equation, the strain – deformation equations, the material constitutive relations, and the strain compatibility equations when applied to a cylindrical geometry, describe the deformation of a cylinder subject to external mechanical loading (see Table 2–1). The exact solution of these equations for a finite length cylindrical shell has not been found. However, use of the Weirstrauss theorem [30], allows the solution of the partial differential equation,

$$\underline{L}(\underline{\Phi}) = \underline{G}$$

to be written in cylindrical coordinates

$$\underline{\Phi}(z,\theta,r) = \sum \Phi^{(j)}(z,\theta)\, P_j(r)$$

where z, θ, and r correspond to the three coordinate axes of a cylindrical coordinate system, (such as illustrated in Figure 3–1), and where the function $\underline{\phi}^{(j)}$ is continuous over the region of interest and $P_j(r)$ form an infinite set of orthogonal functions. This technique forms a basis for the solution of the elasticity equations in a cylindrical geometry. Because of the impracticability of retaining an infinite number of terms, the series is truncated, often after very few terms.

Since the number of papers presented on cylindrical geometries is voluminous, a selection of those using the series solution technique described above will be reviewed. A general review of cylindrical shell theory is available in the literature [31].

2.2 Method of Series Solution as Applied to Cylindrical Shells

Three approaches have been adopted in using an orthogonal series to represent the solution of the elasticity equations as applied to a cylindrical tube. Table 2–2 categorizes the literature reviewed according to series type and solution type.

The most obvious approach is to assume a series form for the displacement variables, and solve the governing differential equations directly or through an energy minimization procedure. Table 2–3 illustrates this procedure as implemented with a power series. In the direct method, the strains are calculated from the assumed displacements using the strain displacement relationships given in equation (2–1). The stresses are then determined from the material constitutive relations (generalized Hooke's law). Weighted integrals of the stresses are calculated through the integration procedure defined in Table 2–3. Because the integration is through the entire cylinder wall, which may be layered, a generalized stiffness is introduced, to make the integration possible. The displacement is a continuous function through the cylinder. A weighted integral form of the stress equilibrium equations (equations 2–4) is introduced, and the stress resultants previously calculated substituted into it. The result is a system of differential equations in the displacement coefficients which must be solved subject to boundary conditions.

Because a deformation representation is used, the compatibility equations are satisfied exactly. The use of a weighted integral form of the stress equilibrium equations precludes an exact equilibrium with a finite number of terms in the series.

The development of a solution using an energy minimization technique proceeds along a somewhat similar path. The variation in elastic strain energy and the work done by the deforming agent are minimized and expressed in terms of weighted integrals of the stress. The resulting equation is identical to the weighted integral form of the stress equilibrium equations. The solution follows the direct method from this point. As with the direct method, equilibrium is not exactly satisfied with a finite number of terms. The solution is completed with the application of the boundary conditions.

Power series, Legendre polynomial series, and an exponential series have been used with this type of solution development. Because of the complexity in retaining a large number of terms in the series, they are severely cropped, often with only two or three terms being retained [40, 50, 51].

Other authors (see Table 2–2) chose to represent the stresses or strains in terms of other series. Because the deformations were usually only necessary for the application of boundary conditions(as illustrated in Table 2–4), they [41, 59] felt that an expansion of the stresses or strains as a series of orthogonal functions would be more mathematically efficient. The series, however, had coefficients that depended on the layer of the material being considered. The series was substituted directly into the stress equilibrium equations, and a solution generated for the series coefficients for each layer. The deformations were calculated by integration of the strain deformation equations. To maintain material continuity, the deformations and radial stress components were matched at the layer interfaces. The application of boundary conditions then solved the problem.

A third approach found in the literature, is a series form for both the displacement and the stresses. These are directly substituted into the stress displacement equations (which are obtained by combining equations (2–1) and (2–3) and the stress equilibrium equations. This gives a series of differential equations in the unknown coefficients valid only for a specific layer. As before, matching has been done on the deformation and radial stress components to achieve a solution. This method has usually been limited to single layer cylinders [43–49].

2.3 Details of the Power Series Approaches

The original use of power series representation for cylinders was in the classical analysis of thin isotropic shells [32]. Transverse normal and transverse shear stresses were considered negligible, and the circumferential, axial, and in–plane shear strains were represented as linear functions of the radial distance from the cylinder mid–plane. The solution followed the direct approach by calculating the stresses and substituting the integrated form of these into the stress resultant equilibrium equations. This laid the basis for further isotropic and non–isotropic cylindrical shell developments. The basic assumptions of thin shell theory are:

(1) planes normal to the shell mid-plane remain planar and normal;
(2) deformations of the shell wall are small;
(3) transverse normal and transverse shearing strains are ignored;
(4) transverse slopes are small enough that a small deflection theory can be used; and
(5) the material is linearly elastic.

Assuming that transverse and normal stresses were vanishingly small, Donnell [33] extended the concepts introduced by Love to cover non-symmetric loading with in-plane shear in an isotropic cylinder. He assumed that the in-plane strains could be represented as a linear function of the radial distance from the cylinder mid-plane. Following classical shell theory, he defined a system of first order stress resultant equilibrium equations. Relating mid-plane displacements and curvatures to his assumed strain field, and further relating the in-plane stresses to the strains and deformations through a linear elastic isotropic constitutive relation, he derived expressions for the stress resultants in terms of mid-plane displacements and rotations. These were substituted into the stress resultant equilibrium equations to give a system of three coupled partial differential equations, one of eighth order and two of fourth order. These equations contain the mid-plane displacements as unknowns. The mid-plane rotations and stress resultants were easily calculable by multiple differentiation of the mid-plane displacements. It should be noted that, to achieve a match between the number of equations and the number of unknowns, an equilibrium equation involving strictly shear terms was ignored.

In 1962, Dong, Pister, and Taylor [34] extended the work of Donnell to laminated anisotropic cylindrical shells. To overcome the fact that material properties were not constant through the cylinder wall, the concept of a generalized stiffness was borrowed from laminated plate theory. Normal and transverse shear stresses were again neglected, and the cylinder was assumed to obey the standard Kirchoff - Love hypothesis. As stated earlier, a series of differential equations were given which allowed the mid-plane deformations to be calculated. These equations demonstrated a coupling between the shell membrane and bending stresses. Most of their work was directed at cylindrical shells where the laminae making up the shell wall were orthotropic and of the same thickness, and the lamina stacking sequence was symmetric about the cylinder mid-plane.

Whitney [35] extended the theory to include the effects of normal stresses on anisotropic cylinders. To include this effect, the radial deformation was expressed as a linear function of the radial distance from the midplane. By integrating the strain displacement equations and ignoring transverse shear strains, the axial deformation was expressed as a quadratic function of the radial displacement from the cylinder mid-plane. Although it was possible to do so, Whitney at this point never considered axial variations of stress or deformation. It should be pointed out that the material modelled was a thin laminated cylinder of orthotropic layers.

Gulati and Essenberg [36] explored the twisting moments introduced by material anisotropy terms.

Several variants of these thin shell theories were published. Whitney and Halpin [37], for example, considered a layered orthotropic cylinder of finite length subject to internal pressure, torque, and axial loading, in a manner similar to a tubular specimen in a tensile test frame. They ignored transverse shear and normal stress components and never looked at the effects near the cylinder ends. Zukas and Vinson [38] added thermal effects to a layered isotropic cylinder. The transverse normal stress as a result of thermal loading was considered.

In an attempt to incorporate transverse shear, Dong and Tso [39] introduced a shear correction factor to account for transverse shear strain variations from layer to layer. They assumed a linear expansion for the axial and circumferential deformations, and a layer dependent radial function for the radial deformation. By using a shear correction factor, an average radial deformation was defined for the cylinder wall and variations of the transverse shear strain in the layers were allowed. End effects were not considered; the solution proceeded in the direction of material oscillations instead. This was a thin shell theory for a layered orthotropic shell of revolution.

Studies up to this date (1974) largely attempted to model a complex stress field with simple mathematical expressions for the deformations – usually linear for the axial and circumferential deformation and constant for the radial deformation through the cylinder wall. The early work of Whitney [35] extended this to a quadratic displacement representation in the axial direction.

Whitney and Sun [40] recognized the need for a more complete radial deformation function if normal and transverse shearing stresses and strains were to be calculated. These they felt would become increasingly important as the thickness of the cylinder increased. They derived a system of differential equations for a layered orthotropic cylinder using a linear deformation through the cylinder wall for the axial and circumferential components, and a quadratic representation for the radial deformation. The principle of stationary potential energy was used to derive the stress resultant equations. Even with this extension to the second order, they found it necessary to introduce a shear correction factor to get solutions that closely matched known exact elasticity solutions. They rather arbitrarily assigned a value of $\pi / \sqrt{12}$ to this correction factor. Although the differential equations were presented, end solutions were not sought. They considered infinitely long cylinders subject to non-symmetric loading situations. A similar procedure has been implemented by Christensen et al for thick flat plates [61, 63].

Vasilenko et al [41] introduced a quadratic correction factor for the transverse shear stresses in a axisymmetric layered orthotropic shell. Loading was axisymmetric and the stiffness was allowed to vary meridionally. A system of ten first order differential equations were solved for some cylindrical examples. Normal strains and stresses were ignored in this development.

Very little work has been done since the mid 1970's to improve the layered orthotropic cylindrical shell models for thicker cylinders using the power series approach. One exception is the FEM element developed by Liu and Reddy [42] which expanded axial and circumferential displacements as cubics in the midplane distance while leaving the normal deformation constant. Since this approach is not of an analytic character, it will not be dealt with here. A similar polynomial plate element of higher order has been developed and implemented by Hansen [79].

One of the most complete deformation analyses available in the literature is due to Librescu [80]. Choosing a coordinate system with the origin located in the wall of a shell of revolution, he expressed the deformation components as a power series in the normal distance from the origin plane. His initial studies were applied to an anisotropic shell where the deformations were assumed to be continuous functions. In later studies [81, 82], he assumed layer specific deformations represented as linear functions in the normal distance from the origin plane. Matching of the stress components σ_{rr}, τ_{rz}, and $\tau_{r\theta}$ as well as the deformation values were done at the interfaces in a laminated anisotropic shell. The analysis procedure in both cases was complex, in that linear elasticity in a tensor format, and a curvilinear coordinate system centered in the shell wall was used. No cylindrical solution examples were offered.

In the approaches considered thus far, either the deformations or the stress or strains were represented as a power series. Widera, in a series of publication spanning three decades of which a few are [43, 44, 45, 46, 47] assumed a power series formulation for both the deformation and the stresses in an anisotropic cylinder. A shell thickness parameter $\lambda = h/r_c$ was introduced and used as the expanding variable for the stresses, displacements, and compliances. These were substituted directly into the stress equilibrium and stress displacement equations. Equation sets were deduced comparing like powers of the shell thickness parameter. The first order comparison yields a standard thin shell theory. The second order term introduces effects due to the transverse stresses. The analysis stops at this point, primarily due to algebraic difficulties, and hence is limited to thin cylinders, although an extension to thick cylinders is possible in principle.

2.4 Legendre Series Expansions

An expansion of the stresses or the deformations in terms of Legendre polynomials has received some attention in the literature (see Table 2–2). Khoma [48] expanded the deformations using Legendre polynomials referenced to the shell mid–plane for an anisotropic shell. After calculating the small deformation strains, an energy functional was formed and minimized. Stress resultants were generated using Legendre polynomials and substituted into an energy minimization equation to yield a system of partial differential equations in the unknown coefficients. This analysis was never applied to any specific shell geometry and generated no specific solutions. Two terms of the expansion were retained for the analysis of a flat transversely isotropic plate. Chepiga [49] followed a similar approach formalizing the procedure, but not analyzing any specific case.

Vinson [50, 51] adopted an alternative approach aimed at generating the stresses in a thick–walled isotropic cylinder. Following the method developed by Soler [52] for plates, he expressed both the stresses and deformations as a series of Legendre polynomials referenced radially to the cylinder mid-plane. These were substituted into the stress equilibrium and a combination of the strain-deformation equations and Hooke's law and solved on a term by term basis. From a practical point of view, only a first order theory was developed, but the author claimed applicability to thick cylinders.

2.5 Eigenvalue Solutions

Some authors [43, 50, 51, 53, 54, 55, 56] assumed constant material properties along the length of the cylinder, and solved the resulting system of differential equations using an eigenvalue technique. For example, Widera [43] assumed an exponentially decaying function for the stresses and displacements and generated a fourth order characteristic equation.

Bazarenko [56] paralleled Widera's early work using expansions in terms of a logarithmic shell thickness parameter for an isotropic cylinder. A comparison of first order terms for this parameter after the usual substitution into the elasticity equations generated a characteristic equation. Three groups of eigenvalues were obtained. The first group was identically zero and corresponded to infinite cylinder solutions. The second group of roots resulted in slowly damped stresses and strains down the cylinder axis, following classical shell theory. The third group of roots corresponded to very quickly decaying stresses not found in classical analysis. This was labelled a boundary layer.

Zukas and Vinson [38] found that the first order expansion in the deformation detailed earlier resulted in a cubic eigenvalue equation for transversely isotropic cylinders. The three eigenvalues were either all real, or one real and two complex conjugates. The solution is an extension of classical analysis in that quickly decaying non-oscillatory stress terms are now observed. Vinson [50, 51] retained the eigenvalue approach when he modelled the thick isotropic cylinder with Legendre polynomials.

Cheng [53, 54] generated a fourth order characteristic equation using a linear displacement field for an orthotropic cylinder.

Li and Wang [55] expanded the shell deformations for an orthotropic shell as a power series in terms such as $e^{\lambda_i \xi}$ where λ_i are the characteristic values of a fourth order equation.

2.6 Remarks

It is apparent from the review presented that little work has been done in exploring the stresses and strains in thick-walled non-isotropic cylinders. This is largely due to premature truncation of the series representing stresses or deformations. Almost without exception, this can be attributed to algebraic difficulties that arise when more than a few terms are retained. In the analysis that follows, it will be shown that a very simple coordinate system change allows the retention of any desired number of terms in a power series expansion for the deformation of a laminated orthotropic cylinder.

Strain–Deformation Equations (Small Deformations) [57]

(2–1)

$$\varepsilon_{zz} = \frac{\partial u_z}{\partial z} \qquad \gamma_{r\theta} = \frac{\partial u_\theta}{\partial r} - \frac{u_\theta}{r} + \frac{1}{r}\frac{\partial u_r}{\partial \theta}$$

$$\varepsilon_{\theta\theta} = \frac{u_r}{r} + \frac{1}{r}\frac{\partial u_\theta}{\partial \theta} \qquad \gamma_{rz} = \frac{\partial u_r}{\partial z} + \frac{\partial u_z}{\partial r}$$

$$\varepsilon_{rr} = \frac{\partial u_r}{\partial r} \qquad \gamma_{z\theta} = \frac{1}{r}\frac{\partial u_z}{\partial \theta} + \frac{\partial u_\theta}{\partial z}$$

Strain Compatibility Equations [58]

(2–2)

$$\frac{\partial^2 \varepsilon_{\theta\theta}}{\partial r^2} + \frac{1}{r^2}\frac{\partial^2 \varepsilon_{rr}}{\partial \theta^2} + \frac{2}{r}\frac{\partial \varepsilon_{\theta\theta}}{\partial r} - \frac{1}{r}\frac{\partial \varepsilon_{rr}}{\partial r} = 2\left(\frac{1}{r}\frac{\partial^2 \gamma_{r\theta}}{\partial r \partial \theta} + \frac{1}{r}\frac{\partial \gamma_{r\theta}}{\partial \sigma}\right)$$

$$\frac{\partial^2 \varepsilon_{\theta\theta}}{\partial z^2} + \frac{1}{r^2}\frac{\partial^2 \varepsilon_{zz}}{\partial \theta^2} + \frac{1}{r}\frac{\partial \varepsilon_{zz}}{\partial r} = 2\left(\frac{1}{r}\frac{\partial^2 \gamma_{\theta z}}{\partial z \partial \theta} + \frac{1}{r}\frac{\partial \gamma_{zr}}{\partial z}\right)$$

$$\frac{\partial^2 \varepsilon_{zz}}{\partial r^2} + \frac{\partial^2 \varepsilon_{rr}}{\partial z^2} = \partial\left(\frac{\partial^2 \gamma_{rz}}{\partial z \partial r}\right)$$

$$\frac{1}{r}\frac{\partial^2 \varepsilon_{zz}}{\partial r \partial \theta} - \frac{1}{r^2}\frac{\partial \varepsilon_{zz}}{\partial \theta} = \frac{\partial}{\partial z}\left(\frac{1}{r}\frac{\partial \gamma_{rz}}{\partial \theta} + \frac{\partial \gamma_{\theta z}}{\partial r} - \frac{\partial \gamma_{r\theta}}{\partial z}\right) - \frac{\partial}{\partial z}\left(\frac{\gamma_{\theta z}}{r}\right)$$

$$\frac{1}{r}\frac{\partial^2 \varepsilon_{rr}}{\partial \theta \partial z} = \frac{\partial}{\partial r}\left(\frac{1}{r}\frac{\partial \gamma_{zr}}{\partial \theta} - \frac{\partial \gamma_{\theta z}}{\partial r} + \frac{\partial \gamma_{r\theta}}{\partial z}\right) - \frac{\partial}{\partial r}\left(\frac{\gamma_{\theta z}}{r}\right) + \frac{2}{r}\frac{\partial \gamma_{r\theta}}{\partial z}$$

$$\frac{\partial^2 \varepsilon_{\theta\theta}}{\partial r \partial z} - \frac{1}{r}\frac{\partial \varepsilon_{rr}}{\partial z^2} + \frac{1}{r}\frac{\partial \varepsilon_{\theta\theta}}{\partial z} = \frac{1}{r}\frac{\partial}{\partial \theta}\left(-\frac{1}{r}\frac{\partial \gamma_{zr}}{\partial z} + \frac{\partial \gamma_{\theta z}}{\partial r} + \frac{\partial \gamma_{rz}}{\partial z}\right) + \frac{1}{r}\frac{\partial}{\partial \theta}\left(\frac{\gamma_{\theta z}}{r}\right)$$

Material Constitutive Relations (Orhotropic) [2]

(2–3)

$$\begin{bmatrix} \sigma_{zz} \\ \sigma_{\theta\theta} \\ \sigma_{rr} \\ \tau_{r\theta} \\ \tau_{rz} \\ \tau_{\theta z} \end{bmatrix} = \begin{bmatrix} Q_{11} & Q_{12} & Q_{13} & 0 & 0 & Q_{16} \\ Q_{12} & Q_{22} & Q_{23} & 0 & 0 & Q_{26} \\ Q_{13} & Q_{23} & Q_{33} & 0 & 0 & Q_{36} \\ 0 & 0 & 0 & Q_{44} & Q_{45} & 0 \\ 0 & 0 & 0 & Q_{45} & Q_{55} & 0 \\ Q_{16} & Q_{26} & Q_{36} & 0 & 0 & Q_{66} \end{bmatrix} \begin{bmatrix} \varepsilon_{zz} \\ \varepsilon_{\theta\theta} \\ \varepsilon_{rr} \\ \gamma_{r\theta} \\ \gamma_{rz} \\ \gamma_{\theta z} \end{bmatrix}$$

Stress Equilibrium Equations [57]

(2–4)

$$\frac{\partial \sigma_{rr}}{\partial r} + \frac{1}{r}\frac{\partial}{\partial \theta}\tau_{r\theta} + \frac{\partial}{\partial z}\tau_{rz} + \frac{\sigma_{rr} - \sigma_{\theta\theta}}{r} = 0$$

$$\frac{\partial}{\partial r}\tau_{r\theta} + \frac{1}{r}\frac{\partial}{\partial \theta}\sigma_{\theta\theta} + \frac{\partial}{\partial z}\tau_{\theta z} + \frac{2}{r}\tau_{r\theta} = 0$$

$$\frac{\partial}{\partial r}\tau_{rz} + \frac{1}{r}\frac{\partial}{\partial \theta}\tau_{\theta z} + \frac{\partial}{\partial z}\sigma_{zz} + \frac{1}{r}\tau_{rz} = 0$$

Table 2–1 Linear Elastic Equations in Cylindrical Coordinates

Method/Series	Power Series	Legendre Series	Other Series
Displacement function assumed	1967 Gulati, Essenberg [36] 1968 Dong, Pister Taylor [34] 1970 Pagano Whitney [70] 1970 Vinson, Zukas [38] 1972 Dong, Tso [39] 1973 Cheng [53] 1973 Whitney, Grimes, Francis [21] 1975 Whitney, Sun [40] 1975 Librescu [80, 81, 82] 1976 Vasilenko [41] 1984 Cheng, He [54] 1986 Liu, Reddy [42]	1973 Khoma [48] 1975 Chepiga [49]	1986 Li & Wang [55]
Stress function (strain) assumed	1967 Bert [60] 1968 Whitney, Halpin [37] 1969 Bazarenko [56] 1971 Whitney [35]	1973 Gregorenko et al [59]	
Stress function and Displacement function assumed	1968–1988 [43–47] Widera et al	1972 Vinson [50] 1975 Vinson [51]	

Table 2–2 Review of Shell Theories According to Solution Type

(A) Direct Method

(1) Assume displacement functions

$$\underset{\sim}{u} = \sum \phi^{(j)} \xi^{j}$$

(2) Calculate strains ε using eqn (2–1) in terms of displacement coefficients.

(3) Calculate stresses σ using eqn (2–5) in terms of displacement coefficients.

(4) Introduce stress resultant and generalized stiffness.

$$\underset{\sim}{N} = \int \underset{\sim}{\sigma} f(\xi) d\xi \quad ; \quad \underset{\approx}{A} = \int \underset{\approx}{Q} f(\xi) d\xi$$

(5) Calculate $\underset{\sim}{N}$ in terms of displacement coefficients.

(6) Generate stress resultant equilibrium equations by multiplying egn (2–4) by $f(\xi)$ and integrating as in (4) above.

(7) Substitute (5) into (6) to get the deformation equilibrium equations.

(8) Solve (6) and (7) subject to boundary conditions.

(B) Method of Stationary Potential

(1) Define strain energy U where

$$U = \frac{1}{2} \int_{V} (\sigma_{rr} \varepsilon_{rr} + \sigma_{\theta\theta} \varepsilon_{\theta\theta} + \sigma_{zz} \varepsilon_{zz} + \tau_{rz} \gamma_{rz} + \tau_{r\theta} \gamma_{r\theta} + \tau_{\theta z} \gamma_{\theta z}) \, dV$$

(2) Define work done W bv deformina aaencv where

$$W = \frac{1}{2} \int_{V} \left\{ \frac{1}{r} \frac{\partial}{\partial r} (r u_r \sigma_{rr} + r u_\theta \tau_{r\theta} + r u_z \tau_{rz}) + \frac{\partial}{\partial z} (u_r \tau_{rz} + u_\theta \tau_{\theta z} + u_z \sigma_{zz}) \right\} dV$$

(3) Substitute (1) and (2) of Part (A) into the above equations.

(4) Form the potential energy functional Γ where

$\Gamma = U - W$

in terms of the coefficients

(5) Find the minimum of Γ by differentiating with respect to the coefficient $\phi^{(j)}$ and setting the result to zero. The result is equation (5) of Part (A).

(6) Repeat procedures (6) and (7) of Part (A)

Table 2–3 Method of Solution if Displacement is a Power Series

For Each Layer

(1) Assume stress or strain variable as power series.

$$\underline{\sigma}, \underline{\varepsilon} = \sum \underline{\phi}^{(j)} \zeta^{j}$$

(2) Calculate strain or stress using eqn (2-3).

(3) Substitute (1) and (2) into the stress equilibrium equation and solve system of differential equations for the coefficients.

(4) Calculate displacement components by solving eqn (2-1).

For Each Layer Interface

(1) Match displacement components

(2) Match transverse normal and transverse shear stress components

Apply boundary conditions

Table 2–4 Method of Solution if Stress or Strain is a Power Series

Chapter 3

A REFINED CYLINDRICAL SHELL THEORY

SUMMARY OF SOLUTION METHOD

A refined cylindrical shell theory of any desired accuracy for a laminated orthotropic material subject to axisymmetric loading is realized by the following method.

(1) The deformations are represented as a power series in a non–dimensional radial coordinate q.

(2) Small deformation strains are calculated in terms of q.

(3) A generalized stress resultant is defined by integrating the product of the stress and q^n through the thickness of the cylinder wall.

(4) The equilibrium equations are multiplied by q^n and integrated through the cylinder wall. The stress resultant definition is used in these equations to generate the stress resultant equilibrium equations.

(5) A generalized stiffness is defined by integrating the product of the reduced stiffnesses and q^n through the cylinder wall.

(6) A generalized linear constitutive relationship for the material plus the generalized stiffnesses are substituted into the generalized stress resultant equations to generate a system of second order ordinary differential equations with the coefficients of the power series being the unknowns.

(7) The differential equation system is transformed to a coordinate system centered at the mid-plane of the laminate. This was observed to improve convergence of the series. The resulting system is then solved subject to boundary conditions, giving the coefficients of the power series expressed in the mid-plane coordinate system.

3.1 Introduction

One technique for finding the solution of a differential equation is to express the dependent variable as a power series in the independent variable. This requires that the function be continuous over the range of interest of the independent variable [30].

As previously reviewed, this technique has been applied to the analysis of laminated plates and shells. An increasing number of terms in a truncated power series representing the solution, usually the deformation of the plate or shell, is used. The independent variable is usually the distance from the mid-plane of the shell or plate to the point of interest, measured normal to the surface of the plate or shell.

As discussed earlier, thin laminates are traditionally analyzed by retaining only the linear terms in a power series representing the deformations or strains.

If ξ is the distance from the laminate mid-plane to the point of interest measured normal to the surface of the laminate, then the deformation of the shell can be approximated as

$$\underline{u} = \underline{\beta}^{(0)} + \underline{\beta}^{(1)} \xi$$

where $$\underline{\beta}^{(0)}(z,\theta) = (\beta_z^{(0)}, \beta_\theta^{(0)}, \beta_r^{(0)})^T$$

and $$\underline{\beta}^{(1)}(z,\theta) = (\beta_z^{(1)}, \beta_\theta^{(1)}, 0)^T$$

$\underline{u}$ is the deformation of the plate or shell, and $\underline{\beta}$ is a vector function independent of r. z, θ, and r represent the axial, circumferential, and radial coordinates of a cylindrical coordinate system. The solution is valid for thin plates and shells where transverse shear effects can be neglected, and for situations with negligible surface normal loadings.

Various authors have added extra terms to this power series to allow a solution where transverse shear and large normal loadings exist. For example [40], a quadratic representation has been used to approximate infinitely long cylinders where the loading creates transverse shear effects.

The deformation $\underline{u}$ was written as

$$\underline{u} = \underline{\beta}^{(0)} + \underline{\beta}^{(1)} \xi + \underline{\beta}^{(2)} \xi^2$$

$$\underline{\beta}^{(0)}(z,\theta) = (\beta_z^{(0)}, \beta_\theta^{(0)}, \beta_r^{(0)})^T$$

$$\underline{\beta}^{(1)}(z,\theta) = (\beta_z^{(1)}, \beta_\theta^{(1)}, \beta_r^{(1)})^T$$

$$\underline{\beta}^{(2)}(z,\theta) = (0, 0, \beta_r^{(2)})^T$$

This representation needs a shear correction factor to adequately handle situations where transverse shear is significant. A cubic representation was used for the solution of thick flat plates subject to large loadings normal to the surface [61]. The deformation was represented by

$$\underline{u} = \underline{\beta}^{(0)} + \underline{\beta}^{(1)}\xi + \underline{\beta}^{(2)}\xi^2 + \underline{\beta}^{(3)}\xi^3$$

$$\underline{\beta}^{(j)}(x,y) = (\beta_x{}^{(j)}, \beta_y{}^{(j)}, \beta_z{}^{(j)})^T \qquad j = 0, 1, 2$$

$$\underline{\beta}^{3}(x,y) = (\beta_x{}^{(3)}, \beta_y{}^{(3)}, 0)$$

This produces deformations of adequate accuracy, however special techniques were needed to achieve the desired accuracy in the calculation of stresses.

The above analyses have been extended in what follows to include any desired number of terms in a power series representation for cylinders. It also allows for the inclusion of boundary or end conditions for finite length cylinders.

3.2 Strain–Deformation Equations

Consider a thick cylinder subject to axisymmetric loading referenced to a cylindrical coordinate system shown in Figure 3–1. The material properties of the cylinder are assumed to be independent of angular position. Let z, θ, and r define the axial, angular, and radial position of any point in the coordinate system.

Further, let the vector

(3–1) $$\underline{u} = (u_z, u_\theta, u_r)^T$$

where $u_j = u_j(z, \theta, r)$; $j = z, \theta, r$

define the deformation at any point in the cylinder wall under the given loading conditions. With material properties and a loading situation that have no angular dependence, we can write

$$\frac{\partial}{\partial \theta}\left\{ \quad \right\} = 0 \tag{3-2}$$

for all variables.

It should be noted that unlike isotropic materials, orthotropic cylinders may rotate under an axisymmetric load. i.e. $u_\theta \neq 0$

Define the strains relative to the coordinate system of Figure 3–1 by the vector

$$\underline{\varepsilon} = (\varepsilon_{zz}, \varepsilon_{\theta\theta}, \varepsilon_{rr}, \gamma_{r\theta}, \gamma_{rz}, \gamma_{\theta z})^T \tag{3-3}$$

Given that the deformations of the cylinder are small, the strains in the cylinder wall can be written [57].

$$\begin{aligned} \varepsilon_{zz} &= \frac{\partial u_z}{\partial z} & \gamma_{r\theta} &= \frac{\partial u_\theta}{\partial r} - \frac{u_\theta}{r} + \frac{1}{r}\frac{\partial u_r}{\partial \theta} \\ \varepsilon_{\theta\theta} &= \frac{1}{r}\frac{\partial u_\theta}{\partial \theta} + \frac{u_r}{r} & \gamma_{rz} &= \frac{\partial u_r}{\partial z} + \frac{\partial u_z}{\partial r} \\ \varepsilon_{rr} &= \frac{\partial u_r}{\partial r} & \gamma_{\theta z} &= \frac{1}{r}\frac{\partial u_z}{\partial \theta} + \frac{\partial u_\theta}{\partial z} \end{aligned} \tag{3-4}$$

Given equation (3–2), the strain displacement equations reduce to

$$\begin{aligned} \varepsilon_{zz} &= \frac{\partial u_z}{\partial z} & \gamma_{r\theta} &= \frac{\partial u_\theta}{\partial r} - \frac{u_\theta}{r} \\ \varepsilon_{\theta\theta} &= \frac{u_r}{r} & \gamma_{rz} &= \frac{\partial u_r}{\partial z} + \frac{\partial u_z}{\partial r} \\ \varepsilon_{rr} &= \frac{\partial u_r}{\partial r} & \gamma_{\theta z} &= \frac{\partial u_\theta}{\partial z} \end{aligned} \tag{3-5}$$

As mentioned, traditional laminate analysis expands the through the wall dependence of the deformation in terms of the distance away from the laminate center retaining only first order terms. Mathematical analysis is greatly simplified if we expand our deformations in terms of a slightly different variable

(3–6) $$q = \frac{r}{r_c}$$

r_c is the radial position of the cylinder wall mid–plane. A transformation will then be applied at the end of the analysis to express the solution in terms of distances away from the cylinder mid–plane.

Let us now expand the cylinder deformation beyond the usual first or second order truncations as

(3–7) $$\underline{u} = \sum_{j=0}^{\infty} \underline{\phi}^{(j)}(z)\, q^{j}$$

where $$\underline{\phi}^{(j)}(z) = (\phi_z^{(j)}, \phi_\theta^{(j)}, \phi_r^{(j)})^T$$

are functions, dependent upon the axial coordinate, that are to be determined.

Substituting equations (3–7) into equations (3–5) gives the strains as a series in terms of the variables q and $\underline{\phi}^{(j)}$, i.e.

$$
(3\text{-}8) \qquad
\begin{Bmatrix} \varepsilon_{zz} \\ \varepsilon_{\theta\theta} \\ \varepsilon_{rr} \\ \gamma_{r\theta} \\ \gamma_{rz} \\ \gamma_{\theta z} \end{Bmatrix}
= \sum_{j=0}^{\infty}
\begin{Bmatrix}
\phi_z'^{(j)} \zeta^{j} \\
\frac{1}{r_c} \phi_r^{(j)} \zeta^{j-1} \\
\frac{j}{r_c} \phi_r^{(j)} \zeta^{j-1} \\
\frac{j-1}{r_c} \phi_\theta^{(j)} \zeta^{j-1} \\
\phi_r'^{(j)} \zeta^{j} + \frac{j}{r_c} \phi_z^{(j)} \zeta^{j-1} \\
\phi_\theta'^{(j)} \zeta^{j}
\end{Bmatrix}
$$

The primes denote differentiation with respect to z, the axial coordinate.

3.3 Stress Resultant Equations

Consider now, an element of the cylinder in the absence of body forces. We denote the stresses in the cylinder by the stress vector

$$
(3\text{-}9) \qquad \underline{\sigma} = (\sigma_{zz}, \sigma_{\theta\theta}, \sigma_{rr}, \tau_{r\theta}, \tau_{rz}, \tau_{\theta z})^{T}
$$

A force balance leads to the following set of the equilibrium equations in the absence of motion or external body forces [57].

$$
(3\text{-}10) \qquad
\begin{aligned}
\frac{\partial \sigma_{rr}}{\partial r} + \frac{1}{r}\frac{\partial \tau_{r\theta}}{\partial \theta} + \frac{\partial \tau_{rz}}{\partial z} + \frac{\sigma_{rr} - \sigma_{\theta\theta}}{r} &= 0 \\
\frac{\partial \tau_{r\theta}}{\partial r} + \frac{1}{r}\frac{\partial \sigma_{\theta\theta}}{\partial \theta} + \frac{\partial \tau_{\theta z}}{\partial z} + \frac{2}{r}\tau_{r\theta} &= 0 \\
\frac{\partial \tau_{rz}}{\partial r} + \frac{1}{r}\frac{\partial \tau_{\theta z}}{\partial \theta} + \frac{\partial \sigma_{zz}}{\partial z} + \frac{1}{r}\tau_{rz} &= 0
\end{aligned}
$$

Changing variables using equation (3–6), and noting equation (3–2) reduces these equations to

$$
\begin{aligned}
& q \frac{\partial \sigma_{rr}}{\partial q} + r_c\, q \frac{\partial \tau_{rz}}{\partial z} + (\sigma_{rr} - \sigma_{\theta\theta}) = 0 \\
(3\text{–}11) \qquad & q \frac{\partial \tau_{r\theta}}{\partial q} + r_c\, q \frac{\partial \tau_{\theta z}}{\partial z} + 2\, \tau_{r\theta} = 0 \\
& q \frac{\partial \tau_{rz}}{\partial q} + r_c\, q \frac{\partial \sigma_{zz}}{\partial z} + \tau_{rz} = 0
\end{aligned}
$$

Traditionaı iaminate analysis considers force and moment resultants by integrating the stress and the stress–displacement product through the thickness of the laminate. This has been extended, [40, 61] to include quadratic and cubic terms in the mid–plane displacement.

We shall extend this to an arbitrary order by defining a generalized stress resultant in terms of q by

$$
(3\text{–}12) \qquad \underline{N}^{(n)} = \int_{q_i}^{q_o} \underline{\sigma}\, q^n\, dq
$$

where q_o and q_i correspond to the outer and inner radii of the cylinder respectively.

If we multiply equations (3–11) by q^n and integrate the result over q through the thickness of the cylinder we get

$$
\begin{aligned}
& \int_{q_i}^{q_o} q^{n+1} \frac{\partial \sigma_{rr}}{\partial q}\, dq + r_c \int_{q_i}^{q_o} q^{n+1} \frac{\partial \tau_{rz}}{\partial z}\, dq + \int_{q_i}^{q_o} (\sigma_{rr} - \sigma_{\theta\theta})\, q^n\, dq = 0 \\
& \int_{q_i}^{q_o} q^{n+1} \frac{\partial \tau_{r\theta}}{\partial q}\, dq + r_c \int_{q_i}^{q_o} q^{n+1} \frac{\partial \tau_{\theta z}}{\partial z}\, dq + 2 \int_{q_i}^{q_o} \tau_{r\theta}\, q^n\, dq = 0 \\
& \int_{q_i}^{q_o} q^{n+1} \frac{\partial \tau_{rz}}{\partial q}\, dq + r_c \int_{q_i}^{q_o} q^{n+1} \frac{\partial \sigma_{zz}}{\partial z}\, dq + \int_{q_i}^{q_o} \tau_{rz}\, q^n\, dq = 0
\end{aligned}
$$

Two terms in this integration are straightforward, i.e.

$$\int_{\xi_i}^{\xi_o} \xi^{n+1} \frac{\partial \sigma_{ij}}{\partial z} d\xi = \frac{\partial}{\partial z} \int_{\xi_i}^{\xi_o} \xi^{n+1} \sigma_{ij}\, d\xi = N_{ij}^{\prime\,(n+1)}$$

$$\int_{\xi_i}^{\xi_o} \xi^{n} \sigma_{ij}\, d\xi = N_{ij}^{(n)}$$

The third integral can be integrated by parts

$$\int_{\xi_i}^{\xi_o} \xi^{n+1} \frac{\partial \sigma_{ij}}{\partial \xi} d\xi = \xi^{n+1} \sigma_{ij} \Big|_{\xi_i}^{\xi_o} - \int_{\xi_i}^{\xi_o} \sigma_{ij}\, (n+1)\, \xi^{n} d\xi$$

$$= \xi^{n+1} \sigma_{ij} \Big|_{\xi_i}^{\xi_o} - (n+1)\, N_{ij}^{(n)}$$

Collecting terms results in the generalized stress resultant equations

$$r_c\, N_{rz}^{\prime\,(n+1)} - n\, N_{rr}^{(n)} - N_{\theta\theta}^{(n)} = f_{rr}^{(n+1)}$$

(3–13) $$r_c\, N_{\theta z}^{\prime\,(n+1)} - (n-1)\, N_{r\theta}^{(n)} = f_{r\theta}^{(n+1)}$$

$$r_c\, N_{zz}^{\prime\,(n+1)} - n\, N_{rz}^{(n)} = f_{rz}^{(n+1)}$$

where

$$f_{rj}^{(n+1)} = - \sigma_{rj}\, \xi^{n+1} \Big|_{\xi_i}^{\xi_o} ; \qquad \begin{array}{l} j = z, \theta, r \\ n = 0, 1, 2, \ldots \end{array}$$

In a subsequent section, this set of equations will be shown to reduce to the usual stress resultant equations of simple cylindrical shell theories.

3.4 Material Properties

Suppose now that the cylinder is made of layers of orthotropic material whose properties do not vary around the circumference of the cylinder. This would be typical of a filament wound composite tube where a unidirectional fibrous material is formed in a cylindrical manner, the direction of the fibers following a cylindrical surface in a helical path.

If the loads are small enough that the material can be treated as linearly elastic, the stresses and the strains are related by the generalized form of Hooke's law which is

$$\underline{\sigma} = \underline{\underline{Q}} \cdot \underline{\varepsilon} \tag{3-14}$$

where the our material properties $\underline{\underline{Q}}$ are given by [2]

$$\underline{\underline{Q}} = \begin{Bmatrix} Q_{11} & Q_{12} & Q_{13} & 0 & 0 & Q_{16} \\ Q_{12} & Q_{22} & Q_{23} & 0 & 0 & Q_{26} \\ Q_{13} & Q_{23} & Q_{33} & 0 & 0 & Q_{36} \\ 0 & 0 & 0 & Q_{44} & Q_{45} & 0 \\ 0 & 0 & 0 & Q_{45} & Q_{55} & 0 \\ Q_{16} & Q_{26} & Q_{36} & 0 & 0 & Q_{66} \end{Bmatrix} \tag{3-15}$$

We are assuming that all analysis is done at constant temperature. If we substitute the strain series equation (3–8) into (3–14), we get the stresses expressed in terms of the power series coefficients $\underline{\phi}^{(j)}$.

$$\begin{Bmatrix} \sigma_{zz} \\ \sigma_{\theta\theta} \\ \sigma_{rr} \\ \tau_{r\theta} \\ \tau_{rz} \\ \tau_{\theta z} \end{Bmatrix} = \sum_{j=0}^{\infty} \begin{Bmatrix} Q_{11} & Q_{12} & Q_{13} & 0 & 0 & Q_{16} \\ Q_{12} & Q_{22} & Q_{23} & 0 & 0 & Q_{26} \\ Q_{13} & Q_{23} & Q_{33} & 0 & 0 & Q_{36} \\ 0 & 0 & 0 & Q_{44} & Q_{45} & 0 \\ 0 & 0 & 0 & Q_{45} & Q_{55} & 0 \\ Q_{16} & Q_{26} & Q_{36} & 0 & 0 & Q_{66} \end{Bmatrix} \begin{Bmatrix} \phi_z'^{(j)} \zeta^{j} \\ \frac{1}{r_c} \phi_r^{(j)} \zeta^{j-1} \\ \frac{j}{r_c} \phi_r^{(j)} \zeta^{j-1} \\ \frac{j-1}{r_c} \phi_\theta^{(j)} \zeta^{j-1} \\ \phi_r'^{(j)} \zeta^{j} + \frac{j}{r_c} \phi_z^{(j)} \zeta^{j-1} \\ \phi_\theta'^{(j)} \zeta^{j} \end{Bmatrix}$$

Upon collecting terms,

$$
(3\text{-}16)\qquad
\begin{Bmatrix} \sigma_{zz} \\ \sigma_{\theta\theta} \\ \sigma_{rr} \\ \tau_{r\theta} \\ \tau_{rz} \\ \tau_{\theta z} \end{Bmatrix}
= \sum_{j=0}^{\infty} q^{j-1}
\begin{Bmatrix}
0 & 0 & \frac{1}{r_c}(Q_{12}+jQ_{13}) & Q_{11}q & Q_{16}q & 0 \\
0 & 0 & \frac{1}{r_c}(Q_{22}+jQ_{23}) & Q_{12}q & Q_{26}q & 0 \\
0 & 0 & \frac{1}{r_c}(Q_{23}+jQ_{33}) & Q_{13}q & Q_{36}q & 0 \\
\frac{j}{r_c}Q_{45} & \frac{j-1}{r_c}Q_{44} & 0 & 0 & 0 & Q_{45}q \\
\frac{j}{r_c}Q_{55} & \frac{j-1}{r_c}Q_{45} & 0 & 0 & 0 & Q_{55}q \\
0 & 0 & \frac{1}{r_c}(Q_{26}+jQ_{36}) & Q_{16}q & Q_{66}q & 0
\end{Bmatrix}
\begin{Bmatrix} \phi_z^{(j)} \\ \phi_\theta^{(j)} \\ \phi_r^{(j)} \\ \phi_z'^{(j)} \\ \phi_\theta'^{(j)} \\ \phi_r'^{(j)} \end{Bmatrix}
$$

Multiplying (3–16) by q^n and integrating through the thickness of the cylinder expresses the generalized stress resultants of equation (3–12) in terms of the stresses as expressed in equation (3–16), that is

$$
(3\text{-}17)\qquad
\begin{Bmatrix} N_{zz}^{(n)} \\ N_{\theta\theta}^{(n)} \\ N_{rr}^{(n)} \\ N_{r\theta}^{(n)} \\ N_{rz}^{(n)} \\ N_{\theta z}^{(n)} \end{Bmatrix}
= \sum_{j=0}^{\infty} \int_{q_i}^{q_o} q^{n+j-1}
\begin{Bmatrix}
0 & 0 & \frac{1}{r_c}(Q_{12}+jQ_{13}) & Q_{11}q & Q_{16}q & 0 \\
0 & 0 & \frac{1}{r_c}(Q_{22}+jQ_{23}) & Q_{12}q & Q_{26}q & 0 \\
0 & 0 & \frac{1}{r_c}(Q_{23}+jQ_{33}) & Q_{13}q & Q_{36}q & 0 \\
\frac{j}{r_c}Q_{45} & \frac{j-1}{r_c}Q_{55} & 0 & 0 & 0 & Q_{45}q \\
\frac{j}{r_c}Q_{55} & \frac{j-1}{r_c}Q_{45} & 0 & 0 & 0 & Q_{55}q \\
0 & 0 & \frac{1}{r_c}(Q_{26}+Q_{36}) & Q_{16}q & Q_{66}q & 0
\end{Bmatrix}
\begin{Bmatrix} \phi_z^{(j)} \\ \phi_\theta^{(j)} \\ \phi_r^{(j)} \\ \phi_z'^{(j)} \\ \phi_\theta'^{(j)} \\ \phi_r'^{(j)} \end{Bmatrix} dq
$$

Carrying the integration through the summation, we note that terms of the form

$$
\int_{q_i}^{q_o} Q_{ij}\, q^n \, dq
$$

are prevalent. For notation purposes, we introduce the a generalized stiffness matrix $\underline{\underline{A}}^{(n)}$ where

$$
(3\text{-}18)\qquad \underline{\underline{A}}^{(n)} = \int_{q_i}^{q_o} \underline{\underline{Q}}\, q^n \, dq
$$

This simplifies equation (3–17) to

$$
(3\text{–}19)\qquad
\begin{Bmatrix} N_{zz}^{(n)} \\ N_{\theta\theta}^{(n)} \\ N_{rr}^{(n)} \\ N_{r\theta}^{(n)} \\ N_{rz}^{(n)} \\ N_{\theta z}^{(n)} \end{Bmatrix}
= \sum_{j=0}^{\infty}
\begin{Bmatrix}
0 & 0 & \frac{1}{r_c}\left(A_{12}^{(m-1)} + jA_{13}^{(m-1)}\right) & A_{11}^{(m)} & A_{16}^{(m)} & 0 \\
0 & 0 & \frac{1}{r_c}\left(A_{22}^{(m-1)} + jA_{23}^{(m-1)}\right) & A_{12}^{(m)} & A_{26}^{(m)} & 0 \\
0 & 0 & \frac{1}{r_c}\left(A_{23}^{(m-1)} + jA_{33}^{(m-1)}\right) & A_{13}^{(m)} & A_{36}^{(m)} & 0 \\
\frac{j}{r_c}A_{45}^{(m-1)} & \frac{j-1}{r_c}A_{55}^{(m-1)} & 0 & 0 & 0 & A_{45}^{(m)} \\
\frac{j}{r_c}A_{55}^{(m-1)} & \frac{j-1}{r_c}A_{45}^{(m-1)} & 0 & 0 & 0 & A_{55}^{(m)} \\
0 & 0 & \frac{1}{r_c}\left(A_{26}^{(m-1)} + jA_{36}^{(m-1)}\right) & A_{16}^{(m)} & A_{66}^{(m)} & 0
\end{Bmatrix}
\begin{Bmatrix} \phi_z^{(j)} \\ \phi_\theta^{(j)} \\ \phi_r^{(j)} \\ \phi_z'^{(j)} \\ \phi_\theta'^{(j)} \\ \phi_r'^{(j)} \end{Bmatrix}
$$

$$m = n + j$$

3.5 Coupled Second–Order Differential Equations

Substitution of equation (3–19) into the stress resultant equilibrium equations (3–13) yields a system of coupled second order ordinary differential equations. This substitution yields after lengthy but simple algebra, the shell deformation equations

$$
(3\text{–}20)\qquad \underline{\underline{A}}\,\underline{\Phi}'' + \underline{\underline{B}}\,\underline{\Phi}' + \underline{\underline{C}}\,\underline{\Phi} + \underline{D} = 0
$$

where

$$
(3\text{–}21)\qquad \underline{\Phi}(z) = \left(\phi_z^{(0)}, \phi_\theta^{(0)}, \phi_r^{(0)}, \phi_z^{(1)}, \phi_\theta^{(1)}, \phi_r^{(1)}, \ldots\right)^T
$$

and the coefficients $\underline{\underline{A}}$, $\underline{\underline{B}}$, and $\underline{\underline{C}}$ and $\underline{D}$ are given in Table 3–1.

It was found that the matrices of this equation are nearly singular, that is, there is very little difference between adjacent rows in the matrices. Any solution scheme must address this.

3.6 Mid–Plane Shift

Using the power series in equation (3–7) offers no guarantee of convergence to a solution. It was observed that this was improved if we transformed our independent variable q to a new variable ξ where

$$(3\text{–}22) \qquad \xi = \frac{r_c - r}{r_c} \qquad -1 < \xi < 1$$

ξ is the radial non–dimensional distance from the shell mid–plane to the point of interest.

The power series definition of the shell deformations then becomes

$$(3\text{–}23) \qquad \underline{u} = \sum_{j=0}^{\infty} \underline{\beta}^{(j)} \xi^{j}$$

where $\qquad \underline{\beta}^{(j)}(z) = (\beta_z^{(j)}, \beta_\theta^{(j)}, \beta_r^{(j)})^T$

which we note is the form of the expansion that when truncated to two or three terms is used traditionally.

As previously mentioned, expansion of the series in terms of the variable q was mathematically simpler. Expansion in terms of ξ however was more convergent.

Equating (3–23) and (3–7) is obviously

$$\sum_{j=0}^{\infty} \underline{\beta}^{(j)} \xi^{j} = \sum_{j=0}^{\infty} \underline{\phi}^{(j)} (1-\xi)^{j}$$

Expanding $(1-\xi)^j$ using Newton's Binomial Expansion gives

$$(1-\xi)^{j} = \sum_{k=0}^{j} \binom{j}{k} (-1)^{k} \xi^{k}$$

where $\binom{j}{k}$ is the number of combination of j items in k groups, and is written as

$$\binom{j}{k} = \frac{j!}{k!\,(j-k)!}$$

Collecting terms and equating equal powers of ξ gives

$$\underline{u} = \sum_{j=0}^{\infty} \left\{ \sum_{k=j}^{\infty} \binom{k}{j} (-1)^{k} \underline{\phi}^{(k)} \right\} \xi^{j}$$

from which

$$\underline{\beta}^{(j)} = \sum_{k=j}^{\infty} \binom{k}{j} (-1)^{j} \underline{\phi}^{(k)}$$

or equivalently

(3–24) $$\underline{\phi}^{(j)} = \sum_{k=j}^{\infty} \binom{k}{j} (-1)^{j} \underline{\beta}^{(k)}$$

If we substitute equation (3–24) into (3–20), the coupled differential equation set becomes

$$\sum_{j=0}^{\infty} \sum_{k=j}^{\infty} (-1)^{j} \binom{k}{j} \left\{ \underline{\underline{A}}_{ij} \underline{\beta}''^{(k)} + \underline{\underline{B}}_{ij} \underline{\beta}'^{(k)} + \underline{\underline{C}}_{ij} \underline{\beta}^{(k)} \right\} + \underline{D}_{i} = 0$$

where the matrices $\underline{\underline{A}}_{ij}$, $\underline{\underline{B}}_{ij}$, and $\underline{\underline{C}}_{ij}$ are the 3 x 3 submatrices of $\underline{\underline{A}}$, $\underline{\underline{B}}$, and $\underline{\underline{C}}$ corresponding to i and j as given in Table 3–1. If we expand this summation and collect like terms in $\underline{\beta}^{(k)}$, these equations can be more conveniently written as

(3–25) $$\underline{\underline{a}}\,\alpha'' + \underline{\underline{b}}\,\alpha' + \underline{\underline{c}}\,\alpha + \underline{D} = 0$$

where $$\underline{\alpha}(z) = \left(\beta_z^{(0)}, \beta_\theta^{(0)}, \beta_r^{(0)}, \beta_z^{(1)}, \beta_\theta^{(1)}, \beta_r^{(1)}, \dots\right)^T$$

and $$\underline{\underline{a}}_{ij} = \sum_{k=0}^{j} \binom{j}{k} (-1)^j \underline{\underline{A}}_{ik}$$
$$\underline{\underline{b}}_{ij} = \sum_{k=0}^{j} \binom{j}{k} (-1)^j \underline{\underline{B}}_{ik}$$
$$\underline{\underline{c}}_{ij} = \sum_{k=0}^{j} \binom{j}{k} (-1)^j \underline{\underline{C}}_{ik}$$

This transformation requires that we calculate the strains in terms of ξ. Equation (3–5) is written now as

$$\text{(3–26)} \qquad \begin{Bmatrix} \varepsilon_{zz} \\ \varepsilon_{\theta\theta} \\ \varepsilon_{rr} \\ \varepsilon_{r\theta} \\ \varepsilon_{rz} \\ \varepsilon_{\theta z} \end{Bmatrix} = \sum_{j=0}^{\infty} \begin{Bmatrix} \beta_z'^{(j)} \xi^j \\ \frac{\beta_\theta^{(j)}}{R} \frac{\xi^j}{1-\xi} \\ -\frac{j}{R} \beta_r^{(j)} \xi^{j-1} \\ -\frac{j}{R} \beta_\theta^{(j)} \xi^{j-1} - \frac{1}{R} \beta_\theta^{(j)} \frac{\xi^j}{1-\xi} \\ \beta_r'^{(j)} \xi^j - \frac{j}{R} \beta_z^{(j)} \xi^{j-1} \\ \beta_z'^{(j)} \xi^j \end{Bmatrix}$$

3.7 Series Truncation

Truncation of the power series is necessary at some point, if a solution is to be realized practically. Each individual series for the radial, the axial, or the circumferential deformations does not necessarily have to be truncated at the same point. This allows in principle an infinite number of truncation schemes.

Two truncation schemes have been utilized in previous studies. In an attempt to improve accuracy in the calculation of ε_{rr}, one more term in the radial deformation has been retained than either the axial or circumferential deformations [40]. It is seen from equation (3–26) that this would maintain ε_{zz}, $\varepsilon_{\theta\theta}$, ε_{rr}, and $\varepsilon_{\theta z}$ to the same degree of accuracy. The out of plane shear terms becomes of mixed accuracy, however. A second technique used in prior studies has been to retain the axial and circumferential deformation expansions to one more term than the radial deformation expansion [34, 37, 39, 53, 66]. This then, allows out of plane shears $\gamma_{r\theta}$ and γ_{rz} to be calculated to the same and internally consistent degree of accuracy. A third method, which has not been used to the author's knowledge, would be to truncate all terms equally. It will be shown later that this is the most quickly converging of the three truncation schemes discussed. It will also be seen, that if a large number of terms in the series are retained, the differences between truncation methods becomes insignificant.

It is of interest at this point to restate the equation sets requiring solutions in terms of the truncation noted above.

The coupled differential equation set (3–25) becomes

(3–27) $$\underline{\underline{a}}\,\underline{\alpha}'' + \underline{\underline{b}}\,\underline{\alpha}' + \underline{\underline{C}}\,\underline{\alpha} + \underline{D} = 0$$

where $$\underline{\alpha} = (\beta_z^{(0)}, \beta_\theta^{(0)}, \beta_r^{(0)}, \cdots, 0, 0, \beta_r^{(N)})^T$$

for the first truncation method,

$$\underline{\alpha} = (\beta_z^{(0)}, \beta_\theta^{(0)}, \beta_r^{(0)}, \cdots, \beta_z^{(N)}, \beta_\theta^{(N)}, 0)^T$$

for the second method, and

$$\underline{\alpha} = (\beta_z^{(0)}, \beta_\theta^{(0)}, \beta_r^{(0)}, \cdots, \beta_z^{(N)}, \beta_\theta^{(N)}, \beta_r^{(N)})^T$$

for the third.

To achieve a match between the number of equations and the number of unknowns, equations must be dropped. It has been observed that if the first truncation method is used, an extra radial equilibrium equation is retained [40]. That is to say, if the axial and circumferential terms are retained to order N, and the radial deformation is retained to order (N+1), then N axial and circumferential equilibrium equations are used, and (N+1) radial equilibrium equations are retained in equations (3–27).

If the second truncation method is used, by a similar reasoning, one radial equilibrium equation has been dropped [66]. That is, if the axial and circumferential terms are retained to order N, and the radial deformation is truncated at order (N–1), then N equilibrium equations are used for the axial and circumferential directions, whereas (N–1) equations are used for the radial direction.

The third truncation scheme does not suffer such a defect since the number of equations automatically equals the number of unknown coefficients.

3.8 Boundary Conditions

In general problems of elastostatics, boundary conditions can take three forms – a stress at a boundary, a displacement at a boundary, or a combination of the two. The same component of the stress and displacement vector cannot be specified simultaneously [62].

The radial boundary conditions have been explicitly incorporated in the stress resultant equilibrium equations (3–13). The stress components σ_{rr}, $\sigma_{r\theta}$, and σ_{rz} are specified on the inner and outer surfaces of the cylinder through the function $f_{rj}^{(n)}$.

We are thus left with specifying conditions on $N_{zz}^{(n)}$, $N_{\theta z}^{(n)}$, and $N_{rz}^{(n)}$ as indicated by equation (3–13), or $\underline{\beta}^{(n)}$ as indicated by equation (3–25) at any boundaries on the z axis. The total number of boundary conditions must equal the number of unknown coefficients that are to be found. The specification of edge loading terms is equivalent to incorporating displacement derivatives as demonstrated by equation (3–19). We can specify either $\beta_z^{(n)}$ or $N_{zz}^{(n)}$, $\beta_\theta^{(n)}$ or $N_{\theta z}^{(n)}$, and $\beta_r^{(n)}$ or $N_{rz}^{(n)}$. This is consistent with the boundary condition formulation given by Whitney and Sun [40].

3.9 Equation Development by the Energy Method

We have seen the development of the power series equations for the thick–walled cylinder subject to axisymmetric loading through the use of the stress equilibrium equations. We shall now develop the same stress resultant equilibrium equations using the principle of stationary potential energy, to show the simplicity of the method and to demonstrate the self–consistency of the equation set.

The principle of minimum potential energy states [63],

An admissible displacement field is the one that makes the potential energy functional a stationary value.

The potential energy functional Γ is defined as

(3–28) $\quad \Gamma = U - W$

where W is the work done in deforming the material and U is the strain energy as a result of the deformation.

In the absence of body forces, the work done by the deforming agent can be derived [64] with the divergence theorem i.e.

$$W = \int_S \sigma_{ij} n_j u_i \, dS$$

becomes

(3–29) $$W = \int_V \left\{ \frac{1}{r}\left(\frac{\partial}{\partial r} r\sigma_{rr}u_r + r\tau_{r\theta} u_\theta + r\tau_{rz}u_z \right) + \frac{\partial}{\partial z}\left(\tau_{rz}u_r + \tau_{\theta z}u_\theta + \sigma_{zz}u_z\right) \right\} dV$$

Integration is performed over the volume of the body.

The strain energy is [65].

(3–30) $$U = \int_V \frac{1}{2}\left(\sigma_{rr}\varepsilon_{rr} + \sigma_{\theta\theta}\varepsilon_{\theta\theta} + \sigma_{zz}\varepsilon_{zz} + \tau_{rz}\gamma_{rz} + \tau_{r\theta}\gamma_{r\theta} + \tau_{\theta z}\gamma_{\theta z}\right) dV$$

where integration is over the volume of the body.

Substituting equation (3–7) into W, we see that

$$W = 2\pi r_c \int_z \int_\xi \sum_{j=0}^{\infty} \frac{1}{2}\Big[\frac{\partial}{\partial \xi}\left\{ \left(\sigma_{rr}\phi_r^{(j)} + \sigma_{\theta\theta}\phi_\theta^{(j)} + \tau_{rz}\phi_z^{(j)}\right) \xi^{j+1} \right\} + \frac{\partial}{\partial z}\left(\tau_{rz}\phi_r^{(j)} + \tau_{\theta z}\phi_\theta^{(j)} + \sigma_{zz}\phi_z^{(j)}\right)\xi^{j+1}\Big] dz\, d\xi$$

This, upon expanding and integrating by parts is

(3–31) $$W = 2\pi r_c \int_z \sum_{j=0}^{\infty} \frac{1}{2}\frac{\partial}{\partial \xi}\left\{ \left(\sigma_{rr}\phi_r^{(j)} + \tau_{r\theta}\phi_\theta^{(j)} + \tau_{rz}\phi_z^{(j)}\right)\xi^{j+1} \right|_{\xi_i}^{\xi_o} dz + \sum_{j=0}^{\infty}\int_z \frac{\partial}{\partial z}\left(N_{rz}^{(j+1)}\phi_r^{(j)} + N_{z\theta}^{(j+1)}\phi_\theta^{(j)} + N_{zz}^{(j+1)}\phi_z^{(j)} \right) dz$$

The strain energy given by equation (3–30) can be expressed in terms of the deformations coefficients using the strain series equations (3–8). That is,

(3–32)
$$\mathcal{U} = 2\pi r_c \sum_{j=0}^{\infty} \int_z \int_\xi \frac{1}{2} \Big\{ \Big[j\,\sigma_{rr}\phi_r^{(j)} + \sigma_{\theta\theta}\phi_r^{(j)} + (j-1)\tau_{r\theta}\phi_\theta^{(j)} \Big] \xi^j + r_c \Big[\sigma_{zz}\phi_z'^{(j)} + \tau_{rz}\phi_r'^{(j)} + \tau_{\theta z}\phi_\theta'^{(j)} \Big] \Big\} \, d\xi \, dz$$

Γ then becomes

(3–33)
$$\begin{aligned} \Gamma = 2\pi r_c \sum_{j=0}^{\infty} \int_z \Big[& \int_\xi \frac{1}{2} \Big\{ j\,\sigma_{rr}\phi_r^{(j)} + \sigma_{\theta\theta}\phi_r^{(j)} + (j-1)\tau_{r\theta}\phi_\theta^{(j)} \Big\} \xi^j \, d\xi \\ & + \frac{r_c}{2} \int_\xi \Big\{ \sigma_{zz}\phi_z'^{(j)} + \tau_{rz}\phi_r'^{(j)} + \tau_{\theta z}\phi_\theta'^{(j)} \Big\} \xi^{j+1} \, d\xi \\ & - \frac{1}{2} \frac{\partial}{\partial \xi} \Big(\sigma_{rr}\phi_r^{(j)} + \tau_{r\theta}\phi_\theta^{(j)} + \tau_{rz}\phi_z^{(j)} \Big) \xi^{j+1} \Big|_{\xi_i}^{\xi_o} \\ & - \frac{\partial}{\partial z} \Big(N_{rz}^{(j+1)}\phi_r^{(j)} + N_{\theta z}^{(j+1)}\phi_\theta^{(j)} + N_{zz}^{(j+1)}\phi_z^{(j)} \Big) \Big] \, dz \end{aligned}$$

Following the Rayleigh–Ritz method [62], the potential energy functional is stationary when its partial derivatives with respect to each of the deformation coefficients is zero, i.e.

(3–34)
$$\frac{\partial \Gamma}{\partial \phi^{(n)}} = 0$$

Applying the Rayleigh–Ritz method to equation (3–33) then gives

(3–35)
$$\begin{aligned} r_c\, N_{rz}'^{(n+1)} - n\, N_{rr}^{(n)} - N_{\theta\theta}^{(n)} &= f_{rr}^{(n+1)} \\ r_c\, N_{\theta z}'^{(n+1)} - (n-1)\, N_{r\theta}^{(n)} &= f_{r\theta}^{(n+1)} \\ r_c\, N_{zz}'^{(n+1)} - n\, N_{rz}^{(n)} &= f_{rz}^{(n+1)} \end{aligned}$$

where
$$f_{rj}^{(n+1)} = -\sigma_{rj}\, \xi^{n+1} \Big|_{\xi_o}^{\xi_i} \qquad j = z, \theta, r \qquad n = 0, 1, 2, \ldots$$

We note that these are identical to equations (3–13) derived through the integration of the stress equilibrium equations. We note also that the σ_{rj} stress components at the radial boundaries are contained in the $f_{rj}^{(n)}$ terms as before, and hence are built into the solution. We shall not develop the deformation equations here because the development would proceed exactly as that done previously.

3.10 Comparison to the Work of Others

To compare how the stress resultant equilibrium equations presented here compare to those of the membrane theory for a cylinder, consider equations (3–13) for n equal to zero. These are simply (neglecting out of plane shearing and normal stresses)

$$
\begin{aligned}
r_c \; N_{zz}'^{(1)} &= 0 \\
r_c \; N_{\theta z}'^{(1)} &= 0 \qquad\qquad (3\text{–}36) \\
N_{\theta\theta}^{(0)} &= -f_{rr}^{(1)}
\end{aligned}
$$

Note that $f_{rr}^{(1)}$ tends to $-p$ as the membrane thickness becomes infinitesimal for a thin cylinder subject to internal pressure.

These equations are the membrane stress resultant equilibrium equations [66] when no angular variation is allowed.

To compare the stress resultant equations to the thin cylindrical shell equations, consider equations (3–13) for n equal to zero and one.

For n = 0

(3–37)

$$r_c N_{rz}^{(1)} - N_{\theta\theta}^{(0)} = f_{rr}^{(1)}$$

$$r_c N_{\theta z}^{(1)} + N_{r\theta}^{(0)} = f_{r\theta}^{(1)}$$

$$r_c N_{zz}^{(1)} = f_{rz}^{(1)}$$

For n = 1

(3–38)

$$r_c N_{rz}'^{(2)} - N_{rr}^{(1)} - N_{\theta\theta}^{(1)} = f_{rr}^{(2)}$$

$$r_c N_{\theta z}'^{(2)} = f_{r\theta}^{(2)}$$

$$r_c N_{zz}'^{(2)} - N_{rz}^{(1)} = f_{rz}^{(2)}$$

Note that the first and third equations of (3–37) and the third equation of (3–38) form the set of equations for the thin cylinder [66] which in our notation can be written

(3–39)

$$N_{zz}'^{(1)} = 0$$

$$N_{rz}^{(1)\prime} - \frac{1}{r_c} N_{\theta\theta}^{(0)} = -P_{in}$$

$$\left(N_{zz}'^{(2)} - N_{zz}'^{(1)}\right) - \frac{1}{r_c} N_{rz}^{(1)} = 0$$

The second equation of equation (3–38) suggests that $N_{\theta z}^{(2)}$ is constant or vanishes since $f_{r\theta}^{(2)}$ is normally zero. This means that $\sigma_{\theta z}$ is constant or zero, which from the second equation of (3–37) gives us that $N_{r\theta}^{(1)}$ is constant or zero. This is consistent with a first order theory that neglects transverse shear stresses. The first equation of (3–38) is a result of allowing the radial deformation to vary through the thickness of the cylinder, hence belongs to a higher order theory.

We can do a similar check against a more refined shell theory for cylinders [40] where the zero, first, and second order equations must be considered. These equations when written in terms of the mid-plane coordinates are, when angular and temperature effects are ignored

$$
\begin{aligned}
&N_z' + q_z = 0 \\
&N_{\theta z}' + \frac{1}{r_c} Q_\theta + q_\theta = 0 \\
&Q_z' - \frac{1}{r_c} N_\theta + q = 0 \\
(3\text{-}40) \qquad &M_z' - Q_z + m_z = 0 \\
&M_{z\theta}' - Q_\theta + m_\theta = 0 \\
&R_z' - \frac{1}{r_c} M_\theta - N_r + m = 0 \\
&S_z' - \frac{1}{r_c} P_\theta - M_r + n = 0
\end{aligned}
$$

The stress resultants are defined by

$$\{N_z, N_r, N_{z\theta}, Q_z\} = \int_{-h/2}^{h/2} (\sigma_{zz}, \sigma_{rr}, \tau_{z\theta}, \tau_{rz})\left(1 + \frac{\xi}{r_c}\right) d\xi$$

$$\{N_\theta, N_{\theta z}, Q_\theta\} = \int_{-h/2}^{h/2} (\sigma_{\theta\theta}, \tau_{\theta z}, \tau_{\theta r})\, d\xi$$

$$\{M_z, M_r, M_{z\theta}, R_z\} = \int_{-h/2}^{h/2} (\sigma_{zz}, \sigma_{rr}, \tau_{z\theta}, \tau_{rz})\left(1 + \frac{\xi}{r_c}\right) \xi\, d\xi$$

$$\{M_\theta, M_{\theta z}, R_\theta\} = \int_{-h/2}^{h/2} (\sigma_{\theta\theta}, \tau_{\theta z}, \tau_{\theta r})\, \xi\, d\xi$$

$$P_\theta = \int_{-h/2}^{h/2} \sigma_{\theta\theta}\, \xi^2 d\xi$$

(3–41)

$$S_z = \int_{-h/2}^{h/2} \tau_{rz} \left(1 + \frac{\xi}{r_c}\right) \xi^2 d\xi$$

$$S_\theta = \int_{-h/2}^{h/2} \tau_{\theta z}\, \xi^2 d\xi$$

$$\{q_z, q_\theta, q\} = \{\tau_{rz}(r_0) g_0 - \tau_{rz}(r_i) g_i,\ \tau_{r\theta}(r_0) g_0 - \tau_{r\theta}(r_i) g_i,\ \sigma_{rr}(r_0) g_0 - \sigma_{rr}(r_i) g_i\}$$

$$\{m_z, m_\theta, m\} = \{\tau_{rz}(r_0) g_0 - \tau_{rz}(r_i) g_i,\ \tau_{r\theta}(r_0) g_0 - \tau_{r\theta}(r_i) g_i,\ \sigma_{rr}(r_0) g_0 - \sigma_{rr}(r_i) g_i\} \frac{h}{2}$$

$$n = \frac{h^2}{8} \{\sigma_{zz}(r_0) g_0 - \sigma_{zz}(r_i) g_i\}$$

for a cylinder of wall thickness h, and q_i and q_o are as defined before.

In our notation

$$\{N_z, N_r, N_{z\theta}, Q_z\} \text{ becomes } r_c\{N_{zz}^{(1)}, N_{rr}^{(1)}, N_{z\theta}^{(1)}, N_{rz}^{(1)}\}$$

$$\{N_\theta, N_{\theta z}, Q_\theta\} \text{ becomes } r_c\{N_{\theta\theta}^{(0)}, N_{z\theta}^{(0)}, N_{r\theta}^{(0)}\}$$

$$\{M_z, M_r, M_{z\theta}, R_z\} \text{ becomes } r_c^2\{N_{zz}^{(2)} - N_{zz}^{(1)}, N_{rr}^{(2)} - N_{rr}^{(1)}, N_{z\theta}^{(2)} - N_{z\theta}^{(1)}, N_{rz}^{(2)} - N_{rz}^{(1)}\}$$

(3–42)

$$\{M_\theta, M_{\theta z}, R_{\theta z}\} \text{ becomes } r_c^2\{N_{\theta\theta}^{(2)} - N_{\theta\theta}^{(1)}, N_{\theta z}^{(2)} - N_{\theta z}^{(1)}, N_{r\theta}^{(2)} - N_{r\theta}^{(1)}\}$$

$$P_\theta \text{ becomes } \tfrac{1}{2} r_c^3\{N_{\theta\theta}^{(2)} - 2N_{\theta\theta}^{(1)} + N_{\theta\theta}^{(0)}\}$$

$$S_z \text{ becomes } \tfrac{1}{2} r_c^3\{N_{rz}^{(3)} - 2N_{rz}^{(2)} + N_{rz}^{(1)}\}$$

$$S_\theta \text{ becomes } \tfrac{1}{2} r_c^3\{N_{r\theta}^{(2)} - 2N_{r\theta}^{(1)} + N_{r\theta}^{(0)}\}$$

If we substitute these into equation (3–40), the first three equations directly become

(3–43)

$$r_c\, N_{rz}'^{(1)} - N_{\theta\theta}^{(0)} = f_{rr}^{(1)}$$

$$r_c\, N_{\theta z}'^{(1)} - N_{r\theta}^{(0)} = f_{r\theta}^{(1)}$$

$$r_c\, N_{zz}'^{(1)} = f_{rz}^{(1)}$$

These are the stress resultant equilibrium equation developed here for n equal to zero.

If we add r_c times equation one, two, and three to four, five, and six

$$
\begin{aligned}
&r_c\, N_{rz}'^{(2)} - N_{rr}^{(1)} - N_{\theta\theta}^{(1)} = f_{rr}^{(2)} \\
(3\text{-}44) \qquad &r_c\, N_{\theta z}'^{(2)} = f_{r\theta}^{(2)} \\
&r_c\, N_{zz}'^{(2)} - N_{rz}^{(1)} = f_{rz}^{(2)}
\end{aligned}
$$

These are the generalized stress resultant equations for n equal to one.

If we subtract $^1/_2 r_c$ times equation three from, and add equation six to equation seven, we get

$$
(3\text{-}45) \qquad r_c\, N_{rz}'^{(3)} - 2\, N_{rr}^{(2)} - N_{\theta\theta}^{(1)} = f_{rr}^{(3)}
$$

This is the first stress resultant equation for n equal to two. The other two equations for n equal to two are not obtained because the comparison solution terminated the expansions for the axial and angular deformation terms with the linear term and carried the radial deformation to the quadratic term.

$$\underline{\underline{A}} = [A]_{nj} \qquad \underline{\underline{B}} = [B]_{nj} \qquad \underline{\underline{C}} = [C]_{nj} \qquad \begin{array}{l} n, j = 0, 1, 2 \cdots \\ m = n + j \end{array}$$

$$[A]_{nj} = \begin{Bmatrix} 0 & 0 & r_c A_{55}^{(m+1)} \\ r_c A_{16}^{(m+1)} & r_c A_{66}^{(m+1)} & 0 \\ r_c A_{11}^{(m+1)} & r_c A_{16}^{(m+1)} & 0 \end{Bmatrix}$$

$$[B]_{nj} \quad \begin{Bmatrix} j A_{55}^{(m)} - n A_{13}^{(m)} - A_{12}^{(m)} & (j-1) A_{45}^{(m)} - n A_{36}^{(m)} - A_{26}^{(m)} & r_c \frac{d}{dz} A_{55}^{(m+1)} \\ r_c \frac{d}{dz} A_{16}^{(m+1)} & r_c \frac{d}{dz} A_{66}^{(m+1)} & A_{26}^{(m)} + j A_{36}^{(m)} + (n-1) A_{45}^{(m)} \\ r_c \frac{d}{dz} A_{11}^{(m+1)} & r_c \frac{d}{dz} A_{16}^{(m+1)} & A_{12}^{(m)} + j A_{13}^{(m)} - n A_{55}^{(m)} \end{Bmatrix}$$

$$[C]_{nj} \quad \begin{Bmatrix} j \frac{d}{dz} A_{13}^{(m)} & (j-1) \frac{d}{dz} A_{55}^{(m)} & -\frac{1}{r_c} \left(A_{22}^{(m-1)} + m A_{23}^{(m-1)} + nj A_{33}^{(m-1)} \right. \\ -\frac{n-1}{r_c} j \, A_{45}^{(m-1)} & -\frac{(n-1)(j-1)}{r_c} A_{44}^{(m-1)} & \frac{d}{dz} \left(A_{26}^{(m)} + j A_{36}^{(m)} \right) \\ -\frac{n}{r_c} j \, A_{55}^{(m-1)} & -\frac{n(j-1)}{r_c} A_{45}^{(m-1)} & \frac{d}{dz} \left(A_{12}^{(m)} + j A_{13}^{(m)} \right) \end{Bmatrix}$$

$$[D]_n \quad \begin{Bmatrix} \sigma_{rr} \, g^{n+1} \Big|_{g_i}^{g_o} \\ \tau_{r\theta} \, g^{n+1} \Big|_{g_i}^{g_o} \\ \tau_{rz} \, g^{n+1} \Big|_{g_i}^{g_o} \end{Bmatrix}$$

Table 3—1 Deformation Coefficients

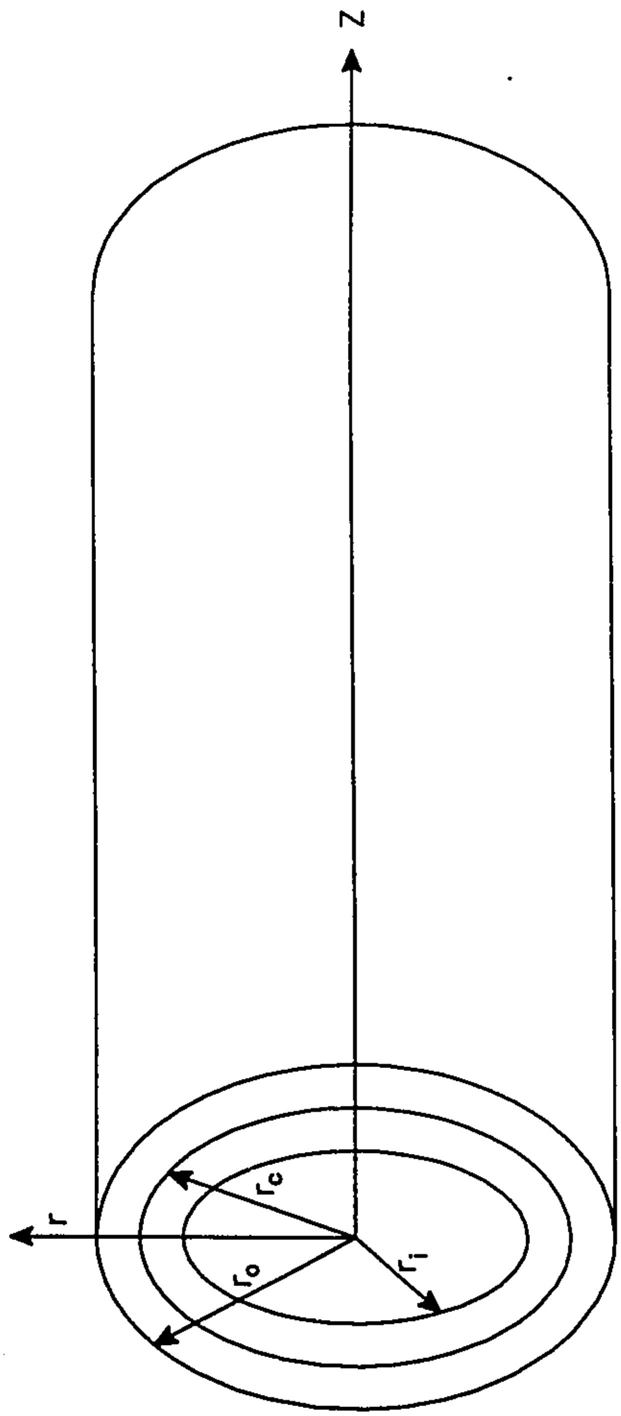

Figure 3–1 Cylinder Geometry

Chapter 4

CYLINDERS WITH CONSTANT MATERIAL PROPERTIES

4.1 Introduction

The second order system of differential equations (3-35) is exceedingly stiff. The stiffness of a differential equation system is the ratio of the largest to smallest real parts of the eigenvalues. A system is stiff when this ratio is large. Sharply rising and decaying terms are present which make the application of numerical approximation techniques very difficult. The problem becomes, for any cylinder of finite length, a very stiff two point boundary value problem.

In an attempt to solve this system, a standard shooting technique [67] was tried. A converging solution was only achieved for two terms in the series representing the deformation. A parallel shooting technique [67] was also tried for the finite length cylinder, stepping in from each end. This did not add more terms to the series or improve the accuracy of the solution.

A power series representation for the deformation along the axis of the cylinder was also tried. Convergence was possible in principle with several hundred terms in the series, at which point, however, accumulated numerical round-off errors became significant.

A successful method was found when the material properties of the cylinder were assumed not to vary along the z axis. This method, a generalized eigenvalue approach, is the topic of this chapter.

4.2 Eigenvalue Solution of the Homogeneous Equation

Consider now, the special case of a cylinder whose material properties do not depend upon the axial coordinate, thus making the coefficients of the differential equation system (3-27) constant. A completely general solution for this system can be obtained by first solving the homogeneous system

$$(4\text{-}1) \qquad \underline{\underline{a}}\, \underline{\alpha}_H' + \underline{\underline{b}}\, \underline{\alpha}_H' + \underline{c}\, \underline{\alpha}_H = 0$$

where $\underline{\alpha}_H$ is the solution of the differential equation set (4-1). Adding the homogeneous solution to any particular solution of equation (3-27) results in the general solution to that system.

The constant coefficients in equation (4-1) suggest an eigenvalue approach, where a solution of the form

$$\underline{\alpha}_H \sim e^{\lambda z} \qquad (\lambda \text{ complex})$$

is assumed.

If this is substituted into (4-1), the resulting eigenvalue equation is

(4–2) $$(\underline{\underline{a}}\,\lambda^2 + \underline{\underline{b}}\,\lambda + \underline{\underline{c}})\,\underline{\alpha}_H = 0$$

If we define a new variable $\underline{\eta}$ by

(4–3) $$\underline{\eta} = (\underline{\alpha}_H{}', \underline{\alpha}_H)^T$$

then equation (4–2) can be rewritten

(4–4) $$\underline{\underline{Q}} \cdot \underline{\eta} = \lambda\, \underline{\underline{R}}\, \underline{\eta}$$

$$\underline{\underline{Q}} = \left[\begin{array}{c|c} -\underline{\underline{b}} & -\underline{\underline{c}} \\ \hline \underline{\underline{I}} & 0 \end{array}\right]$$

$$\underline{\underline{R}} = \left[\begin{array}{c|c} \underline{\underline{a}} & 0 \\ \hline 0 & \underline{\underline{I}} \end{array}\right]$$

Equation (4–4) is a generalized eigenvalue equation, with a non–trivial solution existing only if

(4–5) $$\det(\underline{\underline{Q}} - \lambda\, \underline{\underline{R}}) = 0$$

The matrices $\underline{\underline{a}}$ and $\underline{\underline{b}}$ are very ill–conditioned, and $\underline{\underline{c}}$ is singular. This suggests that any solution technique which involves the inversion of $\underline{\underline{Q}}$ would be limited to at most a few terms in the power series expansion. Although several techniques are available for solving the determinant equation, the LZ algorithm is one which generates a full set of eigenvalues and eigenvectors for this particular problem and does not require the inversion of $\underline{\underline{Q}}$ [68, 69]. In fact, either $\underline{\underline{Q}}$ or $\underline{\underline{R}}$ may be singular.

The details of the LZ algorithm are readily available in the literature [68, 69]. This algorithm is based upon three observations:

(1) The eigenvalue equations

$$\underline{\underline{Q}} \cdot \underline{\eta} = \lambda \underline{\underline{R}}\,\underline{\eta} \tag{4-6}$$

$$\underline{\underline{L}}\,\underline{\underline{Q}}\,\underline{\underline{M}}\,\underline{y} = \lambda \underline{\underline{L}}\,\underline{\underline{R}}\,\underline{\underline{M}}\,\underline{y}$$

have the same eigenvalues if $\underline{\underline{L}}$ and $\underline{\underline{M}}$ are non-singular matrices, and their eigenvalues are related by

$$\underline{\eta} = \underline{\underline{M}}\,\underline{y}$$

(2) There exists matrices $\underline{\underline{L}}$ and $\underline{\underline{M}}$ such that $\underline{\underline{LQM}}$ and $\underline{\underline{LRM}}$ are in upper triangular form and these matrices can be found by simple operations.

(3) If α_i are the diagonal elements of $\underline{\underline{LQM}}$ and βi are the diagonal elements of LRM then the eigenvalues are given by $\alpha i/\beta i$ assuming $\beta i \neq 0$.

The aim of the LZ algorithm is to find matrices $\underline{\underline{L}}$ and $\underline{\underline{M}}$ such that $\underline{\underline{LQM}}$ and $\underline{\underline{LRM}}$ are in upper triangular form.

The algorithm has been coded in Fortran 77 code with the source being publicly available [69].

To illustrate the use of the method, two families of cylinders are considered. In the first family, several isotropic cylinders with differing wall thicknesses are analyzed. This allows the eigenvalues generated to be compared with standard thin wall solutions [66], and solutions generated by a higher order technique for thicker cylinders [50].

The second family consists of generally orthotropic cylinders with differing wall thicknesses. These are compared to some results available in the literature [34] for thin wall cylinders.

The impact of the three series truncation methods, as discussed earlier, will be shown.

4.3 Method of Solution

The generation of the determinant equation (4–5) is straightforward. The requirement, of course, is the determination of matrices $\underline{\underline{a}}$, $\underline{\underline{b}}$, and $\underline{\underline{c}}$. This has been numerically implemented assuming that the cylinder is multi–layered, and that each individual layer is orthotropic. The details of the process are included here for completeness.

Since each layer of the cylinder is orthotropic, the following material properties must be specified for each layer

E_{11}	E_{12}	ν_{12}
E_{22}	E_{13}	ν_{13}
E_{33}	E_{23}	ν_{23}

The inside and outside radii of the layer, in addition to the orientation of the layer with respect to the z axis must be given also.

The stiffnesses of each layer, in the material frame of reference are calculated using well established relationships [2].

$$C_{11} = \frac{1 - \nu_{23}\nu_{32}}{E_2 E_3 \Delta} \qquad C_{12} = \frac{\nu_{12} + \nu_{13}\nu_{32}}{E_1 E_3 \Delta} \qquad C_{44} = E_{23}$$

$$C_{22} = \frac{1 - \nu_{13}\nu_{31}}{E_1 E_3 \Delta} \qquad C_{13} = \frac{\nu_{13} + \nu_{12}\nu_{23}}{E_1 E_2 \Delta} \qquad C_{55} = E_{31} \tag{4-7}$$

$$C_{33} = \frac{1 - \nu_{12}\nu_{21}}{E_1 E_2 \Delta} \qquad C_{23} = \frac{\nu_{23} + \nu_{21}\nu_{13}}{E_1 E_2 \Delta} \qquad C_{66} = E_{12}$$

$$\Delta = \frac{1 - \nu_{12}\nu_{21} - \nu_{23}\nu_{32} - \nu_{13}\nu_{31} - 2\nu_{21}\nu_{32}\nu_{13}}{E_1 E_2 E_3}$$

These are then rotated to the geometrical frame of reference. This is done through the procedure which follows.

If the loads are small enough that the material can be treated as linearly elastic, the stresses and the strains in each layer are related by the generalized form of Hooke's law which is

(4–8) $$\underline{\sigma}_1 = \underline{\underline{C}}\ \underline{\varepsilon}_1$$

where the material properties $\underline{\underline{C}}$ are given by [2]

(4–9) $$\underline{\underline{C}}(z,r) = \begin{Bmatrix} C_{11} & C_{12} & C_{13} & 0 & 0 & 0 \\ C_{12} & C_{22} & C_{23} & 0 & 0 & 0 \\ C_{13} & C_{23} & C_{33} & 0 & 0 & 0 \\ 0 & 0 & 0 & C_{44} & 0 & 0 \\ 0 & 0 & 0 & 0 & C_{55} & 0 \\ 0 & 0 & 0 & 0 & & C_{66} \end{Bmatrix}$$

and $\underline{\sigma}_1$ and $\underline{\varepsilon}_1$ are the principal stresses and strains in the material.

The stresses and strains in the material frame can be related to the geometric frame by introducing the transformation $\underline{\underline{T}}$ such that [2]

(4–10) $$\underline{\sigma}_x = \underline{\underline{T}}^{-1}\ \underline{\sigma}_1$$

where

$$\underline{\underline{T}} = \begin{Bmatrix} m^2 & n^2 & 0 & 0 & 0 & 2mn \\ n^2 & m^2 & 0 & 0 & 0 & -2mn \\ 0 & 0 & 1 & 0 & 0 & 0 \\ 0 & 0 & 0 & m & -n & 0 \\ 0 & 0 & 0 & m & n & 0 \\ -mn & mn & 0 & 0 & 0 & m^2-n^2 \end{Bmatrix}$$

where

$m = \cos(\omega)$

$n = \sin(\omega)$

ω is the orientation of the principal direction with respect to the geometric frame.

A similar relationship can be given for the strains. The strains transform the same as the stresses if a tensor representation is used. If we extend the two dimensional analysis available in the literature [2] to three dimensions, we have

(4–11) $$\underline{\varepsilon}_{px} = \underline{\underline{T}}^{-1}\,\underline{\varepsilon}_{p1}$$

where

$$\underline{\varepsilon}_{px} = \left(\varepsilon_{zz},\ \varepsilon_{\theta\theta},\ \varepsilon_{rr},\ \frac{\gamma_{r\theta}}{2},\ \frac{\gamma_{rz}}{2},\ \frac{\gamma_{\theta z}}{2} \right)^T$$

and

$$\underline{\varepsilon}_{p1} = \left(\varepsilon_{11},\ \varepsilon_{22},\ \varepsilon_{33},\ \frac{\gamma_{23}}{2},\ \frac{\gamma_{31}}{2},\ \frac{\gamma_{12}}{2} \right)^T$$

If we use a three dimensional Reuter matrix $\underline{\underline{R}}$ where

(4–12) $$\underline{\underline{R}} = \begin{bmatrix} 1 & 0 & 0 & 0 & 0 & 0 \\ 0 & 1 & 0 & 0 & 0 & 0 \\ 0 & 0 & 1 & 0 & 0 & 0 \\ 0 & 0 & 0 & 2 & 0 & 0 \\ 0 & 0 & 0 & 0 & 2 & 0 \\ 0 & 0 & 0 & 0 & 0 & 2 \end{bmatrix}$$

then
$$\underline{\varepsilon}_x = \underline{\underline{R}}\,\underline{\varepsilon}_{px}$$
$$\underline{\varepsilon}_1 = \underline{\underline{R}}\,\underline{\varepsilon}_{p1}$$

We can then write

$$\underline{\underline{R}}^{-1}\,\underline{\varepsilon} = \underline{\underline{T}}^{-1}\,\underline{\underline{R}}^{-1}\,\underline{\varepsilon}_1$$

or

$$\underline{\varepsilon}_1 = \underline{\underline{R}}\,\underline{\underline{T}}^{-1}\,\underline{\underline{R}}^{-1}\,\underline{\varepsilon}$$

Substituting this and the stress rotation equation into the generalized form of Hooke's law gives

(4–13) $$\underline{\sigma} = \underline{\underline{T}}^{-1}\,\underline{\underline{C}}\,\underline{\underline{R}}\,\underline{\underline{T}}\,\underline{\underline{R}}^{-1}\,\underline{\varepsilon}$$

Noting that

$$\underline{\underline{T}} = \underline{\underline{T}}(\omega)$$

and that

$$\underline{\underline{R}}^{-1} = \begin{bmatrix} 1 & 0 & 0 & 0 & 0 & 0 \\ 0 & 1 & 0 & 0 & 0 & 0 \\ 0 & 0 & 1 & 0 & 0 & 0 \\ 0 & 0 & 0 & 1/2 & 0 & 0 \\ 0 & 0 & 0 & 0 & 1/2 & 0 \\ 0 & 0 & 0 & 0 & 0 & 1/2 \end{bmatrix}$$

we can write

$$\underline{\sigma} = \underline{\underline{Q}}\,\underline{\varepsilon}$$

which is equation (3–14).

This matrix operation can be expanded to give

$$
\begin{aligned}
Q_{11} &= m^4 C_{11} + 2m^2n^2(C_{12} + 2C_{66}) + n^4 C_{22} \\
Q_{12} &= (C_{11} + C_{22} - 4C_{66})m^2n^2 + (m^4 + n^4)C_{12} \\
Q_{13} &= m^2 C_{13} + n^2 C_{23} \\
Q_{16} &= mn\left(m^2C_{11} - n^2C_{22} - \{m^2 - n^2\}\{C_{12} + 2C_{66}\}\right) \\
Q_{22} &= n^4 C_{11} + 2m^2n^2(C_{12} + 2C_{66}) + m^4 C_{22} \\
Q_{23} &= n^2 C_{13} + m^2 C_{23} \\
Q_{26} &= mn\left(n^2C_{11} - m^2C_{22} + \{m^2 - n^2\}\{C_{12} + 2C_{66}\}\right) \\
Q_{33} &= C_{33} \\
Q_{36} &= mn(C_{13} - C_{23}) \\
Q_{44} &= m^2 C_{44} + n^2 C_{55} \\
Q_{45} &= mn(C_{55} - C_{44}) \\
Q_{55} &= m^2 C_{55} + n^2 C_{44} \\
Q_{66} &= m^2n^2(C_{11} + C_{22} - 2C_{12}) + (m^2 - n^2)^2 C_{66}
\end{aligned}
\tag{4-14}
$$

The rest of the Q_{ij} $i, j = 1, \ldots, 6$ are zero as in equation (3–15).

The generalized stiffnesses are now calculated using equation (3–18). We have assumed that the material properties are constant for each individual layer of material. Equation (3–18) then becomes, for each layer ℓ of material in the cylinder wall,

$$
\underline{\underline{A}}_{\ell}^{(n)} = \underline{\underline{Q}}_{\ell} \int_{q_{\ell i}}^{q_{\ell o}} q^n \, dq \tag{4-15}
$$

where $q_{\ell i}$ is q at the inside radial position of the layer

$q_{\ell o}$ is q at the outside radial position of the layer.

This is easily integrated to give

$$
(4\text{–}16) \qquad
\begin{aligned}
\underline{\underline{A}}_{\ell}^{(n)} &= \underline{\underline{Q}}_{\ell} \, \frac{\varrho_{\ell o}^{\,n+1} - \varrho_{\ell i}^{\,n+1}}{n+1} \; ; \qquad n \geq 0 \\
\underline{\underline{A}}_{\ell}^{(-1)} &= \underline{\underline{Q}}_{\ell} \, \ln\left(\frac{\varrho_{\ell o}}{\varrho_{\ell i}}\right) .
\end{aligned}
$$

We note from Table 3–1 that $\underline{\underline{A}}_{\ell}^{(-1)}$ is required when n and j are zero.

Summing these through the cylinder wall completes the integration. That is,

$$
(4\text{–}17) \qquad
\begin{aligned}
\underline{\underline{A}}_{\ell}^{(n)} &= \sum_{\ell=1}^{NLAYER} \underline{\underline{Q}}_{\ell} \, \frac{\varrho_{\ell o}^{\,n+1} - \varrho_{\ell i}^{\,n+1}}{n+1} \; ; \quad n \geq 0 \\
\underline{\underline{A}}_{\ell}^{(-1)} &= \sum_{\ell=1}^{NLAYER} \underline{\underline{Q}}_{\ell} \, \ln\left(\frac{\varrho_{\ell o}}{\varrho_{\ell i}}\right)
\end{aligned}
$$

where NLAYER is the total number of layers in the laminate.

Having calculated the generalized stiffnesses, the coefficient matrices $\underline{\underline{A}}$, $\underline{\underline{B}}$, and $\underline{\underline{C}}$ of Table 3–1 must be calculated. For a cylinder whose material properties do not vary axially, these reduce to

$$
[A]_{nj} = \left\{ \begin{array}{ccc}
0 & 0 & r_c A_{55}^{(m+1)} \\
r_c A_{16}^{(m+1)} & r_c A_{66}^{(m+1)} & 0 \\
r_c A_{11}^{(m+1)} & r_c A_{16}^{(m+1)} & 0
\end{array} \right\}
$$

$$
(4\text{–}18) \qquad
[B]_{nj} = \left\{ \begin{array}{ccc}
j A_{55}^{(m)} - n A_{15}^{(m)} - A_{12}^{(m)} & (j-1) A_{45}^{(n)} - n A_{36}^{(m)} - A_{26}^{(m)} & 0 \\
0 & 0 & A_{26}^{(m)} + j A_{36}^{(m)} - (n-1) A_{45}^{(m)} \\
0 & 0 & A_{12}^{(m)} + j A_{13}^{(m)} - n A_{55}^{(m)}
\end{array} \right\}
$$

$$
[C]_{nj} = \left\{ \begin{array}{ccc}
0 & 0 & -\frac{1}{r_c} (A_{22}^{(m-1)} + n A_{23}^{(m-1)} + nj A_{33}^{(m-1)} \\
-\frac{(n-1)}{r_c} j A_{45}^{(m-1)} & -\frac{(n+1)(j-1)}{r_c} A_{55}^{(m-1)} & 0 \\
-\frac{nj}{r_c} A_{55}^{(m-1)} & -\frac{n(j-1)}{r_c} A_{45}^{(m-1)} & 0
\end{array} \right\}
$$

The midplane shift as given in equation (3–25) is applied to the matrices $\underline{\underline{A}}$, $\underline{\underline{B}}$, and $\underline{\underline{C}}$ to give the coefficient $\underline{\underline{a}}$, $\underline{\underline{b}}$, and $\underline{\underline{c}}$.

At this point, the matrices $\underline{\underline{Q}}$ and $\underline{\underline{R}}$ of equation (4–4) are formed. An application of the LZ algorithm completes the solution by supplying the eigenvalues and eigenvectors for the problem.

Three series truncation schemes as discussed earlier are used. In the first, the radial deformation is allowed to contain one more term than either the axial or circumferential deformations. One extra radial equilibrium equation is included to match the number of equations to the number of unknowns.

For the second method, the axial and circumferential expansions are taken to one more term than the radial expansion. The axial and circumferential equilibrium equations are likewise carried to one more term.

For the third method, all deformation components are truncated with the same number of terms. No equilibrium equations are dropped.

4.4 Isotropic Cylinders

Thin and thick walled isotropic cylinders under internal pressure were analyzed using the preceding method (see Tables 4–1, 4–2, and 4–3). The thin wall comparison is due to Timoshenko [66]. In his analysis, the radial deformation for an isotropic cylinder subject to a radial pressure only, is given by

(4–19) $$\frac{d^4 u_r}{dz^4} + 4\beta^4 = \frac{P}{D}$$

where

$$\beta^4 = \frac{3(1-\nu^2)}{r_c^2 h^2}$$

$$D = \frac{E h^3}{12(1-\nu^2)}$$

$$h = r_o - r_i$$

The eigenvalues are simply $+\beta$ and $+\bar{\beta}$ where the bar over a variable indicates its complex conjugate value.

The thicker wall comparison is available from Vinson [50], at least for the dominant term.

Several things are evident from this analysis:

(1) The eigenvalues match the thin wall solution (Tables 4–1 and 4–2) to within 0.3% with four terms in the series required for the third truncation method. The first and second methods require more than four terms to achieve the same accuracy.

(2) The eigenvalues match the thick wall solution (Table 4–3) to within 0.4% with four terms in the series for the third truncation method. Similar accuracy is achieved with the other two methods with six terms in the series.

(3) For the thick cylinder, there is little difference between the first two methods of truncation, and this difference vanishes with an increasing number of terms in the series. All three methods converge to the same value if enough terms in the series are used.

(4) The LZ algorithm produces an infinite eigenvalue for the first two truncation methods. This is a result of a diagonal zero in the triangular matrix divisor. The third method did not suffer from this numerical defect.

On the basis of the above observations, the third truncation technique (i.e.. equal number of terms in all the series) was adopted for all calculations other than the infinite length cylinder.

4.5 Orthotropic Cylinders

The results of an analysis of a family of specially orthotropic cylinders is presented in Tables 4–4 and 4–5. The only easily comparable results are those for a thin walled cylinder given by Dong, Pister, and Taylor [34], and simplified by Pagano and Whitney [70]. The solution for a symmetric laminate produces eigenvalues

(4–20) $$\pm\alpha \pm i\beta$$

where $$\begin{pmatrix}\beta \\ \alpha\end{pmatrix} = \left(\frac{b \pm d}{4D_{11}}\right)^{1/2}$$

$$b = \frac{2}{r_c}\left\{D_{11}(\lambda_3 - \lambda_1\lambda_2)\right\}^{1/2} \qquad d = -\frac{D_{16}\lambda_1}{r_c^2}$$

$$\lambda_1 = \frac{S_1}{S_2} \qquad \lambda_2 = \frac{S_1}{A_{11}} \qquad \lambda_3 = \frac{A_{11}A_{22} - A_{12}^2}{A_{11}}$$

$$S_1 = A_{11}A_{26} - A_{12}A_{16} \qquad S_2 = A_{11}A_{66} - A_{16}^2$$

$$(A_{ij}, D_{ij}) = \int_{-h/2}^{h/2} Q_{ij}(1, \zeta^2)\, d\zeta$$

If the principle material axes coincide with the geometric axes, the eigenvalues are easily shown to reduce to

$$\beta^4 = \alpha^4 = \frac{3}{r_c^2 h^2}\left\{\frac{Q_{22}}{Q_{11}} - \left(\frac{Q_{12}}{Q_{11}}\right)^2\right\}$$

A comparison is only presented for a very thin and a thin generally orthotropic cylinder. For these cylinders, a single orthotropic layer was inclined at an angle to the axial direction. The results, presented in Tables 4-6 and 4-7 compare to within 7% of the thin walled analysis discussed earlier. Further comparison or discussion will not be given since the authors of the previous analysis [70] have indicated that their solution is at best an approximate one because of the extreme truncation used for the series representation (deformations were either constant, or varied linearly through the cylinder wall).

4.6 Eigenvalue Groups

By observation, the computed eigenvalues presented previously, occur in three distinct groups.

(1) Pairs of real eigenvalues + λi , − λi occur. The eigenvectors associated with these eigenvalues are real. These eigenvalues add the following to the solution

$$(4\text{–}21) \qquad \underline{\alpha}_H^{(1)} = \sum \left(C_{i1}^{(1)} \underline{X}_{i1} e^{\lambda_i z} + C_{i2} \underline{X}_{i2}^{(1)} e^{-\lambda_i z} \right)$$

where $C_{i1}^{(1)}$ and $C_{i2}^{(1)}$ are constants to be determined and $\underline{X}_{i1}^{(1)}$ and $\underline{X}_{i2}^{(1)}$ are the eigenvectors associated with the eigenvalues.

It is seen that this is a monotonic rising or decaying function with no oscillations in the axial direction. This type of solution has been seen by some authors [38].

(2) Zero eigenvalues appear, with a multiplicity of two. The solution associated with these is a polynomial [71] given by

(4–22) $$\underset{-}{\alpha}_{\mu}^{(2)} = C_1^{(2)} \underline{X}_1^{(2)} + C_2^{(2)} \underline{X}_2^{(2)} z$$

where $C_1^{(2)}$, $C_2^{(2)}$

are coefficients to be determined, and

$$X_1^{(2)}, \quad X_2^{(2)}$$

are the eigenvectors.

This solution can be viewed as that of an infinite cylinder without axial or torque loading. We shall discuss the infinite cylinder in an alternate fashion in a later section.

(3) A third group of eigenvalues appear in the form of complex conjugate pairs K_i and $\overline{K}_i$. The solution associated with these is given by

(4–23) $$\underset{-}{\alpha}_{\mu}^{(3)} = \sum \left(C_{i1}^{(3)} \underline{X}_{i1}^{(3)} e^{K_i z} + C_{i2}^{(3)} \cdot X_{i2}^{(3)} e^{\overline{K}_i z} \right)$$

These correspond to the rising and decaying oscillatory terms more commonly associated with shell theories [66]. Although one could further subgroup these into boundary layer, far field, and several other length related ranges as done by others [43, 56] such an exercise would provide no additional information.

4.7 Homogeneous Solution

We can now write the homogeneous solution as the sum of the parts just described.

(4–24)
$$\underline{\alpha}_H = \sum\left(C_{i1}^{(1)}\,\underline{X}_{i1}^{(1)}\,e^{\lambda_i z} + C_{i2}^{(1)}\,\underline{X}_{i2}\,e^{-\lambda_i z}\right) + C_1^{(2)}\,\underline{X}_1^{(2)} + C_2^{(2)}\,\underline{X}_2^{(2)}\,z + \sum\left(C_{i1}^{(3)}\,\underline{X}_{i1}^{(3)}\,e^{\kappa_i z} + C_{i2}^{(3)}\,\underline{X}_{i2}^{(3)}\,e^{\bar{\kappa}_i z}\right)$$

4.8 Particular Solution

The entire solution for $\underline{\alpha}$ of equation (3–27) is obtained when one adds any particular solution of (3–27) to the homogeneous solution given by equation (4–23). A particular solution which satisfies equation (3–27) is

(4–25)
$$\underline{\alpha}_p' = \text{constant}$$

which must satisfy

(4–26)
$$\underline{\underline{b}}\,\underline{\alpha}_p' + \underline{\underline{c}}\,\underline{\alpha}_p + \underline{D} = 0$$

One particular form of $\underline{\alpha}_p$ which satisfies this is

(4–27)
$$\underline{\alpha}_p = \left(\varepsilon_{zz}^{(0)} z,\ \gamma_{\theta z}^{(1)} r_c z,\ \beta_r^{(0)},\ 0,\ -\gamma_{\theta z}^{(1)} r_c z,\ \beta_r^{(1)},\ 0,\ 0,\ \beta_r^{(2)},\ \ldots\right)^T$$

From this,

$$(4\text{–}28) \qquad \underline{\alpha}_p{}' = \left(\varepsilon_{zz}^{(0)},\ \gamma_{\theta z}^{(1)} r_c,\ 0,\ 0,\ -\gamma_{\theta z}^{(1)} r_c,\ 0,\ 0,\ \cdots \right)^T$$

As will be detailed later, this corresponds to a cylinder experiencing a constant axial strain $\varepsilon_{zz}^{(0)}$ and a uniform shearing strain causing a twisting of the cylinder about its axis. In addition, the cylinder is experiencing a radial deformation constant along its length. This is simply the solution for a cylinder of infinite length subject to axisymmetric loading. The solution, a subject of the next chapter, results when $\underline{\alpha}_p$ and $\underline{\alpha}_p{}'$ as given above are substituted into the governing equation (4–26).

4.9 Total Solution

We can now write the total solution for equation (3–27) for a cylinder whose material properties are constant along its length. It is simply

$$(4\text{–}29) \qquad \underline{\alpha} = \underline{\alpha}_H + \underline{\alpha}_P$$

where $\underline{\alpha}_H$ is the given by equation (4–27)

and $\underline{\alpha}_p$ is given by equation (4–28)

The unknown coefficients in $\underline{\alpha}$ are determined by the application of the boundary conditions.

Truncation Method	Number of Terms in Power Series					Solution comparison	
	2	3	4	6	8	Timoshenko [66]	
	Dominant Eigenvalue						
1	–	–	(±13.07, ±12.95)	(±12.89, ±12.84)	(±12.89, ±12.85)		
2	–	–	(±14.22, ±14.30)	(±12.39, ±12.92)	(±13.41, ±12.56)	(±12.85, ±12.85)	–
3	(±12.23, ±12.20)	(±12.87, ±12.84)	(±12.89, ±12.84)	(±12.89, ±12.85)	(±12.79, ±12.92)		
	% Deviation From Comparison Solution [66]						
1	–	–	(1.71, .778)	(.311, 7.78×10^{-2})	(.311, 0)		
2	–	–	(10.6, 11.3)	(3.56, .545)	(4.36, 2.26)	(0, 0)	–
3	(4.82, 5.06)	(.156, 7.78×10^{-2})	(.311, 7.78×10^{-2})	(.311, 0)	(.466, .545)		

$E = 1.0 \times 10^7$
$G = 3.8462 \times 10^6$
$\nu = 0.3$

$h/r_c = 0.01$
$r_c = 1.0$

Table 4–1 Eigenvalues for a Very Thin Isotropic Cylinder

Truncation Method	Number of Terms in Power Series: 2	3	4	6	8	Solution comparison: Timoshenko [66]	Vinson [51]
	Dominant Eigenvalue						
1	–	–	(±4.308, ±4.166)	(±4.136, ±4.000)	(±4.135, ±3.999)	(±4.065, ±4.065)	(±4.14, ±4.01)
2	–	–	(±4.853, ±4.640)	(±4.134, ±3.999)	(±4.133, ±4.000)		
3	(±3.916, ±3.818)	(±4.123, ±4.011)	(±4.134, ±4.000)	(±4.134, ±4.000)	(±4.135, ±4.000)		
	% Deviation From Comparison Solution [51]						
1	–	–	(4.069, 3.89)	(9.66×10^{-2}, .249)	(.121, .274)	(1.81, 1.38)	(0, 0)
2	–	–	(17.2, 15.7)	(.145, .274)	(.169, .249)		
3	(5.41, 4.79)	(.410, 2.49×10^{-2})	(.145, .249)	(.145, .249)	(.121, .249)		

$E = 1.0 \times 10^7$
$G = 3.8462 \times 10^6$
$\nu = 0.3$

$h/r_c = 0.1$
$r_c = 1.0$

Table 4–2 Eigenvalues for a Thin Isotropic Cylinder

Truncation Method	Number of Terms in Power Series					Solution comparison	
	2	3	4	6	8	Timoshenko [66]	Vinson [51]
	Dominant Eigenvalue						
1	–	(±1.276, ±1.798)	(±3.162, ±2.891)	(±1.996, ±1.686)	(±1.996, ±1.686)		
2	–	(±1.276, ±1.798)	(±3.160, ±2.918)	(±1.996, ±1.686)	(±1.996, ±1.686)	(±1.818, ±1.818)	(±1.99, ±1.68)
3	(±1.876, ±1.643)	(±1.969, ±1.713)	(±1.996, ±1.686)	(±1.996, ±1.686)	(±1.996, ±1.686)		
	% Deviation From Comparison Solution [51]						
1	–	(35.9, 7.02)	(58.9, 72.1)	(.301, .357)	(.301, .357)		
2	–	(35.9, 7.02)	(58.7, 73.7)	(.301, .357)	(.301, .357)	(8.64, 8.21)	(0, 0)
3	(5.72, 2.20)	(1.06, 1.96)	(.301, .357)	(.301, .357)	(.301, .351)		

$E = 1.0 \times 10^7$
$G = 3.8462 \times 10^6$
$\nu = 0.3$

$h/r_c = 0.5$
$r_c = 1.0$

Table 4–3 Eigenvalues for a Thick Isotropic Cylinder

Truncation Method	Number of Terms in Power Series					Comparison Solution [70]
	2	3	4	6	8	
	Dominant Eigenvalue					
1	–	–	(±7.050, ±6.939)	(±7.054, ±6.901)	(±7.059, ±6.902)	(±7.050 ±7.050)
2	–	–	(±7.044, ±6.877)	(±7.030, ±6.840)	(±7.056, ±6.840)	
3	(±7.011, ±6.881)	(±7.025, ±6.895)	(±6.968, ±6.834)	(±7.063, ±6.904)	(±7.063, ±6.904)	
	% Deviation From Comparison Solution [70]					
1	–	–	(0, 1.57)	(5.67×10^{-2}, 2.11)	(.128, 2.10)	(0, 0)
2	–	–	(8.51×10^{-2}, 2.45)	(.283, 2.98)	(8.51×10^{-2}, 2.98)	
3	(.553, 2.40)	(.355, 2.20)	(1.16, 3.06)	(.184, 2.07)	(.184, 2.07)	

$E_{11} = 3.5 \times 10^7$ $\quad G_{12} = 0.75 \times 10^6$ $\quad \nu_{12} = 0.24$

$E_{22} = 2.75 \times 10^6$ $\quad G_{13} = 0.75 \times 10^6$ $\quad \nu_{13} = 0.24$

$E_{33} = 2.75 \times 10^6$ $\quad G_{23} = 0.75 \times 10^6$ $\quad \nu_{23} = 0.25$

$\theta = 0$

$h/r_c = 0.01$ $\quad r_c = 1.0$

Table 4–4 Eigenvalues for a Very Thin Specially Orthotropic Cylinder

Truncation Method	Number of Terms in Power Series					Comparison Solution [70]
	2	3	4	6	8	
	Dominant Eigenvalue					
1	–	(±1.500, ±2.022)	(±1.671, ±1.656)	(±2.438, ±1.941)	(±2.442, ±1.946)	(±2.233 ±2.233)
2	–	(±1.501, ±2.022)	(±2.069, 0)	(±2.439, ±1.948)	(±2.438, ±1.940)	
3	(±2.345, ±1.982)	(±2.349, ±1.986)	(±2.438, ±1.941)	(±2.437, ±1.941)	(±2.438, ±1.941)	
	% Deviation From Comparison Solution [70]					
1	–	(32.8, 9.45)	(25.2, 25.8)	(9.18, 13.1)	(9.36, 12.9)	(0, 0)
2	–	(32.8, 9.45)	(7.34, 100)	(9.22, 12.8)	(9.18, 13.1)	
3	(7.25, 11.2)	(7.43, 11.06)	(9.18), 13.1)	(9.14, 13.1)	(9.18, 13.1)	

$E_{11} = 3.5 \times 10^7$ $\quad G_{12} = 0.75 \times 10^6$ $\quad \nu_{12} = 0.24$

$E_{22} = 2.75 \times 10^6$ $\quad G_{13} = 0.75 \times 10^6$ $\quad \nu_{13} = 0.24$

$E_{33} = 2.75 \times 10^6$ $\quad G_{23} = 0.75 \times 10^6$ $\quad \nu_{23} = 0.25$

$\theta = 0$

$h/r_c = 0.1$ $\quad r_c = 1.0$

Table 4–5 Eigenvalues for a Thin Specially Orthotropic Cylinder

Truncation Method	Number of Terms in Power Series					Comparison Solution [34]
	2	3	4	6	8	
	Dominant Eigenvalue					
1	–	(±8.286, ±14.11)	(±11.86, ±11.76)	(±11.48, ±11.43)	(±11.53, ±11.47)	(±12.57 ±10.84)
2	–	–	(±12.77, ±12.19)	(±12.10, ±11.69)	(±11.66, ±11.59)	
3	(±11.70, ±11.67)	(±11.83, ±11.79)	(±12.42, ±12.09)	(±11.47, ±11.50)	(±11.65, ±11.57)	
	% Deviation From Comparison Solution [34]					
1	–	(34.1, 30.2)	(5.56, 8.49)	(8.67, 5.44)	(8.27, 5.81)	(0, 0)
2	–	–	(1.59, 12.5)	(3.74, 7.84)	(7.24, 6.91)	
3	(6.92, 7.66)	(5.89, 8.76)	(1.19, 11.53)	(8.75, 6.09)	(7.32, 6.73)	

$E_{11} = 3.5 \times 10^7$ $\quad G_{12} = 0.75 \times 10^6$ $\quad \nu_{12} = 0.24$

$E_{22} = 2.75 \times 10^6$ $\quad G_{13} = 0.75 \times 10^6$ $\quad \nu_{13} = 0.24$

$E_{33} = 2.75 \times 10^6$ $\quad G_{23} = 0.75 \times 10^5$ $\quad \nu_{23} = 0.25$

$\theta = 45^{\circ}$

$h/r_c = 0.01$ $\quad r_c = 1.0$

Table 4–6 Eigenvalues for a Very Thin Generally Orthotropic Cylinder

Truncation Method	Number of Terms in Power Series					Comparison Solution [34]
	2	3	4	6	8	
	Dominant Eigenvalue					
1	–	(±3.335, ±3.998)	(±5.018, ±4.826)	(±3.853, ±3.645)	(±3.866, ±3.638)	
2	–	(±3.336, ±4.013)	(±4.675, ±4.566)	(±3.854, ±3.627)	(±3.866, ±3.648)	(±3.975 ±3.428)
3	(±3.766, ±3.651)	(±3.807, ±3.687)	(±3.853, ±3.646)	(±3.858, ±3.641)	(±3.857, ±3.650)	
	% Deviation From Comparison Solution [34]					
1	–	(16.1, 16.6)	(26.2, 40.8)	(3.07, 6.33)	(2.74, 6.13)	
2	–	(16.1, 17.1)	(17.6, 33.2)	(3.04, 5.81)	(2.74, 6.42)	(0, 0)
3	(5.26, 6.51)	(4.23, 7.56)	(3.07, 5.36)	(2.94, 6.21)	(2.97, 6.48)	

$E_{11} = 3.5 \times 10^7$ $\quad G_{12} = 0.75 \times 10^6$ $\quad \nu_{12} = 0.24$

$E_{22} = 2.75 \times 10^6$ $\quad G_{13} = 0.75 \times 10^6$ $\quad \nu_{13} = 0.24$

$E_{33} = 2.75 \times 10^6$ $\quad G_{23} = 0.75 \times 10^6$ $\quad \nu_{23} = 0.25$

$\theta = 45^{\circ}$

$h/r_c = 0.1$ $\quad r_c = 1.0$

Table 4–7 Eigenvalues for a Thin Generally Orthotropic Cylinder

Chapter 5

SOLUTION EXAMPLES USING THE POWER SERIES APPROACH

5.1 Introduction

Three problem types will be analyzed using the power series expansion technique. These are the:

(1) Infinitely long cylinder; a cylinder that is so long that any end restraint effects can be ignored.

(2) Semi–infinite cylinder with one end hinged, where details of the influence of one end restraint are considered.

(3) Semi–infinite cylinder with one end restrained from bending.

The cylinder is assumed to be made of layers of homogeneous orthotropic material. The assumed material properties are listed in Table 5-1. Only an E/XA-S/epoxy composite was considered in the analysis since a complete material data base existed at the University of Ottawa composite material laboratory.

5.2 Transverse Compressive Testing of Composite Laminates

Overview

As mentioned in Chapter 1, the transverse compressive properties of a thick composite shell are considered to be critical for the design of composite pressure vessels at ultra-high pressures. An experimental program was undertaken by the author under a supported research contract [74] to define these material properties.

Specimen Fabrication

The specimens were manufactured by wet filament winding on machinery developed by the author (to be detailed in Chapter 6). The fibers and the matrix system (Shell Epon 825 plus Ancamine 1482 at 19 parts per hundred (by weight), cured for one hour at 100° C) were identical to those used for the entire data base of Table 5-1.

The steel mandrel, shown in Figure 5–1, was designed to produce four angle–plied wet wound laminates at one time.

A schematic of the four sides of the mandrel (unfolded) is shown in Figure 5–2. Because of severe angle changes from one face of the mandrel to the next, it was necessary to incorporate pointed split pins along each corner of the mandrel to prevent axial sliding of the fiber bundles. After five layers of material were wound, ground compression plates were applied to all four faces. C–clamps were used to force the plates together to rest on appropriate spacers. The spacer thicknesses were calculated using tow/roving cross–sectional areas to produce a 65% volume fraction composite for the 6 mm pin spacing on the mandrel.

The composite plates were machined on a water–cooled diamond saw (Figure 5–3). The edges of the specimen were then polished to their final dimensions using 600 grit paper. A typical specimen is shown in Figure 5–4 along with a neat resin specimen.

Specimen Testing

The individual specimens were tested at room temperature (20 $\pm$ 2° C) in the testing jig shown in Figure 5–5. The testing machine employed was an Instron servo–hydraulic machine (Model 1332) equipped with a 100,000 N load cell. The stroke rate was 0.5 mm/minute and the strain was measured with an Instron dynamic extensometer (Model 2620–530) which was attached to the threaded upper and lower platens.

The stress–strain curves for the various materials are similar, and are matrix controlled for all but the 45 degree specimen (Figures 5–6, 5–7, and 5–8). This specimen appeared to be the only one with a well defined ultimate bearing strength. The carbon and S2 glass specimens at 45 degrees exhibited strikingly linear behavior to failure. The Kevlar 49 specimen showed a modulus increase after some resin degradation had occurred. The non–crossply specimens all exhibited a bilinear behavior. This has been postulated by other authors [83] to be associated with a fiber scissoring action. Fiber scissoring (Figure 5–9) was observed in these failed specimens. The unidirectional carbon specimen was other only specimen to show a definite ultimate failure point.

The nature of the stress–strain curve suggests that the linear representation of this in a theoretical analysis would be valid up to 200 MPa normal stress in the case of E/XA–S carbon.

The modulii for a uni–directional E/XA–S composite material is given in Table 5–1.

Discussion

The author believes that it is imperative that basic material properties which are used in the pressure vessel design programs be obtained for the same fibers, matrix, cure schedule and fabrication technique as will be employed in the actual pressure vessels. There is a wide range of transverse compressive mechanical properties in the literature as would be expected for a matrix dominated property. This study has provided preliminary transverse compressive mechanical properties for the calculations given later in this chapter.

The unidirectional stress–strain curves are quite similar to those of the pure resin specimens, thus indicating significant matrix effects on the stress–strain relationships and failure mode. During this study, there has not been any attempt to associate regions of the stress–strain curves with specific failure modes.

5.3 Case I – Infinitely Long Cylinder

Series Approach

Consider a layered orthotropic cylinder of infinite extent, with material properties constant along its length, subject to axisymmetric loadings such as pressure, axial loadings, and torque (see Figure 5–10). The cylinder envisaged is long enough so the 'end effects' are not important and we are left with stresses that are independent of axial position. Given this, and since stiffnesses are independent of the axial coordinate, it follows from equation (3–14) that the strains are also independent of the axial coordinate.

If ε_{rr} and $\varepsilon_{\theta\theta}$ are independent of z, then equation (3–5) suggests that u_r must only depend on the radial position r. That is

$$u_{r\infty} = \sum_{j=0}^{\infty} \phi_{r\infty}^{(j)} q^{j} \qquad (5\text{–}1)$$

where $$q = \frac{r}{r_c}$$

and $\phi_{r\infty}^{(j)}$ are constants to be determined. It is again mathematically simpler to develop the theory in terms of the variable q, and transform the analysis to a mid-plane coordinate system as a later step.

From the second and third equilibrium equations (eqn. 3–11)

$$\frac{d\tau_{r\theta}}{dr} + 2\,\frac{\tau_{r\theta}}{r} = 0$$

$$\frac{d\tau_{rz}}{dr} + \frac{\tau_{rz}}{r} = 0$$

If these shear stresses are to vanish at a free surface, then they must be identically zero through the cylinder wall. From Hooke's law then

$\gamma_{rz}\,,\ \gamma_{r\theta}$ are identically zero.

If ε_{zz} is to be independent of z, then

$$\varepsilon_{zz} = \varepsilon_{zz}(r)$$

implying that (eqn. 3–5)

$$u_z = \varepsilon_{zz}(r)\,z + f_1(r)$$

If $\gamma_{\theta z}$ is to be independent of z, then

$$\gamma_{\theta z} = \gamma_{\theta z}(r)$$

implying that (eqn. 3–5)

$$u_\theta = \gamma_{\theta r}(r)\,z + f_2(r)$$

If $\gamma_{r\theta}$ is zero, then upon substitution into equation 3–5

$$\frac{\partial u_\theta}{\partial r} - \frac{u_\theta}{r} = 0$$

or

$$\frac{d}{dr}\gamma_{\theta z} - \frac{\gamma_{\theta z}}{r} = 0$$

and

$$\frac{df_2}{dr} - \frac{f_2}{r} = 0$$

suggesting that

$$\gamma_{\theta z} = \gamma_{\theta z}^{(1)}\,r$$

and

$$f_2 = k\,r \qquad k \text{ constant}$$

Without loss of generality, we can write

(5–2) $$u_\theta = \gamma_{\theta z}^{(1)} r z$$

where $\gamma_{\theta z}^{(1)}$ is a constant

Similarly, for γ_{rz} to be identically zero

$$\frac{\partial u_r}{\partial z} + \frac{\partial u_z}{\partial r} = 0$$

or

$$\frac{d}{dr} \varepsilon_{zz}(r) \cdot z + \frac{df_1}{dr} = 0$$

suggesting $$\varepsilon_{zz}(r) = \varepsilon_{zz}^{(0)}$$

$$f_1(r) = \text{constant} = k_1$$

thus $$u_z = \varepsilon_{zz}^{(0)} z + k_1$$

Without loss of generality, we can write

(5–3) $$u_z = \varepsilon_{zz}^{(0)} z$$

where $\varepsilon_{zz}^{(0)}$ is a constant

This implies that

(5–4) $$\phi_z^{(0)} = \varepsilon_{zz}^{(0)} z$$

$$\phi_\theta^{(1)} = \gamma_{\theta z}^{(1)} z$$

Substituting these into equations (3–5) gives us that

(5–5) $$\gamma_{r\theta} = 0$$

$$\gamma_{rz} = 0$$

Given this,

(5-6) $$\bar{\Phi}_\infty = \left(\varepsilon_{zz}^{(0)} z,\ 0,\ \phi_{r\infty,0}^{(0)},\ \gamma_{\theta z}^{(1)},\ \phi_{r\infty}^{(1)},\ 0,\ 0,\ \phi_{r\infty}^{(2)},\ \ldots\right)^T$$

This must satisfy equation (4-25), namely

(5-7) $$\underline{\underline{B}}\ \underline{\Phi}_\infty' + \underline{\underline{C}}\ \underline{\Phi}_\infty + \underline{D} = 0$$

This is the particular solution that when shifted to a mid-plane coordinate system is given by equations (4-25) and (4-26).

We note that the terms $\underline{\underline{C}} \cdot \varepsilon_{zz}^{(0)}$ and $\underline{\underline{C}} \cdot \gamma_{\theta z}^{(1)}$ vanish because they are identically zero. We also note that this equation set is missing two additional independent conditions to allow complete specification of the $\phi_{r\infty}^{(j)}$. These can be determined by considering the axial and torque loading on the cylinder.

Pressure and axial loading on the ends of the cylinder result in an axial stress resultant given by

(5-8) $$N_{zz}^{(1)} = \int_{\xi_i}^{\xi_o} \sigma_{zz}\, \xi\, d\xi = \frac{F_z}{2\pi r_c^2}$$

where F_z is any axial loading imposed away from the analysis point on the cylinder.

Any applied torque loading is expressed as

(5-9) $$N_{\theta z}^{(2)} = \int_{\xi_i}^{\xi_o} \tau_{\theta z}\, \xi^2\, d\xi = \frac{\tau}{2\pi r_c^3}$$

where τ is the circumferential torque.

Expanding equation (5-7) using (5-6) generates the basic set of equations for the infinite cylinder. Substituting equations (5-8) and (5-9) into equations (3-19) adds the remaining two equations to give the following set of simultaneous equations

$$\underline{\underline{S}} \cdot \underline{Y} = \underline{P} \tag{5-10}$$

where

$$
\begin{aligned}
S_{11} &= A_{11}^{(1)} \\
S_{12} &= A_{16}^{(2)} \\
S_{1\,j+3} &= \frac{1}{r_c}\left(A_{12}^{(j)} + j\,A_{13}^{(j)}\right) \\
S_{21} &= A_{16}^{(2)} \\
S_{22} &= A_{66}^{(3)} \\
S_{2\,j+3} &= \frac{1}{r_c}\left(A_{26}^{(j+1)} + j\,A_{36}^{(j+1)}\right) \\
S_{n+3\,1} &= A_{12}^{(n)} + n\,A_{13}^{(n)} \\
S_{n+3\,2} &= A_{26}^{(n)} + n\,A_{36}^{(n)} \\
S_{n+3\,j+3} &= \frac{1}{r_c}\left\{A_{22}^{(n+j-1)} + (n+j)\,A_{23}^{(n+j-1)} + nj\;A_{33}^{(n+j-1)}\right\} \\
P_1 &= F_z / 2\pi r_c^2 \\
P_2 &= \tau / 2\pi r_c^3 \\
P_{n+3} &= -P_i\left(\frac{r_i}{r_c}\right)^{n+1} + P_o\left(\frac{r_o}{r_c}\right)^{n+1}
\end{aligned}
$$

and

$$\underline{Y} = \left(\varepsilon_{zz}^{(0)},\ \gamma_{\theta z}^{(1)},\ \phi_{r\infty}^{(0)},\ \phi_{r\infty}^{(1)},\ \ldots\right)^T$$

The matrix $\underline{\underline{S}}$ in equation (5–10) is termed an ill conditioned matrix. This means that the determinant of $\underline{\underline{S}}$ is nearly zero. The thinner the shell, the more ill conditioned the matrix becomes. This fortunately, does not limit our solution, since standard equation solving techniques yield solutions for a truncated series with sufficient number of terms for accurate calculation of stresses and strains.

Equation (5–10) becomes upon shifting to laminated centered coordinates using equations (3–24)

$$R \cdot X = P \qquad (5\text{-}11)$$

where $$[R_{ij}] = \sum_{k=0}^{j} \binom{j}{k} (-1)^k [S_{ik}]$$

$$X = \left(\varepsilon_{zz}^{(0)}, \gamma_{\theta z}^{(1)}, \beta_{r\infty}^{(0)}, \beta_{r\infty}^{(1)}, \ldots \right)^T$$

is the mid-plane shifted form of $\underline{\underline{S}}$ in equation (5-10).

The resulting matrix equation (5-11) is solved using a recursive Gauss-Jordan elimination.

The deformations and strains are calculated using

$$(5\text{-}12) \qquad \begin{aligned} u_\theta &= \gamma_{\theta z}^{(1)} \, r \, z \\ u_z &= \varepsilon_{zz}^{(0)} \, z \\ u_r &= \sum_{j=0}^{\infty} \beta_{r\infty}^{(j)} \, \xi^{j} \end{aligned}$$

Noting that $\gamma_{r\theta}$ and γ_{rz} are zero, equation (3-26) and (5-12) give the cylinder strains as

$$\begin{aligned} \varepsilon_{zz} &= \varepsilon_{zz}^{(0)} \\ \gamma_{\theta z} &= \gamma_{\theta z}^{(1)} \, r \\ \varepsilon_{rr} &= \sum_{j=0}^{\infty} -\frac{j \beta_r^{(j)}}{r_c} \, \xi^{j-1} \\ \varepsilon_{\theta\theta} &= \sum_{j=0}^{\infty} \frac{\beta_r^{(j)}}{r_c} \, \frac{\xi^{j}}{1-\xi} \end{aligned}$$

The stresses are calculated using the generalized form of Hooke's law equation (3-14). A flowchart for a numerical implementation of this is given in the appendices.

Exact Solution

The exact solution for the layered orthotropic cylinder of infinite length has been calculated using elasticity methods, [11] and is included here for comparison purposes.

Noting equations (5–2), (5–3), and (5–5), the strain–deformation equations can be written, following equation (3–5) as

$$
\text{(5–13)} \qquad
\begin{aligned}
\varepsilon_{zz} &= \varepsilon_{zz}^{(0)} \\
\varepsilon_{\theta\theta} &= \frac{u_r}{r} \\
\varepsilon_{rr} &= \frac{du_r}{dr} \\
\gamma_{\theta z} &= \gamma_{\theta z}^{(1)}\, r
\end{aligned}
$$

Substituting these into the stress equilibrium equations (3–10) and eliminating $\frac{\partial \tau_{rz}}{\partial z}$ gives the following second order ordinary differential equation,

$$
\text{(5–14)} \qquad u_r'' + \frac{1}{r} u_r' - \frac{\alpha^2}{r^2} u_r = \beta_1 \frac{\varepsilon_{zz}^{(0)}}{r} + \beta_2 \gamma_{\theta z}^{(1)}
$$

where

$$
\begin{aligned}
\alpha^2 &= \frac{Q_{22}}{Q_{33}} \\
\beta_1 &= \frac{Q_{12} - Q_{13}}{Q_{33}} \\
\beta_2 &= \frac{Q_{26} - 2Q_{36}}{Q_{33}}
\end{aligned}
$$

and

$$
\varepsilon_{zz}^{(0)}, \quad \gamma_{\theta z}^{(1)}
$$

are constants as given in equations (5–2) and (5–3).

The general solution to this differential equation is

$$(5\text{–}15) \qquad u_r^{(i)} = A_i r^{\alpha_i} + B_i r^{-\alpha_i} + \frac{\beta_1^{(i)} \varepsilon_{zz}^{(o)}}{1-\alpha_i^2} r + \frac{\beta_2^{(i)} \gamma_{\theta z}^{(o)}}{4-\alpha_i^2} r^2$$

for each layer i in the cylinder.

If the cylinder is subject to an internal pressure p_i and an external pressure p_o, then the following conditions apply.

$$(5\text{–}16) \qquad \begin{aligned} \sigma_{rr} &= -p_i \; ; \quad r = r_{in} \\ \sigma_{rr} &= -p_o \; ; \quad r = r_{out} \end{aligned}$$

For this problem, equations (5–8) and (5–9) can be written

$$(5\text{–}17) \qquad \int_{r_{in}}^{r_{out}} \sigma_{zz}\, r\, dr = \frac{F_z}{2\pi}$$

and

$$(5\text{–}18) \qquad \int_{r_{in}}^{r_{out}} \tau_{\theta z}\, r^2 dr = \frac{T}{2\pi}$$

If more than one layer of material is present, material continuity between layers is expressed as

$$(5\text{–}19) \qquad u_r^{(i+1)} = u_r^{(i)} \; ; \qquad r = r_i$$

where the superscripts identify the layer number, r_i is the radial position of the interface between the i^{th} and the $(i+1)^{th}$ layer.

Further,

$$(5\text{-}20) \qquad \frac{du_r}{dr}^{(i+1)} = \frac{du_r}{dr}^{(i)} \quad ; \quad r = r_i$$

If we express equations (5–16) through (5–20) in terms of u_r by using equation (5–13) and (3–14), the following system of equations is obtained which when solved gives u_r and our constant strains $\varepsilon_{zz}^{(0)}$ and $\gamma_{\theta z}^{(1)}$ through the thickness of the cylinder wall.

$$(5\text{-}21) \qquad \underline{\underline{B}} \cdot \underline{\Phi} = \underline{P}$$

where the coefficients of $\underline{\underline{B}}$ and $\underline{P}$ are given in Table 5–1 and

$$(5\text{-}22) \qquad \underline{\Phi} = \left(A_1, B_1, A_2, B_2, \ldots, A_N, B_N, \varepsilon_z^{(0)}, \gamma_{\theta z}^{(1)} \right)^T$$

This system has been solved numerically using a Gauss–Jordan elimination technique with iteration.

The flowchart for this solution (EXACT) is included in the appendices. It is a user friendly routine that allows operator specification of the cylinder geometry and material stacking sequence where each layer is an orthotropic material whose principle direction is inclined to the cylinder axis. Material properties are included in an easily expandable material subroutine.

The solution is generated using the method described, and the stresses and strains are outputted for each lamina at the inner lamina surface, the lamina mid–plane, and the outer lamina surface. These are calculated using equations (5–15), (5–13), and (3–14).

Solutions Comparisons

To check the initial validity of both the series and the exact solution algorithms, the standard analytical solution for a thick isotropic cylinder subject to radial pressure only was used. The stresses in a thick isotropic cylinder with internal pressure is given by [72].

$$\sigma_{rr} = \frac{P_i \, r_{in}^2}{r_{out}^2 - r_{in}^2} \left\{ 1 - \frac{r_{out}^2}{r^2} \right\}$$

(5–23)

$$\sigma_{\theta\theta} = \frac{P_i \, r_{in}^2}{r_{out}^2 - r_{in}^2} \left\{ 1 + \frac{r_{out}^2}{r^2} \right\}$$

For external pressure

$$\sigma_{rr} = \frac{-P_o \, r_{out}^2}{r_{out}^2 - r_{in}^2} \left\{ 1 - \frac{r_{in}^2}{r^2} \right\}$$

(5–24)

$$\sigma_{\theta\theta} = \frac{-P_o \, r_{out}^2}{r_{out}^2 - r_{in}^2} \left\{ 1 + \frac{r_{in}^2}{r^2} \right\}$$

The comparison between the series solution and the analytic solution [72] is shown for a very thick cylinder in Tables 5–3 and 5–4 to be negligible (less that .25% on the radial stresses). The solution is also shown for the one generated by the EXACT routine – again within negligible error.

A comparison is also made to a pair of thick orthotropic cylinders as given in the literature [73]. Agreement is within 4% as shown in Tables 5–5 and 5–6, a tolerable figure when comparison data is extracted from a published graph. It should be pointed out that Tsai [73] modelled the orthotropic cylinder as +θ, −θ laminae pairs. This formulation was in fact published prior to the work of Tsai by the author [74]. The +θ, −θ restriction was removed for a layered orthotropic cylinder in a later algorithm [78].

The solutions have been calculated in a series manner for thin and thick generally orthotropic tubes with a single layer and multiple layers inclined in a helical manner for comparison with the EXACT prediction. The results of this calculation are shown in Table 5−7 through Table 5−9. It is clear that for the thin tube, three terms presents an accurate solution for the problem (within 1% if radial stresses are not considered). For the thick tube however, it is seen that convergence to an accurate solution is slower, and that three or four terms are not adequate to accurately represent the solution. The solution in Table 5−9 is presented to show the much more strenuous case of a multi−layer solution with different properties in adjacent layers. Convergence is indicated in all cases.

5.4 Semi−infinite Cylinder Hinged at the Origin

Solution Method

Consider the cylinder of Case I near the origin, where it is restrained from moving either axially or circumferentially. Assume that the radial deformation is specified, and that the cylinder is allowed to bend freely. These conditions can be expressed as

$$
\begin{aligned}
u_z(0, \theta, r) &= 0 \\
u_\theta(0, \theta, r) &= 0 \qquad (5\text{-}25) \\
u_r(0, \theta, r) &= u_{r0}(r)
\end{aligned}
$$

Equation (5–25) suggests that

$$
\begin{aligned}
\beta_z^{(j)}(0) &= 0 \\
\beta_\theta^{(j)}(0) &= 0 \qquad (5\text{–}26)\\
\beta_r^{(j)}(0) &= \beta_{ro}^{(j)} \quad ; \quad j = 0, 1, 2, \ldots
\end{aligned}
$$

where $\beta_{ro}^{(j)}$ are known constants.

At a sufficient distance away from the origin, the solution of Case II must approach that of Case I. An examination of equation (4–23) then requires that

$$
\begin{aligned}
c_{ij}^{(1)} &= 0 \qquad \text{if} \quad \lambda_i \geq 0 \\
c_i^{(2)} &= 0 \qquad (5\text{–}27)\\
c_{ij}^{(3)} &= 0 \qquad \text{if} \quad \text{Real}(\kappa_i) \geq 0
\end{aligned}
$$

The remaining constants can be determined by applying boundary conditions (5–26) to equation (4–29).

At $z = 0$ then

$$
\begin{aligned}
&\sum_i \left\{ c_{i2}^{(1)} \underline{X}_{i2}^{(1)} \right\} + \sum_i \left\{ c_{i1}^{(3)} \underline{X}_{i1}^{(3)} + c_{i2}^{(3)} \underline{X}_{i2}^{(3)} \right\} \\
(5\text{–}28) \quad &+ \left(0, 0, \beta_{r\infty}^{(0)}, 0, 0, \beta_{r\infty}^{(1)}, \ldots \right)^T \\
&= \left(0, 0, \beta_{ro}^{(0)}, 0, 0, \beta_{ro}^{(1)}, \ldots \right)^T
\end{aligned}
$$

Since the eigenvalues are complex, special techniques are required to solve equation (5–28). If we write

$$(5\text{-}29) \qquad \underline{\delta} = \left(0, 0, \beta_{r0}^{(0)} - \beta_{r\infty}^{(0)}, 0, 0, \beta_{r0}^{(1)} - \beta_{r\infty}^{(1)}, \dots \right)^T$$

then equation (5–28) can be written.

$$(5\text{-}30) \qquad \underline{\underline{X}} \cdot \underline{C} = \underline{\delta}$$

where the eigenvectors $\underline{X}_i$ have been put in matrix form $\underline{\underline{X}}$ and the scalar coefficients C_i have been grouped into a vector $\underline{C}$.

Expanding $\underline{\underline{X}}$ and $\underline{C}$ into real and imaginary parts, equation (5–30) becomes

$$(5\text{-}31) \qquad \left\{ \begin{array}{c|c} \mathrm{Real}(\underline{\underline{X}}) & -\mathrm{Imag}(\underline{\underline{X}}) \\ \hline \mathrm{Imag}(\underline{\underline{X}}) & \mathrm{Real}(\underline{\underline{X}}) \end{array} \right\} \left\{ \begin{array}{c} \mathrm{Real}(\underline{C}) \\ \hline \mathrm{Imag}(\underline{C}) \end{array} \right\} = \left\{ \begin{array}{c} \underline{\delta} \\ \hline 0 \end{array} \right\}$$

This matrix is solved using a recursive Gauss–Jordan technique. The coefficients thus generated are substituted into the general solution given by equation (4–29). Knowing the deformation coefficients allows the deformation series given by equation (3–23) to be evaluated. A flowchart for the numerical solution of this problem is given in the appendices.

Solution Comparisons

A standard comparison for this technique is the thin wall isotropic cylinder subject to internal pressure as presented by Timoshenko [66]. His analysis is accurate to first order in the mid–plane strains. Since these depend upon the derivatives of the deformations, one would expect a comparable solution for a deformation series between two and three terms in length.

Figure 5–11 illustrates this comparison. It is seen that the Timoshenko solution falls between the series expansions for two and three terms. Convergence of the solution after the third term is also evident.

A non–series analysis is available for comparison for a thin orthotropic cylinder. Pipes and Whitney [23] did their analysis using a finite difference technique. The comparison for this case is illustrated in Figure 5–12.

5.5 Semi–Infinite Cylinder Rigidly Held at One End

Solution Method

Consider now, a cylinder of semi–infinite length, restrained at the origin from moving radially. Assume also, that the edge of the cylinder at the origin has bending moments $N_{zr}^{(n)}$ applied such that u_r' is zero at the origin, where the prime indicates differentiation in the axial direction. That is, the edge is rigidly held in the radial direction. In addition, assume circumferential rigidity through the application of $N_{\theta z}^{(n)}$ forcing u_θ' to zero at the origin.

The above conditions can be expressed as

$$
\begin{aligned}
u_\theta'(0, \theta, r) &= 0 \\
u_r'(0, \theta, r) &= 0 \qquad (5\text{–}32) \\
u_r(0, \theta, r) &= 0
\end{aligned}
$$

Equation (3–23) suggests that (as before)

$$
\begin{aligned}
(5\text{-}33) \qquad & \beta_\theta'^{(j)}(0) = 0 \\
& \beta_r'^{(j)}(0) = 0 \\
& \beta_r^{(j)}(0) = 0
\end{aligned}
$$

As with case II, at a sufficient distance away from the origin, the solution must approach that of an infinite cylinder. Equation (5–27) therefore applies.

The remaining unknown constants are obtained by substituting equation (5–33) into equation (4–29) for $\beta_r^{(j)}$ and the derivative form of equation (4–29) for $\beta_\theta'^{(j)}$ and $\beta_r'^{(j)}$.

At z = 0 then

$$
\begin{aligned}
(5\text{-}34) \qquad & \sum_i C_i \underline{X}_{ir} + \alpha_{pr} = 0 \\
& \sum_i K_i C_i \underline{X}_{i\theta} + \alpha_{p\theta}' = 0 \\
& \sum_i K_i C_i \underline{X}_{ir} + \alpha_{pr}' = 0
\end{aligned}
$$

where the subscripts r and θ refer to the components of the eigenvectors associated with $\beta_r^{(j)}$, $\beta_\theta'^{(j)}$, and $\beta_r'^{(j)}$.

If one forms the matrix

$$
(5\text{-}35) \qquad \underline{\underline{S}} = \begin{Bmatrix} \underline{X}_{ir} \\ K_i \underline{X}_{i\theta} \\ K_i \underline{X}_{ir} \end{Bmatrix}
$$

then the equation (5–34) can be written

$$
(5\text{-}36) \qquad \underline{\underline{S}} \cdot \underline{C} = \underline{\delta}
$$

where $\underline{\delta} = (\alpha_{pr}(0),\ \alpha_{p\theta}'(0),\ \alpha_{pr}'(0))^T$

We note that from equation (5–33)

$$(5\text{–}37) \qquad \begin{aligned} \alpha_{pr}(0) &= (\beta_{r\infty}^{(0)}, \beta_{r\infty}^{(1)}, \ldots)^T \\ \alpha'_{p\theta}(0) &= (\cdot \cdot \gamma_{\theta z}^{(1)} r_1, -\gamma_{\theta z}^{(1)} r_1, 0, \ldots)^T \\ \alpha'_{pr}(0) &= 0 \end{aligned}$$

The solution is obtained by the application of equation (5–31) and the techniques developed for Case II.

Solution Comparisons

The standard solution fo a thin isotropic cylinder subject to a radially directed uniform pressure, and rigidly clamped at the origin is given by Timoshenko [66]

$$(5\text{–}38) \qquad u_r = \frac{Q_0}{2\beta^3 D} e^{-\beta z} \cos \beta z$$

where

$$Q_0 = \frac{-2\beta^3 d^2 p}{12(1-\nu^2)}$$

$$\beta = \left\{ \frac{3(1-\nu^2)}{a^2 h^2} \right\}^{1/4}$$

$$D = \frac{E h^3}{12(1-\nu^2)}$$

This is compared to the series solution presented here, for several terms. It is seen in Figure 5–13 that the Timoshenko solution falls between the two and three term expansion as was the situation with case II. The ill–conditioned nature of the matrix makes the determination of solutions beyond those presented very difficult.

For a clamped generally orthotropic cylinder, for strains ε_{zz} and $\gamma_{\theta z}$ linear in ξ and $\varepsilon_{\theta\theta}$ quadratic in ξ subject to axisymmetric loading, the solution is for Whitney, Francis, and Grimes [21]

$$(5\text{-}39) \qquad \frac{u_r}{u_{r\infty}} = \left\{ 1 - e^{-\alpha z} \left(\cos \beta z + \frac{\alpha}{\beta} \sin \beta z \right) \right\}$$

where

$$\alpha = \frac{(2b-d)^{\frac{1}{2}}}{2} \qquad \beta = \frac{(2b+d)^{1/2}}{2}$$

$$b = r_c \left(\frac{\lambda_3}{\lambda_1} \right)^{1/2} \qquad d = \frac{\lambda_2}{\lambda_1}$$

$$\lambda_1 = D_{11} - \frac{1}{D r_c^2} \left\{ D_{11}^2 \bar{A}_{66} - 4 D_{11} D_{16} \bar{A}_{16} + 4 D_{16}^2 A_{11} \right\}$$

$$\lambda_2 = \frac{2}{D} \left\{ \bar{A}_{66} A_{12} D_{11} - 2 A_{12} \bar{A}_{16} D_{16} \right\}$$

$$\lambda_3 = \bar{A}_{22} - \frac{A_{12}^2 \bar{A}_{66}}{D}$$

$$\bar{A}_{16} = \frac{D_{16}}{r_c^2} \qquad \bar{A}_{66} = A_{66} + \frac{3 D_{66}}{r_c^2} \qquad \bar{A}_{22} = A_{22} + \frac{D_{22}}{r_c^2}$$

$$D = A_{11} \bar{A}_{66} - \bar{A}_{16}^2$$

$$(A_{ij}, D_{ij}) = 2 \int_0^{h/2} Q_{ij} (1, \xi^2)\, d\xi \qquad i, j = 1, 2, \cdots, 6$$

A comparison of the refined theory to equation (5–39) is presented in Figure 5–14. The comparison falls between the solution for two and three terms. The ill–conditioned nature of the matrix does not allow the inclusion of more terms in the series.

In the preceding two chapters, the following observations were made

(1) For the thin–walled isotropic and generally orthotropic cylinder subject to internal pressure, the solution for the refined shell theory is in agreement with the accepted shell theory for all regions of the cylinder.

(2) For a thin-walled orthotropic cylinder subject to axial tension, the solution for the refined theory is in general agreement with an elasticity solution generated by a finite difference technique.

(3) For a thin or thick-walled isotropic cylinder, and for a thin-walled orthotropic cylinder, the eigenvalues generated by the refined theory are in agreement with those of standard thin shell theories, and with those of a refined thick shell theory.

(4) For a thin or thick walled, isotropic, or orthotropic cylinder of infinite length, the solution for the refined theory is in agreement with those of elasticity theory.

On the basis of the above, it is proposed that the refined shell theory developed in Chapter 3, and solved in Chapters 4 and 5, is in fact a correct representation of the stressed state in a thick walled orthotropic cylinder subject to axisymmetric loading. Lack of an existing solution for a thick-walled orthotropic cylinder prevents a comparison to the presented series solution. Instead, as detailed in the next chapter, plans to manufacture an actual thick-walled orthotropic tube subject to internal pressure, are detailed. The surface strains, as will be shown, if compared to those predicted by the refined shell theory, show the necessity of retaining more than two or three terms to obtain an adequate prediction of the strains.

Measured Values:

Specimen Type	Modulus (GPa.)	Volume Fraction (%)	Reference
Longitudinal Tension	156.0 ± 3.2*	64.3	76
Transverse Tension	8.5 ± 0.7	62.1	76
Transverse Compression (bearing)	5.42 ± 1.12	64.5 ± 0.7	75
Shear (in-plane)	4.59 ± .42	n/a	78

* – mean ± standard deviation
n/a – not available or assumed

Assumed Values:

ν_{12} = 0.29 [76]
ν_{13} = 0.29
ν_{23} = 0.25
G_{13} = 4.58 GPa.
G_{23} = 7.20 GPa.

Table 5–1 E/XA–S/Epoxy Material Data

Table 5–2 Exact Solution Matrix Coefficients

$$\underline{\underline{B}} \cdot \underline{\Phi} = \underline{P}$$

where

$$B_{11} = \left(Q_{23}^{(1)} + \alpha_1 Q_{33}^{(1)} \right) r_{in}^{\alpha_1 - 1}$$

$$B_{12} = \left(Q_{23}^{(1)} - \alpha_1 Q_{33}^{(1)} \right) r_{in}^{-\alpha_1 - 1}$$

$$B_{1\,2N+1} = \left(Q_{13}^{(1)} + \frac{\beta^{(1)}}{1-\alpha_1^2} \left[Q_{23}^{(1)} + Q_{33}^{(1)} \right] \right)$$

$$B_{1\,2N+2} = \left(Q_{36}^{(1)} + \frac{\beta^{(1)}}{4-\alpha_1^2} \left[Q_{23}^{(1)} + 2 Q_{33}^{(1)} \right] \right) r_{in}$$

$$B_{21} = \left(Q_{23}^{(N)} + \alpha_N Q_{33}^{(N)} \right) r_{out}^{\alpha_N - 1}$$

$$B_{22} = \left(Q_{23}^{(N)} - \alpha_N Q_{33}^{(N)} \right) r_{out}^{-\alpha_N - 1}$$

$$B_{2\,2N+1} = \left(Q_{13}^{(N)} + \frac{\beta^{(N)}}{1-\alpha_N^2} \left[Q_{23}^{(N)} + Q_{33}^{(N)} \right] \right)$$

$$B_{2\,2N+2} = \left(Q_{36} + \frac{\beta^{(N)}}{4-\alpha_N^2} \left[Q_{23}^{(N)} + 2 Q_{33}^{(N)} \right] \right) r_{out}$$

$$B_{2i\,2i-1} = r_i^{\alpha_i}$$

$$B_{2i\,2i} = r_i^{-\alpha_i}$$

$$B_{2i\,2i+1} = - r_i^{\alpha_i}$$

$$B_{2i\,2i+2} = r_i^{-\alpha_i}$$

$$B_{2i\,2N+1} = \frac{\beta^{(i+1)}}{1-\alpha_{i+1}^2} - \frac{\beta^{(i)}}{1-\alpha_i^2}$$

$$B_{2i\,2N+2} = \left(\frac{\beta^{(i+1)}}{4-\alpha_{i+1}^2} - \frac{\beta^{(i)}}{4-\alpha_i^2} \right) r_i$$

$$B_{2i+1\,2i-1} = \alpha_i r_i^{\alpha_i}$$

$$B_{2i+1\,2i} = \alpha_i r_i^{-\alpha_i}$$

$$B_{2i+1\,2i+1} = -\alpha_i r_i^{\alpha_i}$$

$$B_{2i+1\,2i+2} = \alpha_i r_i^{-\alpha_i}$$

$$B_{2i+1\,2N+1} = \left(\frac{\beta^{(i)}}{1-\alpha_i^2} - \frac{\beta^{(i+1)}}{1-\alpha_{i+1}^2} \right) r_i$$

$$B_{2i+1\,2N+2} = \left(\frac{\beta^{(i)}}{4-\alpha_i^2} - \frac{\beta^{(i+1)}}{4-\alpha_{i+1}^2} \right) \cdot 2\, r_i^2$$

$$B_{2N+1\,2i-1} = \frac{Q_{12}^{(i)} + \alpha_i Q_{13}^{(i)}}{\alpha_i + 1} \left(r_i^{\alpha_i+1} - r_{i-1}^{\alpha_i+1} \right)$$

$$B_{2N+1\,2i} = \frac{Q_{12}^{(i)} - \alpha_i Q_{13}^{(i)}}{-\alpha_i - 1} \left(r_i^{-\alpha_i + 1} - r_{i-1}^{-\alpha_i + 1} \right)$$

$$B_{2N+1\,2N+1} = \sum_{j=1}^{N} \frac{1}{2} \left\{ Q_{11}^{(j)} + \frac{\beta^{(j)}}{1 - \alpha_i^2} \left(Q_{12}^{(j)} + Q_{13}^{(j)} \right) \right\} \left\{ r_j^2 - r_{j-1}^2 \right\}$$

$$B_{2N+1\,2N+2} = \sum_{j=1}^{N} \frac{1}{3} \left\{ Q_{16}^{(j)} + \frac{\beta^{(j)}}{4 - \alpha_i^2} \left(Q_{12}^{(j)} + 2Q_{23}^{(j)} \right) \right\} \left\{ r_j^3 - r_{j-1}^3 \right\}$$

$$B_{2N+2\,2i-1} = \frac{Q_{26}^{(i)} + \alpha_i Q_{36}^{(i)}}{\alpha_i + 2} \left(r_i^{\alpha_i + 2} - r_{i-1}^{\alpha_i + 2} \right)$$

$$B_{2N+2\,2i} = \frac{Q_{26}^{(i)} - \alpha_i Q_{36}^{(i)}}{-\alpha_i + 2} \left(r_i^{-\alpha_i + 2} - r_{i-1}^{-\alpha_i + 2} \right)$$

$$B_{2N+2\,2N+1} = \sum_{j=1}^{N} \left\{ Q_{16}^{(j)} + \frac{\beta^{(j)}}{1 - \alpha_i^2} \left(Q_{26}^{(j)} + Q_{36}^{(j)} \right) \right\} \left\{ \frac{r_i^3 - r_{i-1}^3}{3} \right\}$$

$$B_{2N+2\,2N+2} = \sum_{j=1}^{N} \left\{ Q_{66}^{(j)} + \frac{\beta^{(j)}}{4 - \alpha_i^2} \left(Q_{26}^{(j)} + 2Q_{36}^{(j)} \right) \right\} \left\{ \frac{r_i^4 - r_{i-1}^4}{4} \right\}$$

$$P_1 = -p_{in}$$

$$P_2 = -p_{out}$$

$$P_3 = P_4 = \cdots = P_{2N} = 0$$

$$P_{2N+1} = F_z$$

$$P_{2N+2} = \frac{T}{2\pi}$$

VARIABLE	Location	NUMBER OF TERMS IN SERIES 1	2	3	4	5	10	EXACT ALGORITHM	EQUATION (5-23)
$\sigma_{\theta\theta}$ (x E7)	Inner	1.5839	2.0619	1,8833	1.7296	1.6821	1.6668	1.6667	1.6667
	Middle	0.94961	0.90836	0.84911	0.92309	0.92955	0.92595	0.92593	0.92593
	Outer	0.63224	0.33160	0.76459	0.63745	0.67381	0.66672	0.66667	0.66667
σ_{rr} (x E7)	Inner	0.63529	0.33680	-0.58659	-0.87235	-0.96912	-0.99975	-1.0000	-1.0000
	Middle	0.31717	-0.24170	-0.39863	-0.25921	-0.25196	-0.25922	-0.25926	-0.25926
	Outer	0.15811	-0.53094	0.20561	-0.05770	0.01428	0.00001	0.0000	0.0000

Inner Radius (M.)	0.030	Internal Pressure (MPa.)	10.0
Outer Radius (M.)	0.060	Applied Torque (Nt. M.)	0.0
Fiber Orientation (Deg.)	Isotropic	External Axial Load (Nt.)	0.0
		External Pressure (MPa.)	0.0

E_{11} = 71.0E6 MPa.	E_{12} = 2.66E6 MPa.	ν_{12} = 0.334
E_{22} = 71.0E6 MPa.	E_{13} = 2.66E6 MPa.	ν_{13} = 0.334
E_{33} = 71.0E6 MPa.	E_{23} = 2.66E6 MPa.	ν_{23} = 0.334

Deviation of Solutions From Comparisons (%)

VARIABLE	Location	NUMBER OF TERMS IN SERIES 1	2	3	4	5	10	EXACT ALGORITHM	EQUATION (5-23)
$\sigma_{\theta\theta}$ (x 10^7)	Inner	4.97	23.71	13.0	3.77	.924	6.00×10^{-3}	0	0
	Middle	2.57	1.89	8.29	.296	.401	1.30×10^{-2}	0	0
	Outer	5.16	-50.3	14.7	4.38	1.07	7.49×10^{-3}	0	0
σ_{rr} (x 10^7)	Inner	36.5	66.3	47.3	12.8	3.09	2.50×10^{-2}	0	0
	Middle	22.1	6.99	53.4	.635	3.04	.246	0	0
	Outer	-	-	-	-	-	-	0	0

Table 5-3 Isotropic Cylinder Subject to Internal Pressure

VARIABLE	Location	NUMBER OF TERMS IN SERIES 1	2	3	4	5	10	EXACT ALGORITHM	EQUATION (5–23)
$\sigma_{\theta\theta}$ (x E7)	Inner	−3.1679	−3.0619	−2.8833	−2.7296	−2.6821	−2.6668	−2.6667	−2.6667
	Middle	−1.8992	−1.9084	−1.8491	−1.9231	−1.9295	−1.9259	−1.9259	−1.9259
	Outer	−1.2649	−1.3316	−1.7646	−1.6375	−1.6738	−1.6667	−1.6667	−1.6667
σ_{rr} (x E7)	Inner	−1.2706	−1.3368	−0.47341	−0.12765	−0.03088	−.00002	0.0000	0.0000
	Middle	−0.63434	−0.75830	−0.60137	−0.74079	−0.74804	−0.74078	−0.74074	−0.74074
	Outer	−0.31621	−0.46906	−1.2056	−0.94230	−1.0143	−1.0001	−1.0000	−1.000

Inner Radius (M.)	0.030	Internal Pressure (MPa.)	10.0
Outer Radius (M.)	0.060	Applied Torque (Nt. M.)	0.0
Fiber Orientation (Deg.)	Isotropic	External Axial Load (Nt.)	0.0
		External Pressure (MPa.)	10.0

E_{11} = 71.0E6 MPa.	E_{12} = 2.66E6 MPa.	ν_{12} = 0.334
E_{22} = 71.0E6 MPa.	E_{13} = 2.66E6 MPa.	ν_{13} = 0.334
E_{33} = 71.0E6 MPa.	E_{23} = 2.66E6 MPa.	ν_{23} = 0.334

Deviation of Solutions From Comparisons (%)

VARIABLE	Location	NUMBER OF TERMS IN SERIES 1	2	3	4	5	10	EXACT ALGORITHM	EQUATION (5–23)
$\sigma_{\theta\theta}$ (x 10^7)	Inner	18.8	14.8	8.12	2.36	.577	3.76×10^{-3}	0.0	0.0
	Middle	1.39	.909	3.99	.145	.135	0.0	0.0	0.0
	Outer	24.1	20.1	5.85	1.77	.408	0.0	0.0	0.0
σ_{rr} (x 10^7)	Inner	–	–	–	–	–	–	–	0.0
	Middle	14.4	2.37	18.8	.142	.985	5.40×10^{-3}	0.0	0.0
	Outer	68.4	53.2	20.6	5.77	1.43	1.00×10^{-2}	0.0	0.0

Table 5–4 Isotropic Cylinder Subject to External Pressure

VARIABLE	Location	1	2	3	4	5	10	EXACT ALGORITHM	TSAI [73]
		NUMBER OF TERMS IN SERIES							
$\sigma_{\theta\theta}$ (x E7)	Inner	–	5.39	5.62	5.60	5.59	5.59	5.598	5.67
	Middle	–	3.95	3.80	3.81	3.81	3.81	3.814	3.78
	Outer	–	2.79	3.19	3.16	3.17	3.17	3.169	3.15
σ_{rr} (x E7)	Inner	–	–.368	–.891	–.981	–.997	–.999	–1.0	–1.0
	Middle	–	–.396	–.422	–.380	–.380	–.381	–.3807	n/a
	Outer	–	–.419	.071	–0.12	.0011	.0004	0.0	0.0

Inner Radius (M.)	0.8888	Internal Pressure (MPa.)	10.0
Outer Radius (M.)	1.1111	Applied Torque (Nt. M.)	0.0
Fiber Orientation (Deg.)	± 55.5	External Axial Load (Nt.)	0.0
		External Pressure (MPa.)	0.0

E_{11} = 181.0×10^9 MPa.	E_{12} = 4.58×10^9 MPa.	ν_{12} = 0.28
E_{22} = 10.3×10^9 MPa.	E_{13} = 4.58×10^9 MPa.	ν_{13} = 0.28
E_{33} = 5.42×10^9 MPa.	E_{23} = 7.17×10^9 MPa.	ν_{23} = 0.24

Deviation of Solutions From Comparisons (%)

VARIABLE	Location	1	2	3	4	5	10	EXACT ALGORITHM	TSAI [73]
		NUMBER OF TERMS IN SERIES							
$\sigma_{\theta\theta}$ (x 10^7)	Inner	–	4.9	.88	1.2	1.4	1.4	1.3	0
	Middle	–	4.5	.53	.79	.79	.79	.79	0
	Outer	–	11.4	1.3	.32	.63	.63	.63	0
σ_{rr} (x 10^7)	Inner	–	63.2	10.9	1.9	.10	.10	0	0
	Middle	–	–	–	–	–	–	–	–
	Outer	–	–	–	–	–	–	–	–

Table 5–5 Thick Specially Orthotropic Cylinder Subject to Internal Pressure

VARIABLE	Location	NUMBER OF TERMS IN SERIES 1	2	3	4	5	10	EXACT ALOGRITHM	TSAI [73]
$\sigma_{\theta\theta}$ (x E7)	Inner	–	3.76	4.36	4.35	4.34	4.34	4.339	4.40
	Middle	–	1.90	1.64	1.66	1.68	1.68	1.678	1.65
	Outer	–	.659	1.13	1.08	1.10	1.09	1.095	1.05
σ_{rr} (x E7)	Inner	–	–.262	–.746	–.930	–.997	–.999	–1.0	–1.0
	Middle	–	–.298	–.335	–.259	–.257	–.261	–.2611	–.25
	Outer	–	–.323	.120	–.037	.008	.0003	0.0	0.0

Inner Radius (M.)	1.200	Internal Pressure (MPa.)	10.0
Outer Radius (M.)	.80	Applied Torque (Nt. M.)	0.0
Fiber Orientation (Deg.)	± 55.5	External Axial Load (Nt.)	0.0
		External Pressure (MPa.)	0.0

E_{11} = 181.0 x 10^9 MPa.	E_{12} = 4.58 x 10^9 MPa.	ν_{12} = 0.28
E_{22} = 10.3 x 10^9 MPa.	E_{13} = 4.58 x 10^9 MPa.	ν_{13} = 0.28
E_{33} = 5.42 x 10^9 MPa.	E_{23} = 7.12 x 10^9 MPa.	ν_{23} = 0.24

Deviation of Solutions From Comparisons (%)

VARIABLE	Location	NUMBER OF TERMS IN SERIES 1	2	3	4	5	10	EXACT ALOGRITHM	TSAI [73]
$\sigma_{\theta\theta}$ (x 10^7)	Inner	–	14.5	.91	1.1	1.4	1.4	1.4	0
	Middle	–	15.2	.61	.61	1.8	1.8	1.7	0
	Outer	–	37.2	7.6	2.9	4.8	3.80	4.3	0
σ_{rr} (x 10^7)	Inner	–	13.8	25.4	7.0	.30	.10	0	0
	Middle	–	19.2	34.0	3.6	2.8	4.4	4.4	0
	Outer	–	–	–	–	–	–	–	–

Table 5–6 Very Thick Specially Orthotropic Cylinder Subject to Internal Pressure

VARIABLE	NUMBER OF TERMS IN SERIES							EXACT ALGORITHM
	Location	1	2	3	4	5	6	
ϵ_z (x E−2)	Inner	0.29223	0.32442	0.32445	0.32445	0.32445	0.32445	0.32445
	Middle	0.29223	0.32443	0.32445	0.32445	0.32445	0.32445	0.32445
	Outer	0.29223	0.32443	0.32445	0.32445	0.32445	0.32445	0.32445
$\gamma_{\theta z}$ (x E−2)	Inner	−0.73723	−0.76873	−0.76702	−0.76706	−0.76706	−0.76706	−0.76706
	Middle	−0.77410	−0.80507	−0.80537	−0.80541	−0.80541	−0.80541	−0.80541
	Outer	−0.81096	−0.84341	−0.84372	−0.84377	−0.84377	−0.84377	−0.84377
U_r (x E−3)	Inner	0.12804	0.13539	0.13598	0.13599	0.13599	0.13599	0.13599
	Middle	0.12804	0.13142	0.13123	0.13123	0.13124	0.13124	0.13124
	Outer	0.12804	0.12744	0.12797	0.12798	0.12798	0.12798	0.12798
σ_{zz} (x E8)	Inner	0.59928	0.64269	0.62173	0.62902	0.62888	0.62887	0.62887
	Middle	0.47717	0.47721	0.47461	0.47594	0.47596	0.47595	0.47595
	Outer	0.36055	0.32094	0.34084	0.33821	0.33835	0.33834	0.33834
$\sigma_{\theta\theta}$ (x E8)	Inner	1.3628	1.4970	1.4947	1.4915	1.4913	1.4913	1.4913
	Middle	0.99712	0.99516	0.98772	0.98932	0.98937	0.98936	0.98936
	Outer	0.64676	0.52237	0.55454	0.55143	0.55160	0.55159	0.55159
σ_{rr} (x E7)	Inner	1.0883	−0.32333	−0.89761	−.99454	−0.99969	−0.99999	−1.0000
	Middle	1.0397	−0.39872	−0.41202	−0.36487	−0.36481	−0.36492	−0.36492
	Outer	0.9956	−0.46818	0.08861	−0.00468	0.00027	0.00002	0.0000
$\sigma_{\theta z}$ (x E8)	Inner	0.21680	0.28806	0.29383	0.29341	0.29339	0.29339	0.29339
	Middle	0.00511	0.00624	0.00241	0.00260	0.00263	0.00263	0.00263
	Outer	−0.19780	−0.26083	−0.26161	−0.26205	−0.25203	−0.25203	−0.25203

Inner Radius (M.)	0.030	Internal Pressure (MPa.)	10.0
Outer Radius (M.)	0.033	Applied Torque (Nt. M.)	0.0
Fiber Orientation (Deg.)	60.0	External Axial Load (Nt.)	0.0
		External Pressure (MPa.)	0.0

E11 = 156.0E9 MPa.	E12 = 4.58E9 MPa.	V12 = 0.29
E22 = 8.53E9 MPa.	E13 = 4.58E9 MPa.	V13 = 0.29
E33 = 5.42E9 MPa.	E23 = 7.20E9 MPa.	V23 = 0.25

Deviation of Solutions From Comparisons (%)

VARIABLE	NUMBER OF TERMS IN SERIES							EXACT ALGORITHM
	Location	1	2	3	4	5	6	
σ_{zz} (x 10^7)	Inner	4.61	2.23	1.14	2.38×10^{-2}	1.59×10^{-3}	0.0	0
	Middle	.256	.264	.282	2.10×10^{-3}	2.10×10^{-3}	0.0	0
	Outer	6.56	5.14	.739	3.84×10^{-2}	2.95×10^{-3}	0.0	0
$\sigma_{\theta\theta}$ (x 10^7)	Inner	8.21	.382	.228	1.34×10^{-2}	0.0	0.0	0
	Middle	.784	.576	.166	4.64×10^{-3}	1.01×10^{-3}	0.0	0
	Outer	17.6	5.30	.535	2.90×10^{-2}	1.80×10^{-3}	0.0	0
σ_{rr} (x 10^7)	Inner	8.63	67.7	10.2	.546	3.10×10^{-2}	1.00×10^{-3}	0
	Middle	184.9	9.26	12.9	1.37×10^{-2}	2.74×10^{-3}	0.0	0
	Outer	–	–	–	–	–	–	0
$\sigma_{\theta z}$ (x 10^7)	Inner	26.1	1.82	.150	6.82×10^{-3}	0.0	0.0	0
	Middle	94.3	137.3	6.37	1.14	0.0	0.0	0
	Outer	21.5	3.49	.167	7.95×10^{-3}	0.0	0.0	0

Table 5−7 Thin Uni−Angular Cylinder Subject to Internal Pressure

VARIABLE	NUMBER OF TERMS IN SERIES							EXACT ALGORITHM
	Location	1	2	3	4	5	10	
ε_z (x E−4)	Inner	1.5712	1.9413	1.9285	1.9531	1.9536	19537	1.9537
	Middle	1.5712	1.9413	1.9285	1.9531	1.9536	1.9537	1.9537
	Outer	1.5712	1.9413	1.9285	1.9531	1.9536	1.9537	1.9537
$\gamma_{\theta z}$ (x E−4)	Inner	−3.0917	−2.7254	−2.6363	−2.7973	−2.8067	−2.8082	−2.8082
	Middle	−4.6376	−4.0881	−3.9545	−4.1960	−4.2101	−4.2122	−4.2122
	Outer	−6.1835	−5.4508	−5.2727	−5.5947	−5.6135	−5.6163	−5.6163
U_r (x E−5)	Inner	1.2646	1.4522	1.7814	1.9495	1.9697	1.9724	1.9724
	Middle	1.2646	1.0720	0.86816	0.93208	0.97549	0.97541	0.97540
	Outer	1.2646	0.69179	0.88141	0.92399	0.92918	0.92986	0.92986
σ_{zz} (x E7)	Inner	1.0382	1.3167	1.5524	1.5666	1.5436	1.5354	1.5351
	Middle	0.36213	0.35872	0.24994	0.28147	0.30577	0.30422	0.30419
	Outer	−.10550	−0.23449	−0.02600	−0.13770	−0.11783	−0.11435	−0.11446
$\sigma_{\theta\theta}$ (x E7)	Inner	2.9469	3.7667	4.7135	5.0386	5.0285	5.0191	5.0188
	Middle	.89540	0.81697	0.48469	0.51447	0.59868	0.59330	0.59328
	Outer	−.49773	−0.98273	−0.50163	−0.68043	−0.65696	−0.65283	−0.65295
σ_{rr} (x E6)	Inner	0.97539	−0.27316	−3.6776	−7.43527	−9.6907	−9.9884	−10.0000
	Middle	0.66571	−0.77931	−1.1196	0.24950	0.14723	0.01549	0.01533
	Outer	0.49031	−0.10505	2.0997	−0.84455	−0.11951	0.00038	0.00000
$\sigma_{\theta z}$ (x E7)	Inner	1.3016	1.7687	2.2988	2.5008	2.5229	2.25218	2.5218
	Middle	0.15113	0.17464	0.01876	0.00003	0.04331	0.00041	0.00041
	Outer	−0.66545	−0.83510	−0.61694	−0.69348	−0.69206	−0.69152	−0.69153

Inner Radius (M.)	0.030	Internal Pressure (MPa.)	10.0
Outer Radius (M.)	0.060	Applied Torque (Nt. M.)	0.0
Fiber Orientation (Deg.)	60.0	External Axial Load (Nt.)	0.0
		External Pressure (MPa.)	0.0

E11 = 156.0E9 MPa.	E12 = 4.56E9 MPa.	ν_{12} = 0.29
E22 = 6.53E9 MPa.	E13 = 4.56E9 MPa.	ν_{13} = 0.29
E33 = 5.42E9 MPa.	E23 = 7.20E9 MPa.	ν_{23} = 0.25

Deviation of Solutions From Comparisons (%)

VARIABLE	NUMBER OF TERMS IN SERIES							EXACT ALGORITHM
	Location	1	2	3	4	5	10	
σ_{zz} (x 10^7)	Inner	32.4	14.2	1.13	3.35	.554	1.95×10^{-2}	0
	Middle	19.0	17.9	17.8	7.47	.519	9.86×10^{-3}	0
	Outer	7.83	104.8	77.3	20.3	2.94	9.61×10^{-2}	0
$\sigma_{\theta\theta}$ (x 10^7)	Inner	41.3	24.9	6.08	.395	.193	5.99×10^{-3}	0
	Middle	50.9	37.7	18.3	13.3	.910	3.37×10^{-3}	0
	Outer	23.8	83.9	22.6	4.21	.614	.0184	0
σ_{rr} (x 10^6)	Inner	90.2	97.3	63.2	25.5	3.09	.116	0
	Middle	4242	4983	7203	1527	860	1.04	0
	Outer	–	–	–	–	–	–	0
$\sigma_{\theta z}$ (x 10^7)	Inner	48.4	29.9	8.86	.833	4.36×10^{-2}	0	0
	Middle	36760	42495	4476	92.7	951	0	0
	Outer	3.77	20.8	10.6	.282	7.66×10^{-2}	1.45×10^{-3}	0

Table 5–8 Thick Uni–Angular Cylinder Subject to Internal Pressure

VARIABLE	Location	NUMBER OF TERMS IN SERIES 1	2	3	4	5	10	EXACT ALGORITHM
ϵ_z (x E−4)	Inner	0.28503	1.0117	1.0312	1.0085	1.0060	1.0060	1.0109
	Middle	0.28503	1.0117	1.0312	1.0085	1.0060	1.0060	1.0109
	Outer	0.28503	1.0117	1.0312	1.0085	1.0060	1.0060	1.0109
$\gamma_{\theta z}$ (x E−4)	Inner	0.57999	−0.11819	−0.10340	−0.11376	−0.11564	−0.11227	−0.11403
	Middle	0.86998	−0.17729	−0.15510	−0.17065	−0.17347	−0.16840	−0.17104
	Outer	1.1600	−0.23638	−0.20680	−0.22753	−0.23129	−0.22454	−0.22806
U_r (x E−5)	Inner	0.42385	0.83770	1.2114	1.3103	1.3262	1.3279	1.3269
	Middle	0.42385	0.29054	0.12101	0.11879	0.15432	0.15365	0.15251
	Outer	0.42385	−0.25662	−0.01939	−0.02904	−0.02743	−0.02700	−0.02917
σ_{zz} (x E7)	Inner	0.48441	0.94714	1.2141	1.2234	1.1983	1.1840	1.1787
	Middle	0.32037	0.36975	0.24077	0.26497	0.28989	0.28486	0.28367
	Outer	0.24564	0.05120	0.26165	0.19355	0.22390	0.21898	0.21614
$\sigma_{\theta\theta}$ (x E7)	Inner	1.4361	2.7910	3.8415	4.0406	4.0409	4.0281	4.0197
	Middle	0.92589	0.91977	0.55328	0.68204	0.65844	0.65005	0.64833
	Outer	0.69144	−0.05800	0.41661	0.33033	0.36893	0.36161	0.35741
σ_{rr} (x E7)	Inner	0.03173	−0.13764	−0.49825	−0.78363	−0.92397	−0.98229	−1.0000
	Middle	0.02234	−0.17778	−0.21052	−0.11378	−0.10699	−0.12000	−0.12668
	Outer	0.01776	−0.19814	−0.14294	−0.07812	0.02581	0.01169	0.0000
$\sigma_{\theta z}$ (x E7)	Inner	−0.73741	1.4502	2.0321	2.1681	2.1858	2.1866	2.1845
	Middle	−0.46830	−0.52214	−0.33822	−0.34147	−0.37972	−0.37671	−0.37695
	Outer	−0.34733	−0.03044	−0.22804	−0.21271	−0.21963	−0.21718	−0.21684

Inner Radius (M.)	0.030	Internal Pressure (MPa.)	10.0
Outer Radius (M.)	0.060	Applied Torque (Nt. M.)	0.0
Fiber Orientation (Deg.)	(60, −60, 60, −60, 60, −60)	External Axial Load (Nt.)	0.0
		External Pressure (MPa.)	0.0

E11 = 156.0E9 MPa.	E12 = 4.58E9 MPa.	ν_{12} = 0.29
E22 = 8.53E9 MPa.	E13 = 4.58E9 MPa.	ν_{13} = 0.29
E33 = 5.42E9 MPa.	E23 = 7.20E9 MPa.	ν_{23} = 0.25

Deviation of Solutions From Comparisons (%)

VARIABLE	Location	NUMBER OF TERMS IN SERIES 1	2	3	4	5	10	EXACT ALGORITHM
σ_{zz} (x 10^7)	Inner	59.2	20.2	2.28	3.07	.952	.252	0
	Middle	12.9	28.8	15.1	6.60	2.19	.419	0
	Outer	13.6	76.3	21.1	10.5	3.59	1.31	0
$\sigma_{\theta\theta}$ (x 10^7)	Inner	64.3	30.6	4.43	.520	.527	.209	0
	Middle	42.8	41.9	14.7	10.2	1.56	.265	0
	Outer	93.5	83.8	16.6	7.58	3.22	1.18	0
σ_{rr} (x 10^7)	Inner	96.8	86.2	50.2	21.6	7.60	1.77	0
	Middle	82.4	40.3	66.2	10.2	16.6	5.27	0
	Outer	–	–	–	–	–	–	0
$\sigma_{\theta z}$ (x 10^7)	Inner	66.2	33.6	6.98	.751	5.04×10^{-2}	9.61×10^{-2}	0
	Middle	24.2	38.5	10.8	9.41	.735	6.37×10^{-2}	0
	Outer	60.2	85.9	5.17	1.90	1.29	.157	0

Table 5−9 Thick Multi−layer Cylinder Subject to Internal Pressure

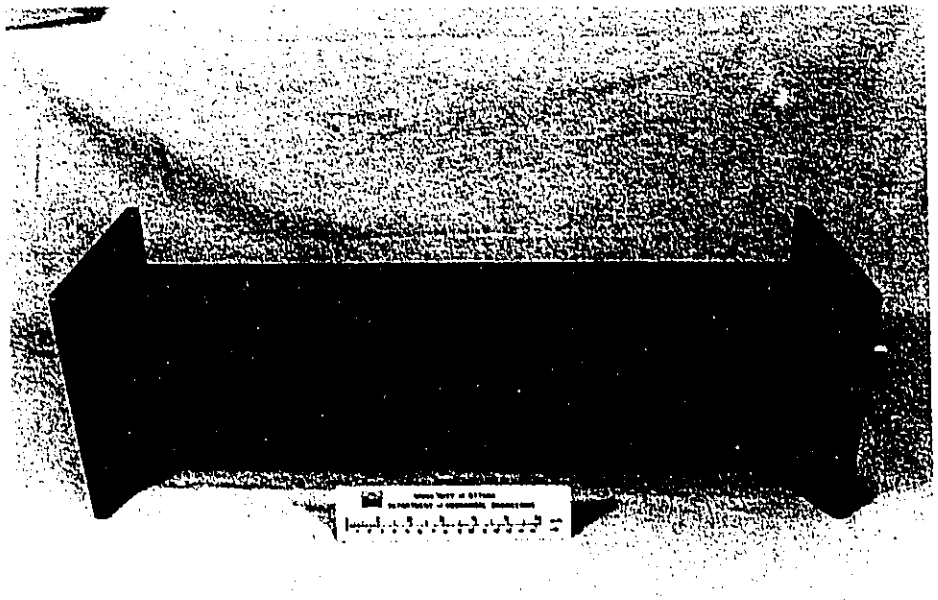

Figure 5–1 Steel Mandrel for Fabricating Angle–Ply Fiber Composites (Without Split Pins)

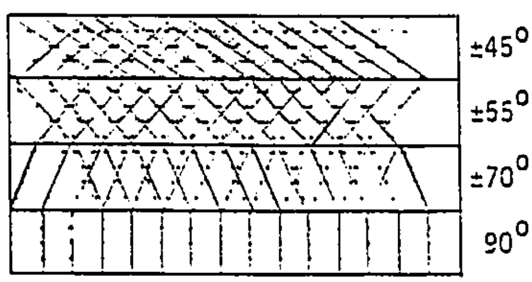

Figure 5–2 Schematic of Winding Patterns on the Four Sides of the Steel Mandrel of Figure 5–1

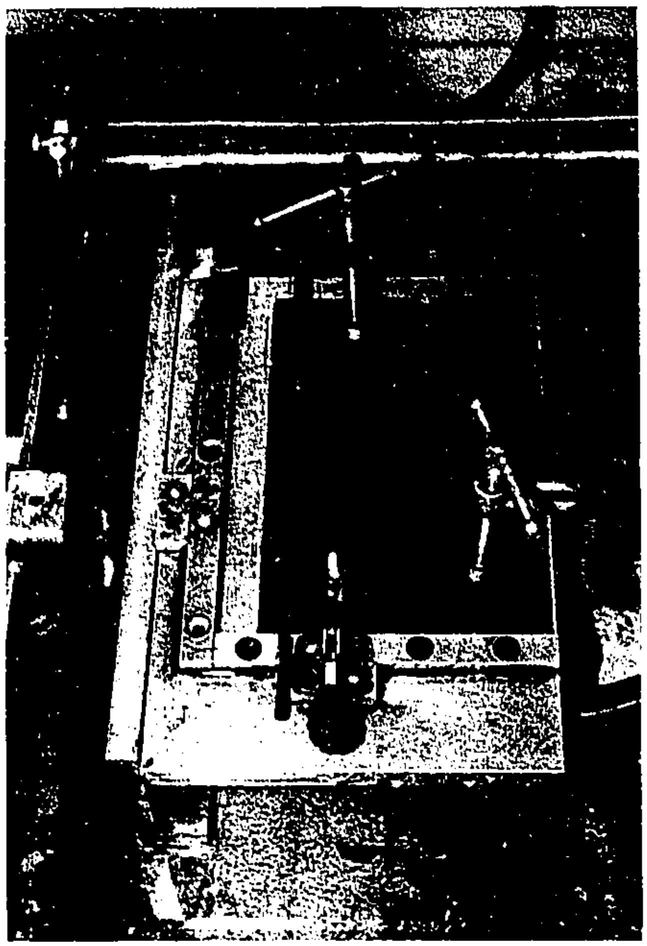

Figure 5–3 Sectioning of a Grafil E/XA–S Carbon/Epoxy Composite Plate with a Water–Cooled Diamond Saw

Figure 5-4 Typical Transverse Compressive Specimens (clockwise from lower left: resin, E/XA-S carbon, Kevlar 49, S2-glass).

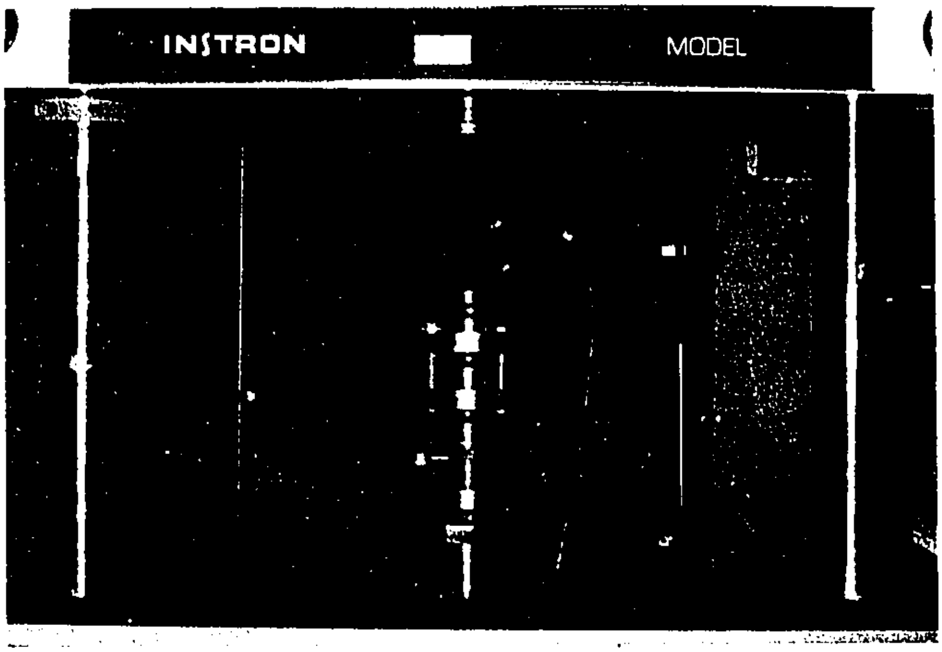

Figure 5–5 Transverse Compressive Testing Fixture

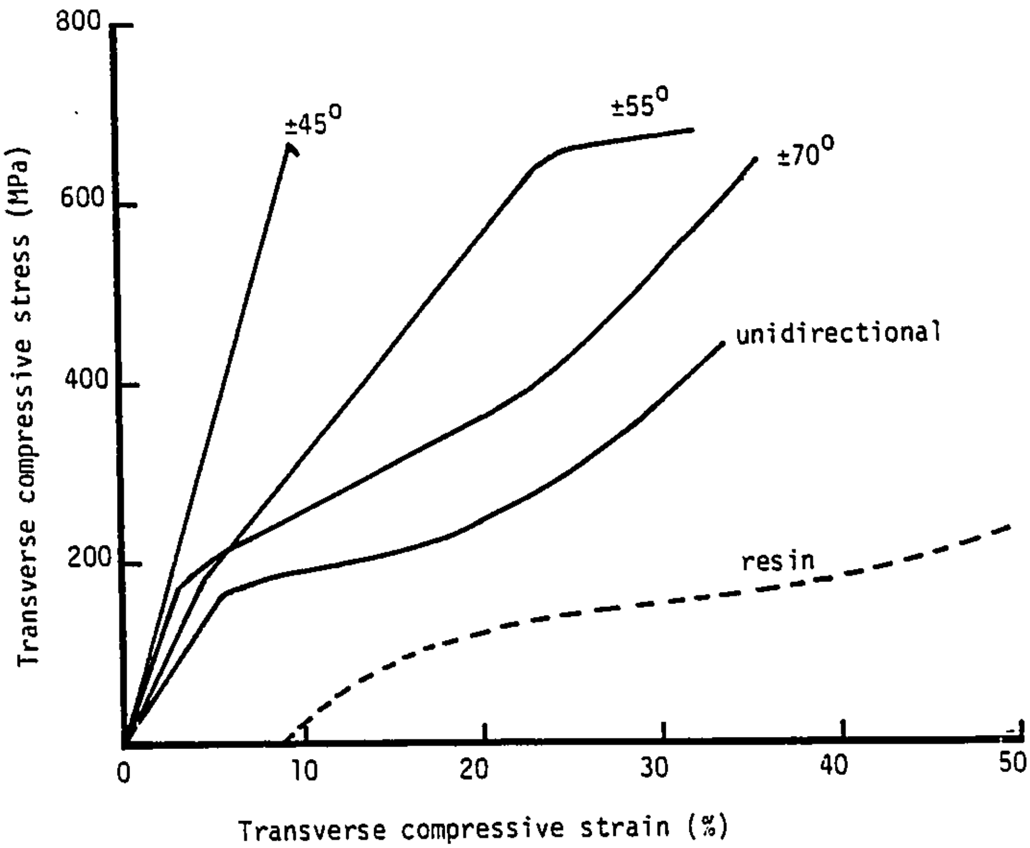

Figure 5–6 Stress–Strain Curves for Transverse Compressive Testing of S2–Glass Angle–Plied Composites

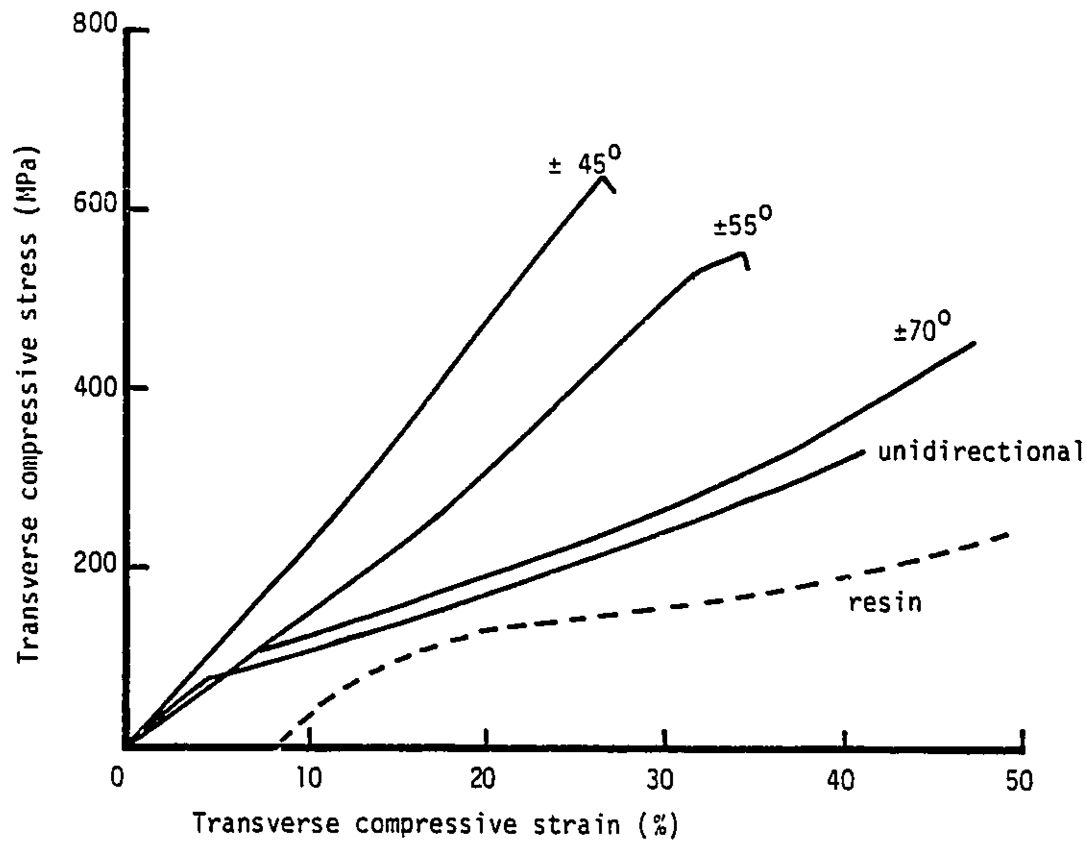

Figure 5–7 Stress–Strain Curves for Transverse Compressive Testing of Kevlar 49 Angle–Plied Composites

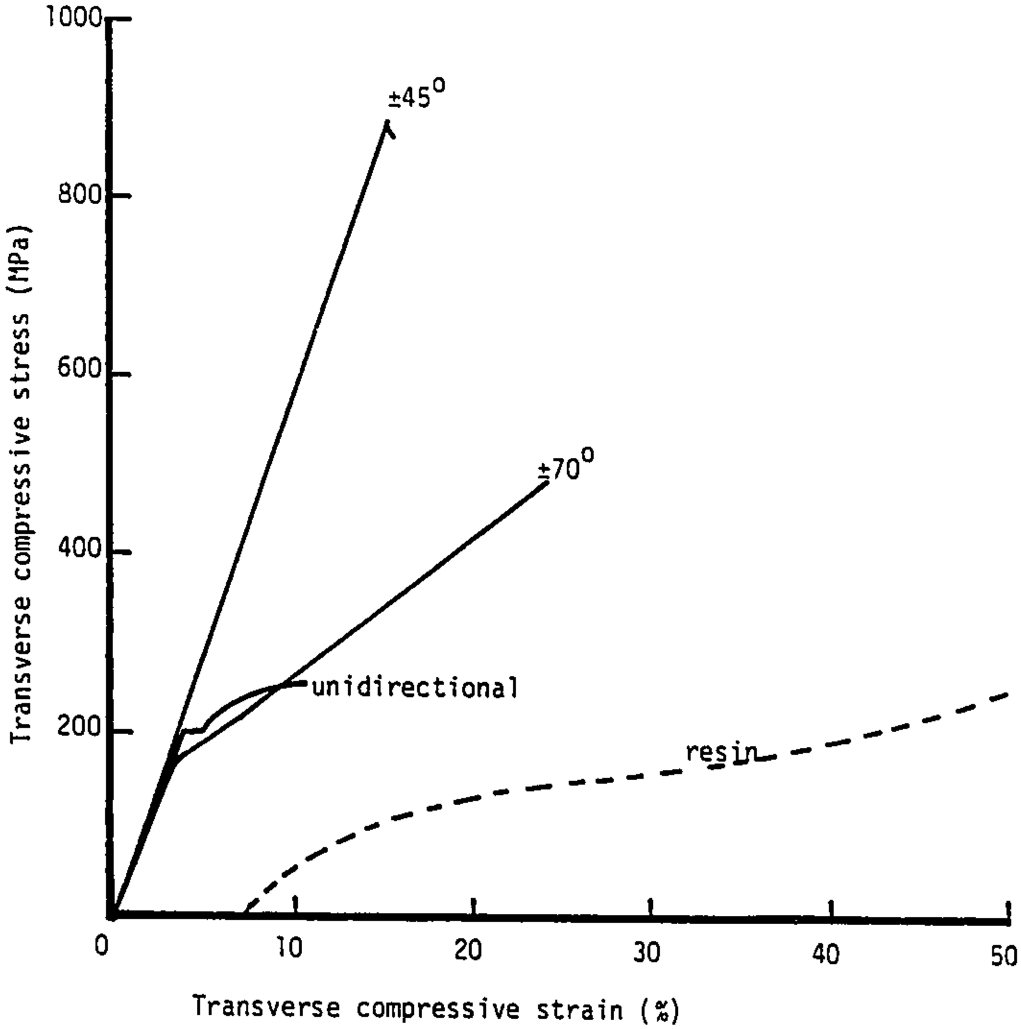

Figure 5–8 Stress–Strain Curves for Transverse Compressive Testing of E/XA–S Carbon Angle–Plied Composites

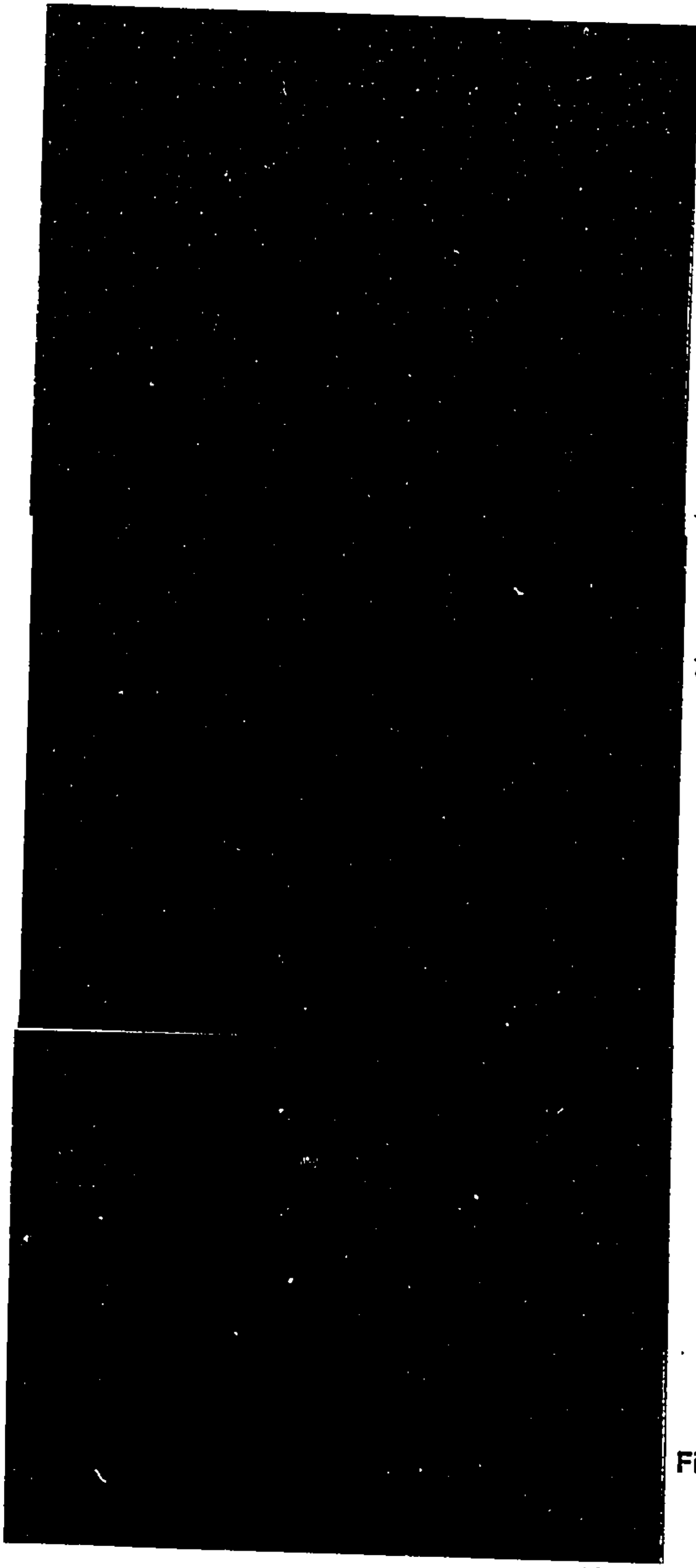

S2-glass composite specimens (clockwise from lower right: unidirectional, ± 70°, ± 55°, ± 45°)

Kevlar 49 composite specimens (clockwise from lower right: unidirectional, ± 70°, ± 55°, ± 45°)

E/XA-S carbon composite specimens (upper: ± 45°; left: unidirectional; right: ± 70°)

Figure 5–9 Failed Composite Specimens

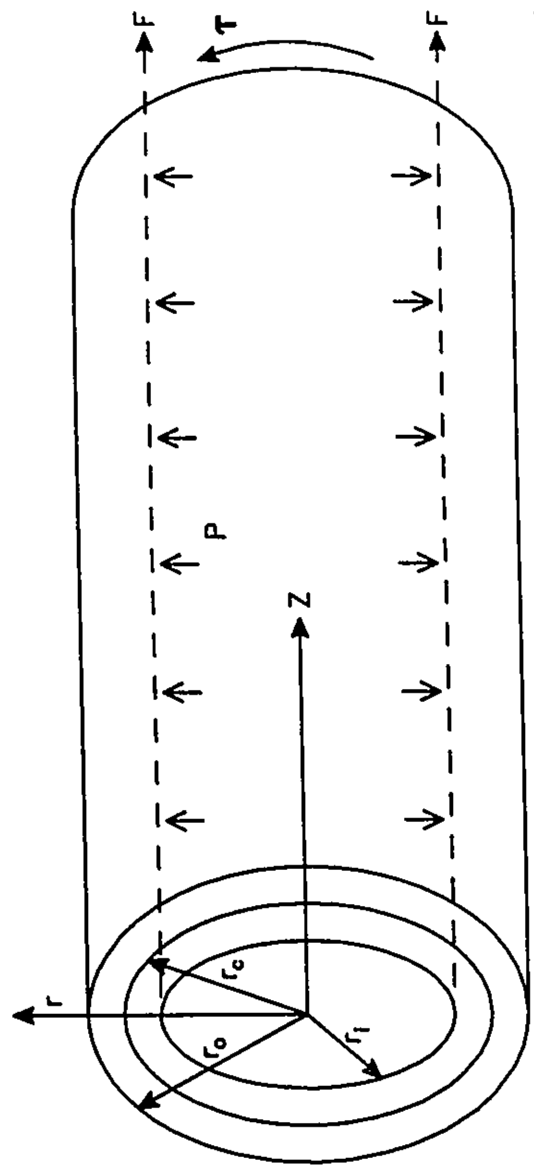

Figure 5–10 Cylinder Geometry

Figure 5–11 Semi–infinite Cylinder Hinged at the Origin

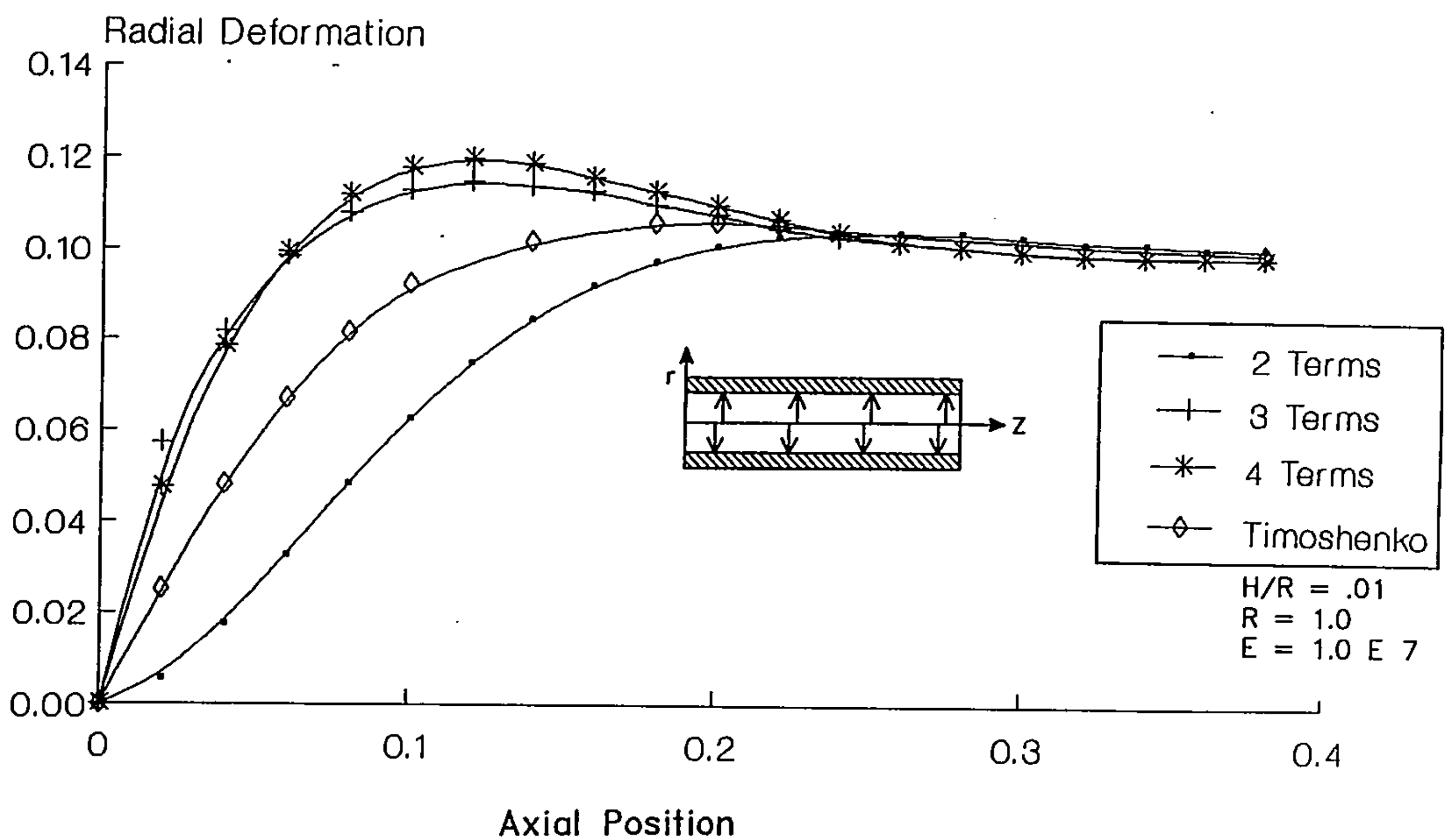

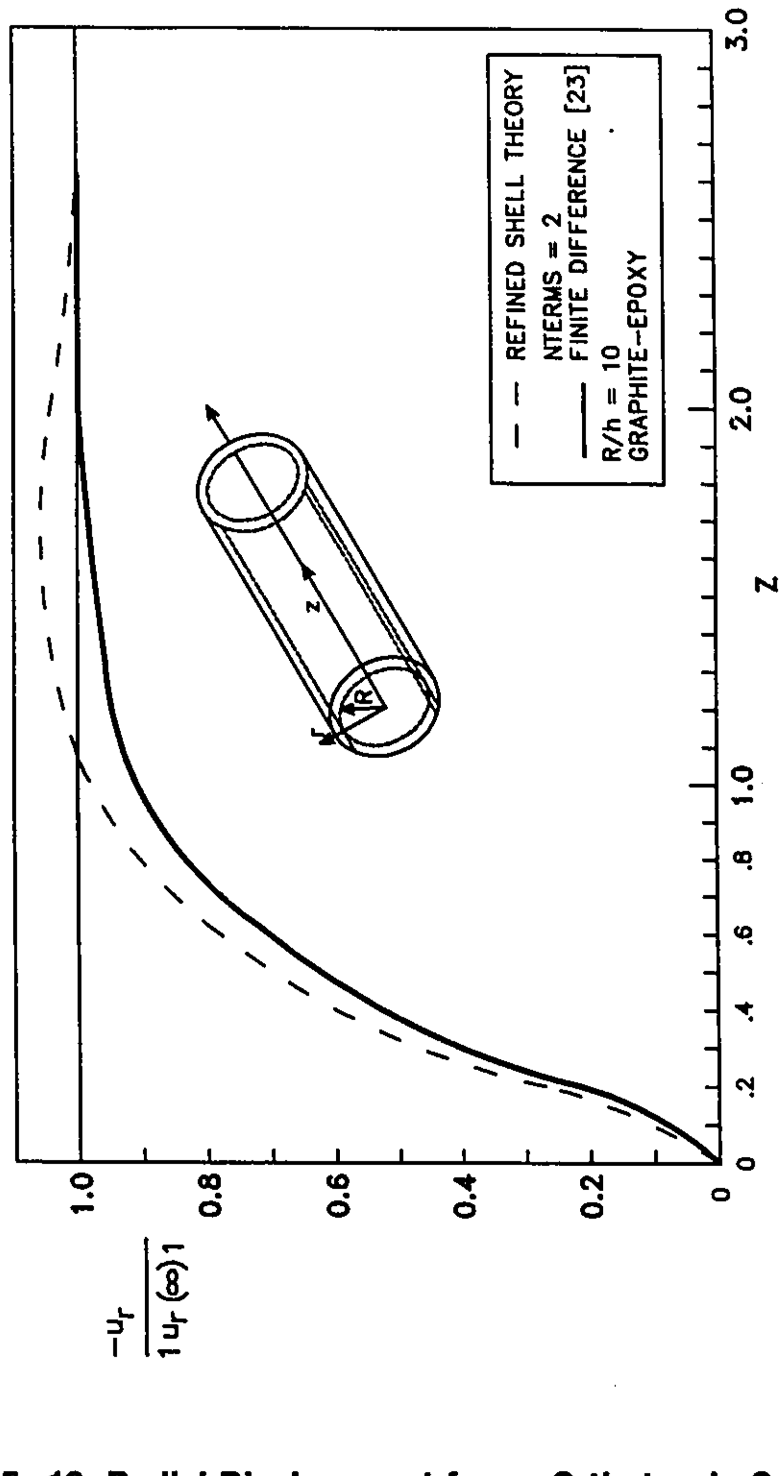

Figure 5–12 Radial Displacement for an Orthotropic Cylinder of Finite Length

Figure 5–13 Thin Isotropic Cylinder Rigidly Clamped at the Origin

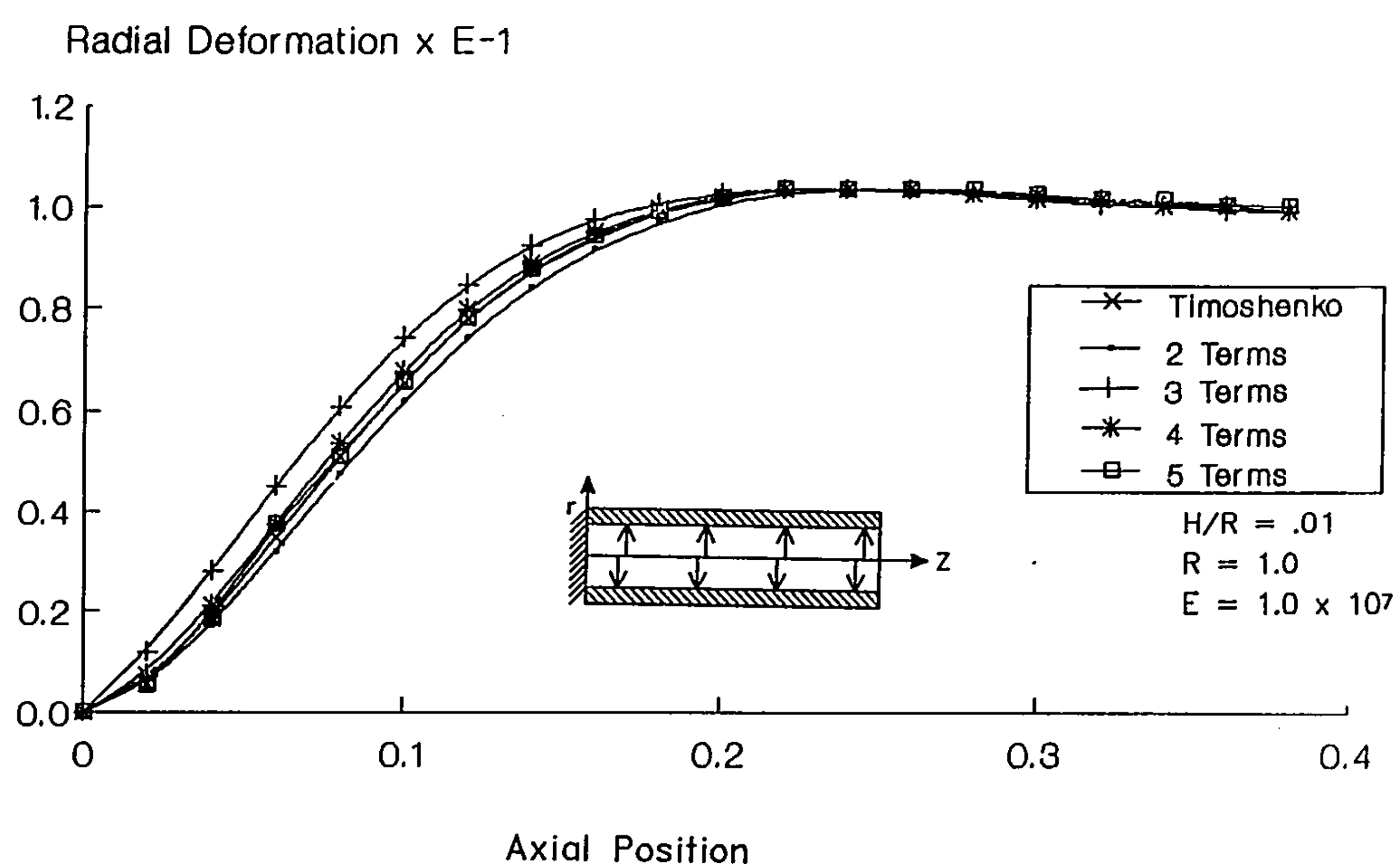

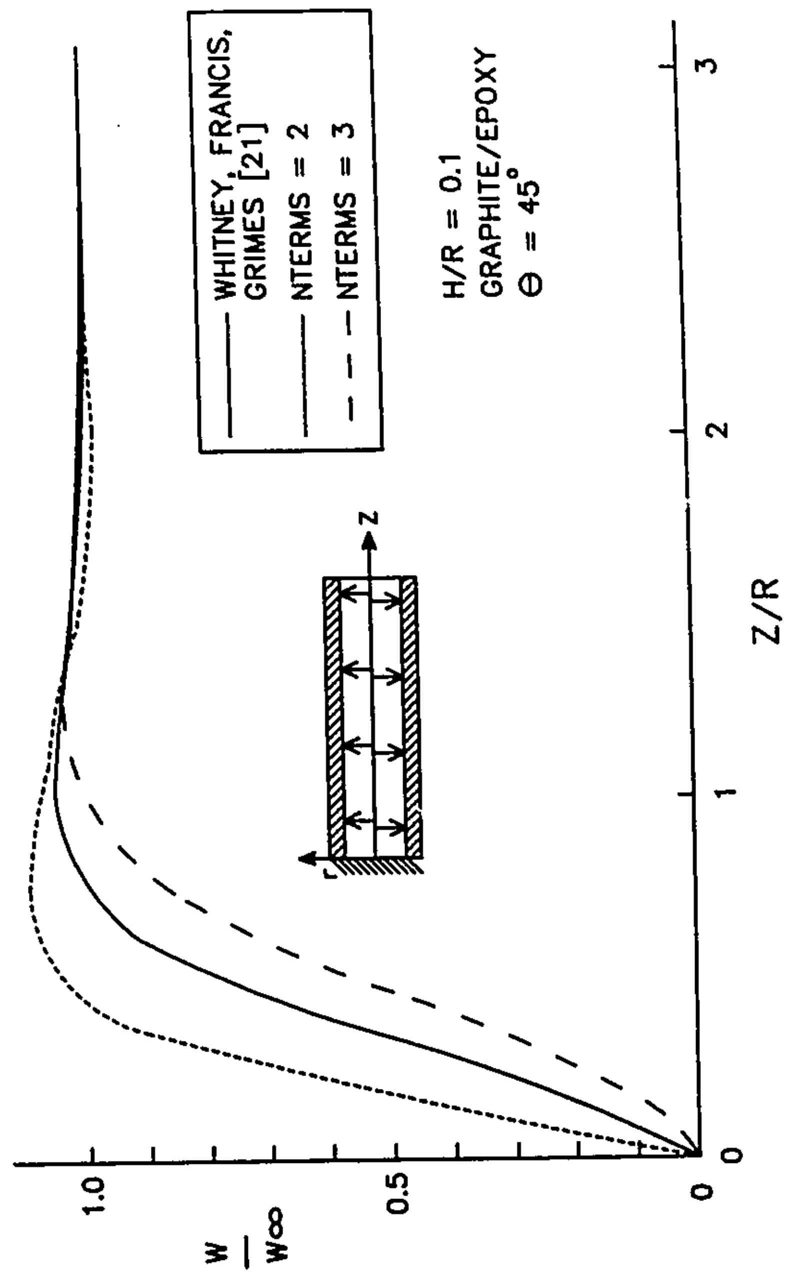

Figure 5–14 Thin Orthotropic Cylinder Clamped at the Origin

Chapter 6

EXPERIMENTAL CONFIRMATION OF THE THICK SHELL THEORY

6.1 Thick Shell Comparison

Because thick wall comparisons, either experimentally or theoretically, are not available to test the multi-term refined shell theory, it was decided to manufacture a thick wall cylinder from a material that could be classed as orthotropic. Internal pressure was chosen as the loading mechanism since it simultaneously provided a radial and an axial load to the closed ended tube.

A continuous fiber composite laminate, if it is to be orthotropic, must consist of parallel fibers aligned in a helical path on a cylindrical surface (Figure 6–1). The entire wall is of necessity, uni–angular, thereby eliminating the interaction effects of an interwoven laminate (Figure 6–2).

Further, to be valuable as a confirmation tool, this specimen would have to be thick enough to require five, six, or more terms to adequately express its surface strains, yet be flexible enough that surface strains of monitorable size would be seen with pressurization sources available.

Such a specimen is detailed in Table 6–1; surface strains along the tube axis are shown in Figures 6–3, 6–4, and 6–5. This specimen will be fabricated on a filament winding apparatus developed by the author and subsequently tested in hydrotest facilities also developed by the author. Details of the specimen manufacturing and test procedure will be provided later in this chapter.

6.2 Review of Tubular Test Data

Although the cylinder has been extensively used to determine the response of a composite material to a uni–axial or biaxial stress field [15, 16, 17, 18, 19], little work has been done on the actual monitoring of end–effect strains in such specimens. No results are available for thick–walled composite cylinders.

In a recent study [22], a tubular specimen using a thickened wall at the grip attachment area was developed. Finite element studies confirmed the hypothesized gradual increase of stresses from the clamp to the specimen mid–span values. This type of configuration cannot be directly compared to the results of the analysis of the previous chapter.

Guess and Haizlip [20] reported experimental measurements on rigidly clamped orthotropic thin walled tubes. Insufficient experimental details were presented to give a comparison of actual results to values calculated by a Case III analysis.

An experimental comparison is available in an early work of Whitney, Grimes, and Francis [21]. They presented experimental data for a thin orthotropic tube subjected to axial loading. A comparison to a Case III analysis is presented in Figure 6-6. Because of the thin-walled nature of the specimen, the use of higher order terms in a shell theory is not required.

6.3 Filament Winder Development

The filament winding process consists of depositing resin impregnated fibers on a rotating mandrel, in a predetermined and controlled manner. A typical process is the wet winding process, where dry fibers are passed through a bath of liquid resin for impregnation before being wound on the mandrel. The wound structure is subsequently cured.

Filament winding machines must control a sizable number of manufacturing variables if defect free composite tubes are to be produced. A summary of these are included in Table 6-2. It is apparent that a relatively sophisticated piece of manufacturing equipment is required.

Extensive modifications were undertaken to convert an existing laboratory computer controlled single axis hoop winder to a computer controlled five axis helical winder (Figure 6-7). Stepper motors coupled to low friction linear drives provided the linear payout eye motions. A stepper motor driven rotary table provided payout eye rotation. The completed filament winder is shown in Figure 6-8.

The original winder as developed by the author, provided moment to moment control of the stepper motor positions by an open loop control system driven by two Z-80 microprocessor controllers. An Apple II microcomputer acted originally as the host computer to direct the simultaneous motions of the stepper motors (see Figure 6-9). Modifications to the machinery subsequently recommended by the author have replaced the eight bit micro system with much faster 16 bit controllers and a 32 bit microcomputer.

Operational software for the winder was developed in two forms:

(1) dedicated routines to perform a specific task written in BASIC.

(2) a general routine (developed by Center Computer Consultants of State College, Pennsylvania) which allowed general helical patterns to be wound.

The basic concept was that a series of data tables were prepared as instructions for each of the five motors. The control program stepped each motor simultaneously for a defined mandrel rotation step size. The program also checked that the limit switches had not been closed, and for operator instructions.

The capabilities of the winder (other than its slow winding speed) met or exceeded commercial units available at the time. The overall cost was much less than that of a commercial unit. Development time including designing, fabrication, and extensive debugging, was approximately three years.

The positional accuracy for the filament winder was measured and found to be less than 2.5×10^{-2} mm on the X, Y, and Z positions. Rotational accuracies were not measured but because of the large stepper motor size, these can be assumed to be $\pm$ 1/2 pulse on a 200 pulse/rotation stepper motor. The need for precise filament placement, as postulated in Chapter 1, had been met.

6.4 Specimen Development and Manufacture

The development of a thick-walled specimen for the experimental confirmation of the developed theory proceeded in three relatively distinct stages:

(1) helically wound Kevlar 49 vessels with a thin aluminum liner

(2) helically wound E/XA-S vessels with a thin aluminum liner

(3) uni-angular E/XA-S vessels with an elastomeric liner

The first task of the specimen manufacturing program was to develop the specimen winding procedure itself. Shallow angle Kevlar 49 specimens were wet woundon a precision thin-walled aluminum mandrel which acted as the vessel liner. To prevent slippage on the dome end of the specimen, winding along the geodesic path that provided zero transverse forces was accomplished.

For a composite pressure vessel, the wind angles are determined by considerations of the results of stress analysis and of winding geometry limitations. In helical filament winding of closed-end cylindrical pressure vessels, the ends are filament wound at the same time as the cylindrical portion. There is a specific path that the strand or tow follows over the cylinder and end domes. A single path is shown in Figures 6-10 and 6-11.

For the strand or tow path to be tangent to the polar boss, each point on the path is defined by two radii, r_1 and r_2 [84]:

(6-1) $$r_1 = \frac{-\left[1+(y')^2\right]^{\frac{3}{2}}}{y''}$$

(6-2) $$r_2 = \frac{-x\left[1+(y')^2\right]^{\frac{1}{2}}}{y'}$$

For a balanced stress condition (based upon netting analysis)

(6–3) $$\frac{r_2}{r_1} = 2 - \tan^2 \omega^*$$

In order to prevent slipping, the path must be the geodesic, i.e.

(6–4) $$X \sin \omega^* = \text{constant}$$

Substituting equations 6–1, 6–2, and 6–3 gives

(6–5) $$x \frac{d^2y}{dx^2} + \left(\frac{dy}{dx}\right)^3 (\tan^2\omega^* - 2) + \frac{dy}{dx}(\tan^2\omega^* - 2) = 0$$

where $$\omega^* = \sin^{-1} \frac{R_c \sin \omega}{x}$$

and ω= helical wind angle in cylindrical portion of vessel.

The boundary conditions are:

(6–6) $$\begin{aligned} y &= 0 \\ y' &= -\infty \qquad \text{at} \quad r = R_c \end{aligned}$$

The solution of equation 6–5 will produce the dome contour (geodesic isotensoid).

In order to follow the path shown in Figure 6–10, it is necessary to coordinate the position on the dome with mandrel rotation, ϕ. Hofeditz [85] has suggested a digital method. This has been converted to a differential equation form

(6–7) $$\frac{d\phi}{dx} = \frac{d\omega^*}{dx} \left(1 + \left(\frac{dy}{dx}\right)^2\right)^{1/2}$$

where at $x = R_c$

(6–8) $$\phi = 0$$ $$\frac{d\phi}{dx} = 0$$

The actual solution of these equations could not be found in the literature. They do exist as proprietary programs of the suppliers of computer controlled filament winders. Both equation 6–5 and 6–7 are very dependent on $\frac{dy}{dx}$ which for both is initially very large. Thus, a change of variables was employed where

(6–9) $$x' = R_c - x$$ $$g = 1/\left(\frac{dy}{dx'}\right)$$

Equations 6–5 and 6–7 then become:

(6–10) $$\frac{dg}{dx'} = -\left(g + \frac{1}{g}\right)\left(2 - \tan^2 \omega^*(x')\right)$$

(6–11) $$\frac{d\phi}{dx} = \frac{d\omega^*(x)}{dx}\left(1 + \frac{1}{g^2}\right)^{1/2}$$

where $$\omega^*(x) = \sin^{-1}\left(\frac{R_c \sin\omega}{R_c - x'}\right)$$

and at $$x' = 0\ ; \quad g = 0\ , \quad \phi = 0$$

Both equations 6–10 and 6–11 were solved using a 4th order Runge–Kutta routine. The assumption of an isotensoid dome is valid up to $\omega^* = \mathrm{Tan}^{-1}\sqrt{2}$. In general, a spherical radius to a junction with the polar boss is then used to complete the contour.

This portion of the program generated two items of note. The first was that although the vessel winding software performed in an excellent manner, the process was very slow. The second item was that an elastomeric bladder was required inside the aluminum shell to prevent premature leakage at the aluminum weld sites. A silicone thermosetting elastomer was centrifugally cast in the specimen to alleviate this defect. The completed specimens are shown in Figure 6–12.

The second specimen development task saw the abandonment of the geodesic pattern on the vessel domes in favor of the much faster linear velocity ramp internal to the stepper motor controllers. Slippage now occurred on the domes however which was eliminated with a circumferential ring of pins at the dome cylinder juncture. The liner mandrel was also redesigned so that the ends were made of steel, and reusable, and the central section was a threaded aluminum tube. The internal elastomeric bladder was changed to a thermosetting polyurethane potting compound. This series of four vessels (Figure 6–13) attained an ultimate pressure capacity in excess of 100 MPa.

For completeness, the manufacturing details and test results for the Kevlar 49 and the E/XA–S vessels are shown in Tables 6–3 and 6–4.

The third specimen development session saw the introduction of a uni–angular wall, were a single angle material could be tested. To eliminate the effects of the metallic liner, various dissolvable mandrels were tried. In early attempts, I used a water soluble polyvinyl alcohol as a binder for various bits of granular material such as sawdust, clay, etc. Brittleness, cracking, and shrinkage prevented the development of this type of dissolvable mandrel. A second mandrel development used a water soluble glued paper pressed into a cylindrical paper laminate and machined to shape. This was dissolved after the vessel was cured by soaking in water for ten hours. The vessel was subsequently lined with a polyurethane elastomer. A twenty degree single angle vessel was wound over this mandrel to test the concept which structurally proved adequate.

The process of manufacturing a cylinder with a fiber composite at a single angle requires the complete stopping and reversal of the rotating mandrel. A dual row of pins not only provided anti-slip guides for the fibers at the specimen domes, but also mandrel reversal so that the mandrel could be stopped and reversed without the fibers falling from the mandrel.

This process of fiber placement has not, to the best of the authors knowledge, been performed by others. Only recently, have commercial machines become available that allow the option of mandrel reversal, a requirement for such a process.

The manufacture of uni-angular composite tubes by a continuous filament winding process required a unique "pinned" mandrel design [74], developed earlier by the author for thin walled pressure vessel studies (see Figure 6-14). Fiber placement proceeded as follows:

(1) With the mandrel advancing in a given rotational direction, the fiber payout eye placed a helix of fibers on the mandrel surface. The payout eye motion paralleled the surface of the mandrel, allowing the fibers to be caught and retained by the pins.

(2) When a pass along the length of the mandrel was completed, the transverse motion would stop, the mandrel would rotate a predefined angle and then stop (a dwell).

(3) The traverse motion would reverse itself along the mandrel length. The fibers would be caught in the first set of pins, at which time the mandrel would begin rotation in a reversed direction.

(4) This process would be repeated at each end of the mandrel until the lamina was complete.

The result was a continuous fiber uni–angular lamina (see Figure 6–15) in a tubular geometry. Several lamina could be stacked to get a uni–angular laminate, or lamina angles could be varied through the wall.

The laminate will be made of materials detailed in Table 6–5. This particular vessel will be fabricated and tested by M. Tenace as part of his MSc. thesis research. The graphite is wet wound with an epoxy matrix onto the surface of the mandrel. A clamped end is manufactured by overwrapping the specimen end with alternating layers of hoop and axial fibers. A teflon ring is used to provide a 'clean' edge on the retaining clamp. The composite is to be consolidated with a wrap of heat shrink tape as detailed in Table 6–6. Upon curing, the heat shrink tapes would shrink, squeezing excess resin into the absorbent cloth sandwiched in between the two heat shrink tape layers. In addition to a consolidated composite, this technique provides a smooth surface on the tube for strain gauge application.

A uni–angular composite tube can retain very little internal pressure without developing a leak path between the fibers. To avoid this difficulty, a low modulus, high elongation polyurethane liner can be centrifugally cast on the tube's interior. The details of the liner are provided in Table 6–7.

Triple gauge strain rosettes (0, 45°, 90°) are to be installed along the length of the specimen in a hoop–axial direction to complete the specimen.

6.5 Pressure Test Facility

Pressurization and containment of the specimen can be done with an apparatus developed by the author. The pressure source is a 70 MPa. hydraulic cylinder mounted in an Instron tensile test frame, as shown in Figure 6–16. This arrangement allows pressures up to 70 MPa. for specimen testing. The pressure rise could take several forms:

(1) A constant rate of pressure increase was obtained by controlling the Instron servo–hydraulic mechanism with a pressure transducer in a feed–back loop (on a strain gauge input channel).

(2) A constant volume flow could be obtained by allowing the tensile tester ram to move with constant velocity.

(3) A cyclic pressure change was available when the tensile machine was in the cyclic test mode. This could be either pressure or volume controlled.

The use of this pressure source by the author is documented [75].

The containment facility shown in Figure 6–17, houses the specimen during pressure testing. This chamber, along with its internal mirrors and lights allows the video taping of the specimen during hydrotesting (for failure analysis purposes). All parts of the specimen were visible on the three internal mirrors.

6.6 Specimen Data

After purging the specimen of any entrapped air, the internal pressure in the specimen is to be raised at a rate of 300 KPa/min with strains and pressure monitored with a data acquisition unit.

The computed curves (Figures 6–3, 6–4, and 6–5) are from data collected at the University of Ottawa composite material facility for the same graphite/epoxy material as used in the specimen. This data is included in Appendix A of this report.

An examination of the axial surface strain curves reveals several interesting points:

(1) Two or three terms in the power series do not adequately describe the end effects for a thick clamped generally orthotropic tube (at least six are required).

(2) A sharp concentration of axial strain exists near the clamped edge.

(3) The infinite cylinder axial strain is relatively insensitive to the number of terms in the power series expansion.

The other strain variations along the cylinder would suggest that:

(1) $\gamma_{\theta z}$ has a sharp singularity near the clamped edge.

(2) More than three terms are required to adequately describe $\gamma_{\theta z}$ in the vicinity of the clamped edge.

(3) The circumferential strains approach zero at the clamped edge.

(4) $\varepsilon_{\theta\theta}$ is sensitive to the number of terms in the series in the vicinity of the origin.

(5) $\gamma_{\theta z}$ is not sensitive to the number of terms in the series three or more pipe radii away from the clamped edge, whereas $\varepsilon_{\theta\theta}$ is.

As mentioned earlier, lack of time has prevented the final completion of the vessel at the time of writing. Details of the results of this program will appear in the MSc. thesis of Mr. Tenace.

VARIABLE	SPECIFICATION
inside radius	0.0295 m
outer radius	0.0492 m
fiber orientation	30^o
material	graphite/epoxy $V_f = 65\%$
length	greater than .2 m
end configuration	clamped
typical strains	0.1 – 0.2% at 55 MPa

Table 6–1 Clamped Cylindrical Specimen Geometry

VARIABLE	RESULT IF NOT CONTROLLED
Fiber/resin ratio	wall thickness variations volume fraction variations non-homogeneties in wall
Fiber wet out	volume fraction variations
Resin viscosity	fiber wet-out voids
Fiber Tension	fiber pre-stress variations void content fiber bridging
Fiber position control – mandrel rotation position – pay out eye X axis Y axis Z axis rotation	laminate mechanical property variations fiber gaps

Table 6–2 Variables for Filament Winding

Table 6–3 Composite Pressure Vessel Testing

VESSEL NO.	TESTING SYSTEM		ULTIMATE FAILURE PRESSURE (MPa)	FAILURE DETAILS
	TYPE	LOCATION		
K49-21-1	70 MPa hand pump	Mech. Eng., U. of O.	5.6	- failure of weld between end and test section due to leakage of hydraulic oil past mechanical seal
K49-21-2	70 MPa hand pump	Mech. Eng., U. of O.	7.0	- failure of weld between end (with flexible aluminium joint) and test section due to leakage of oil past flexible aluminium joint
K49-21-3	70 MPa hand pump	Mech. Eng., U. of O.	8.4	- failure of weld between end test section due to leakage of oil past aerated silicone rubber seal
K49-21-4	70 MPa hand pump	Mech. Eng., U. of O.	12.4	- failure in test section
XAS-48-5	70 MPa hand pump	Mech. Eng., U. of O.	24.8	- failure of weld in test section due to improper cooling of welded test section
XAS-48-6	70 MPa hand pump	Mech. Eng., U. of O.	42.7	- failure in test section.
XAS-48-7	490 MPa intensifier pump	DME, NRCC	62.0	- failure in test section.
XAS-48-8	490 MPa intensifier pump	DME, NRCC	$>$ 102.0	- pre-mature failure of pressurization connection.

Table 6–4 Composite Pressure Vessel Fabrication

VESSEL NO.	COMPOSITE WALL			LINER				
	HELICAL WIND ANGLE	THICKNESS (mm)	END OVERWRAP	TYPE	TEST SECTION			INTERIOR SEAL
					TYPE	THICKNESS (mm)	MATERIAL	
K49-21-1	21.3°	1.865	-	3 piece, welded	extruded tube	1.25	6061-T6	-
K49-21-2	21.3°	1.865	-	3 piece, welded	extruded tube	1.25	6061-T6	flexible aluminum joint
K49-21-3	21.3°	1.865	-	3 piece, welded	machined tube	1.25	6061-T6	flexible aluminum joint + 1.5mm thick silicone elastomer layer (GE RTV 615)
K49-21-4	21.3°	1.865	90° carbon composite	3 piece, welded	machined tube	1.25	6061-T6	flexible aluminum joint + 1.5mm thick polyurethane elastomer layer (H.B. Fuller, SF 2012)
XAS-48-5	48.2°	0.673	90° carbon composite	3 piece, threaded, with end pins	machined tube	1.25	test-section, 6061-T6: ends, mild steel	O-ring seals between test section and ends.
XAS-48-6	48.2°	1.346	90° carbon composite	3 piece, welded, with end pins	machined tube	1.25	6061-T6	flexible aluminum joint + 1.5mm thick polyurethane elastomer layer (H.B. Fuller, SF 2012)
XAS-48-7	48.2°	2.794	90° carbon composite	3 piece, welded, with end pins	machined tube	1.25	6061-T6	flexible aluminum joint + 1.5 mm thick polyurethane elastomer layer (H.B. Fuller, SF 2012)
XAS-48-8	48.2°	5.727	90° carbon composite	3 piece, welded, with end pins	machined tube	1.25	6061-T6	flexible aluminum joint + 1.5 mm thick polyurethane elastomer layer (H.B. Fuller, SF 2012)

MATERIAL	DESCRIPTION
Resin (1)	Shell Epon 825 Epoxy
Hardener (1,	Pacific Anchor Chemicals Ancamine 1482
Fibers (2)	Hysal Grafil E/XAS 12K
	Dupont Kevlar 49 1420 dernier

(1) Resin to hardener ratio was 100:19, (by wt.) heated to 50° C for wet winding, and cured for 1 hour at 100° C

(2) Fiber volume fraction 65%

Table 6–5 Laminate Construction Materials

MATERIAL	DESCRIPTION
inner releasing shrink film	Airtech International
sandwich absorbent cloth	Airtech International
over high shrink film	Airtech International

Table 6–6 Laminate Consolidation Tape

COMPONENT	AMOUNT (GRAMS)
Component A (1)	50
Component B (1)	26

Preheat resin and hardener at 40° C for 1 hour prior to mixing. Mix components by hand for 1–2 minutes. Pour immediately into the specimen and start rotation.

Mount heat gun from the upper frame of the payout eye assembly directed at the cylinder. Keep the cylinder at a temperature that is warm to the touch (about 50° C) for about 4 hours.

(1) SF2012 from H B Fuller (Canada) Ltd.

Table 6–7 Polyurethane Liner Mixture

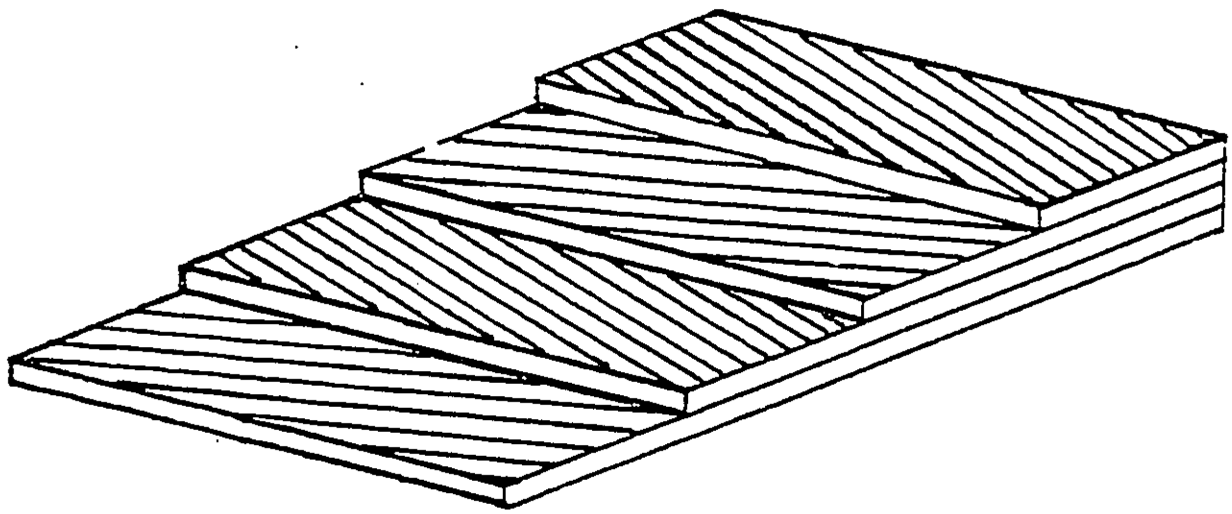

Figure 6–1 Layered Laminae

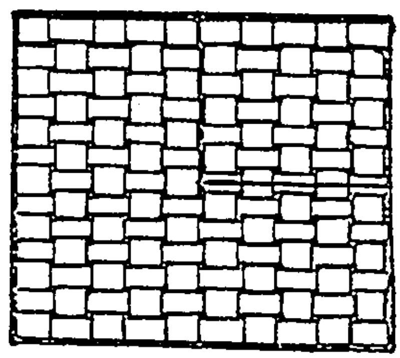

Figure 6–2 Interwoven Lamina

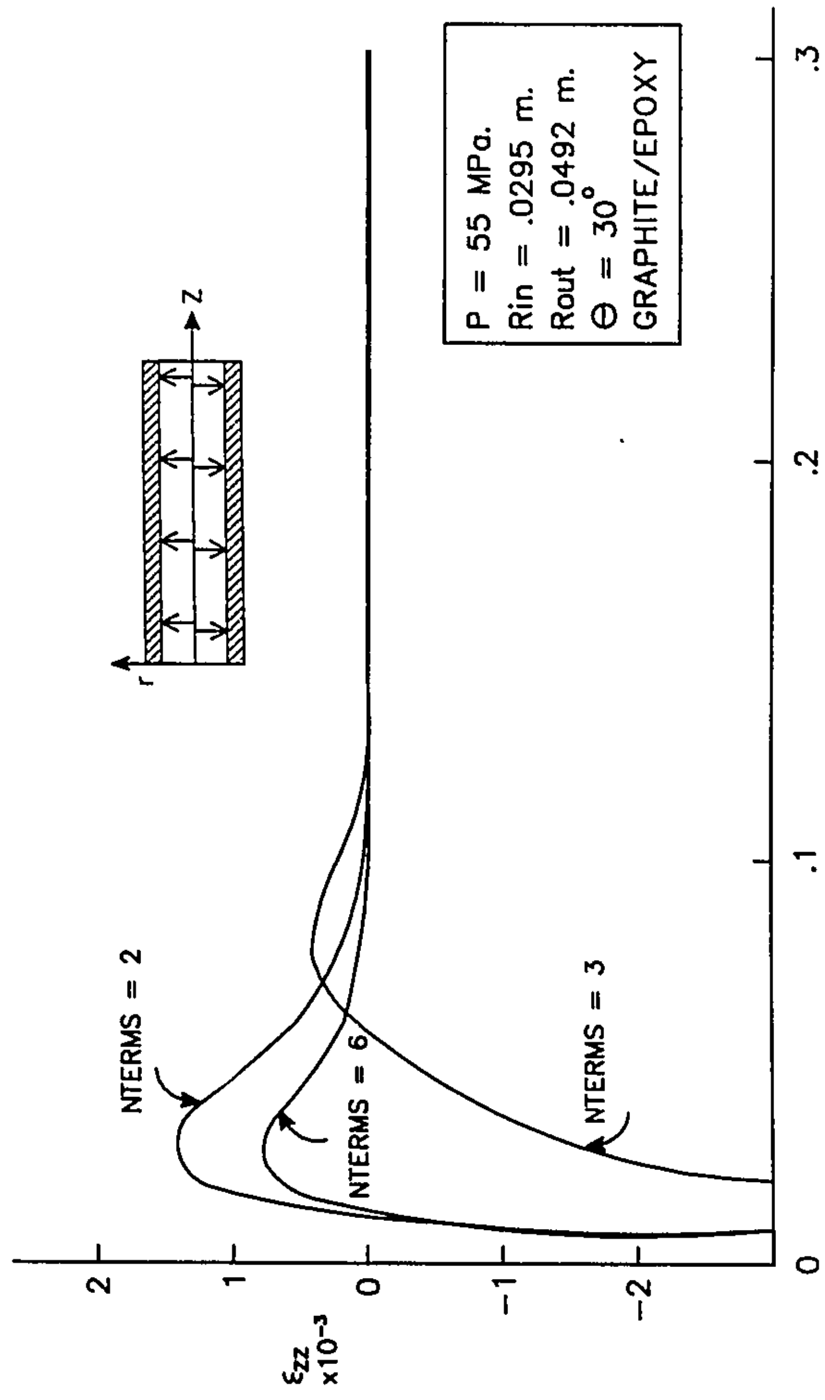

Figure 6–3 Outer Surface Axial Strain Along the Length of a Thick Orthotropic Cylinder

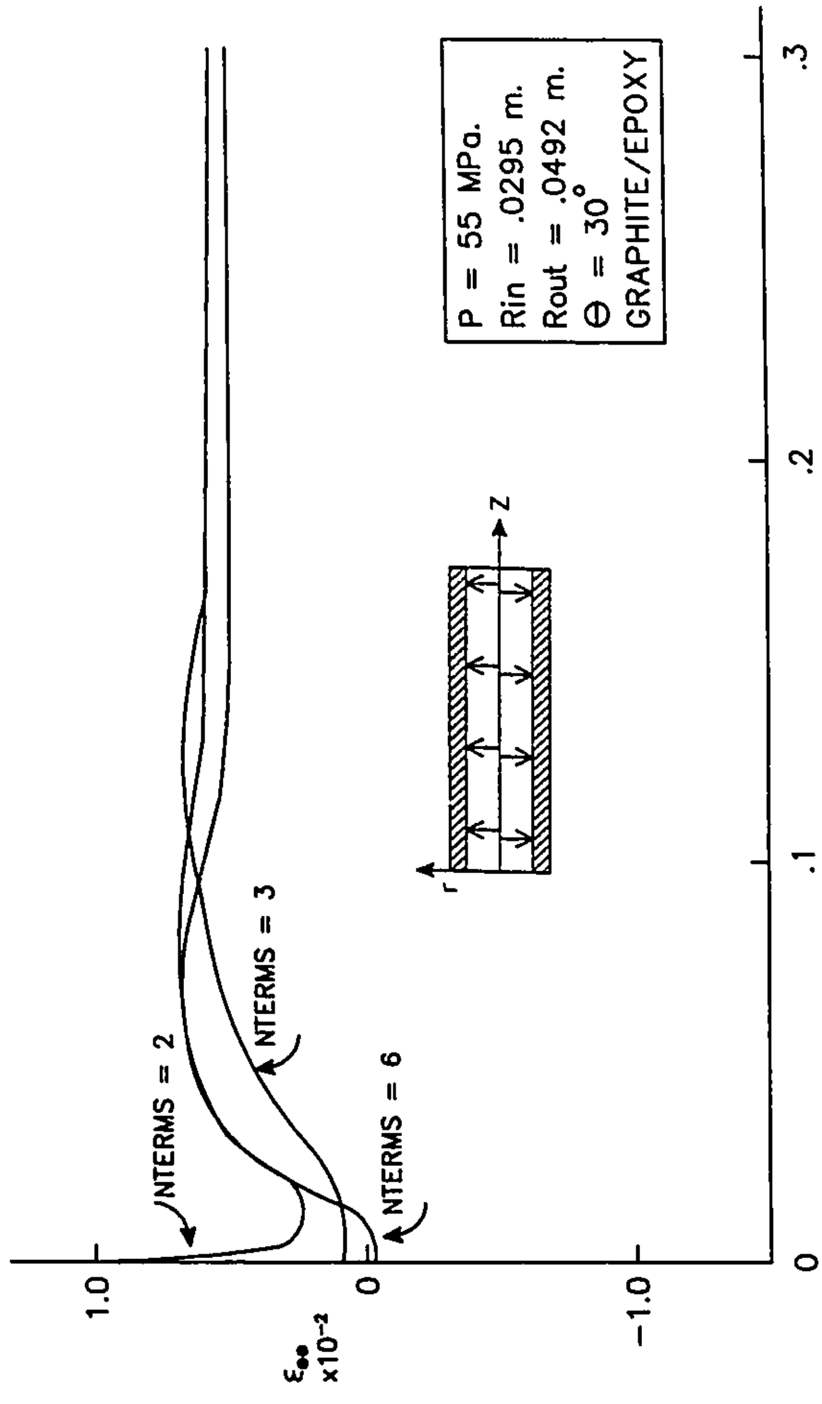

Figure 6–4 Outer Surface Hoop Strain Along the Length of a Thick Orthotropic Cylinder

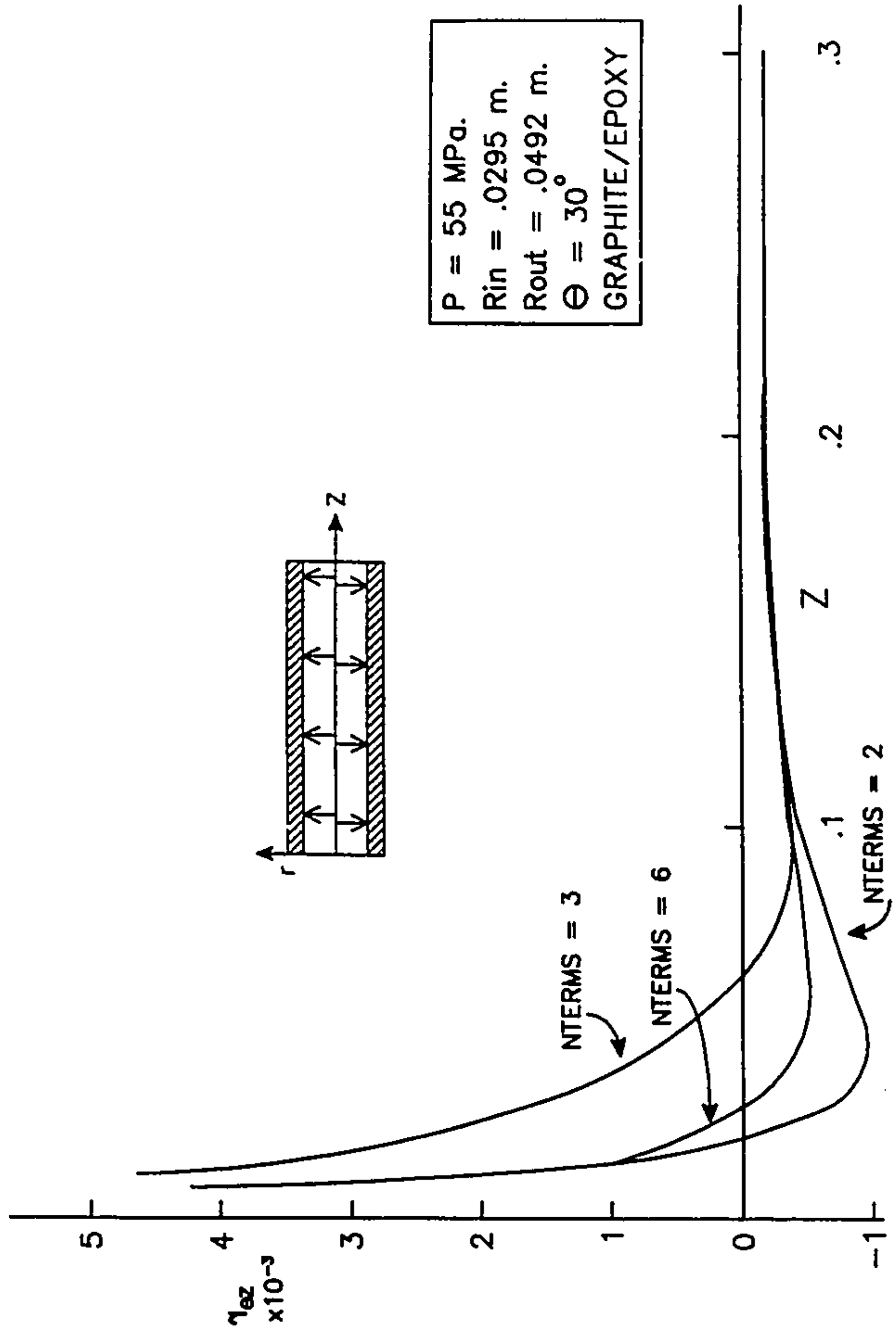

Figure 6–5 Outer Surface In–Plane Shear Stresses Along the Length of a Thick Orthotropic Cylinder

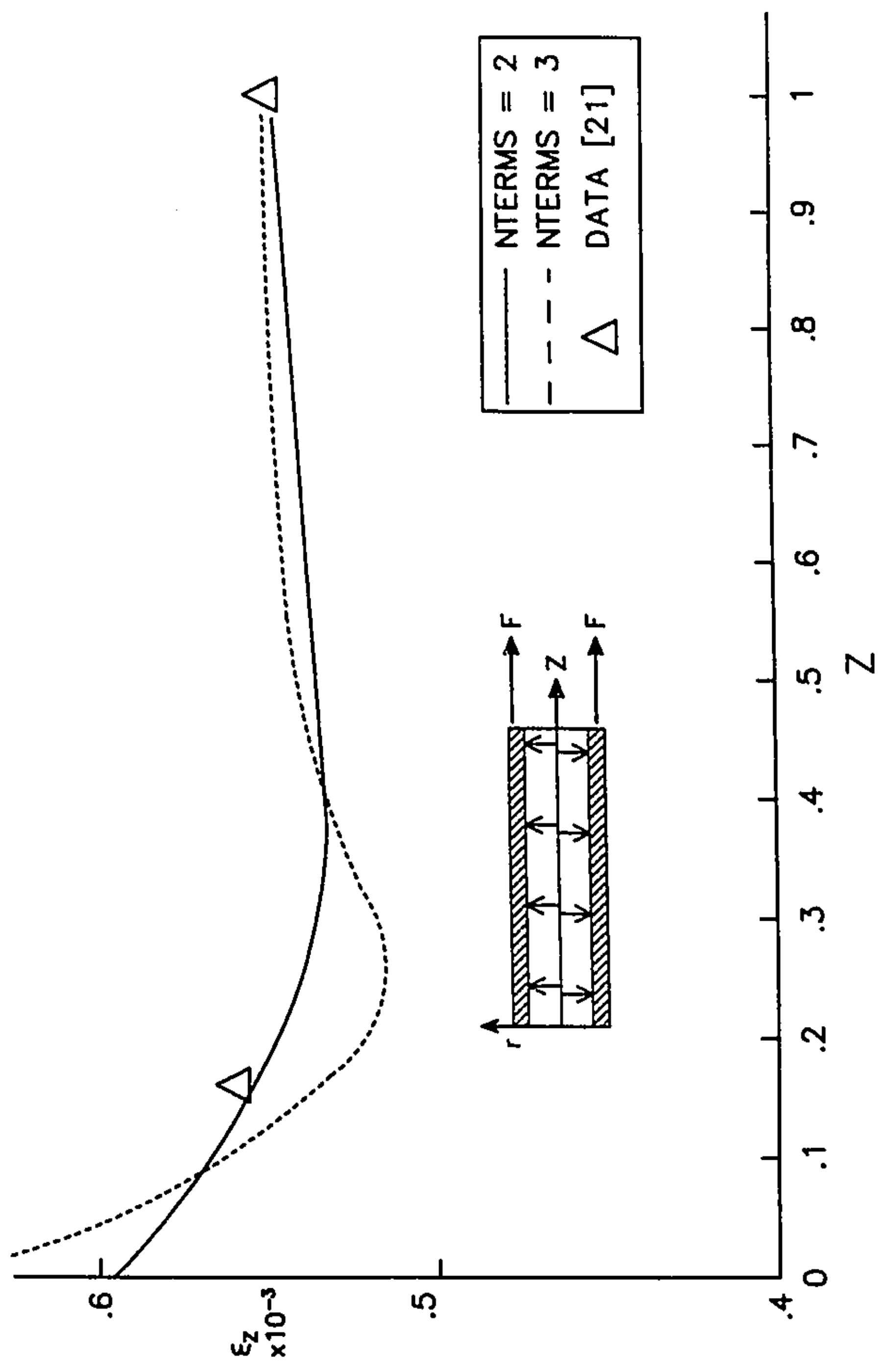

Figure 6–6 Outer Surface Axial Strains for a Orthotropic Cylinder Subject to Axial Tension

Figure 6–7 Original One–Axis Computer Controlled Filament Winder

Figure 6–8 Five–Axis Computer Controlled Filament Winder

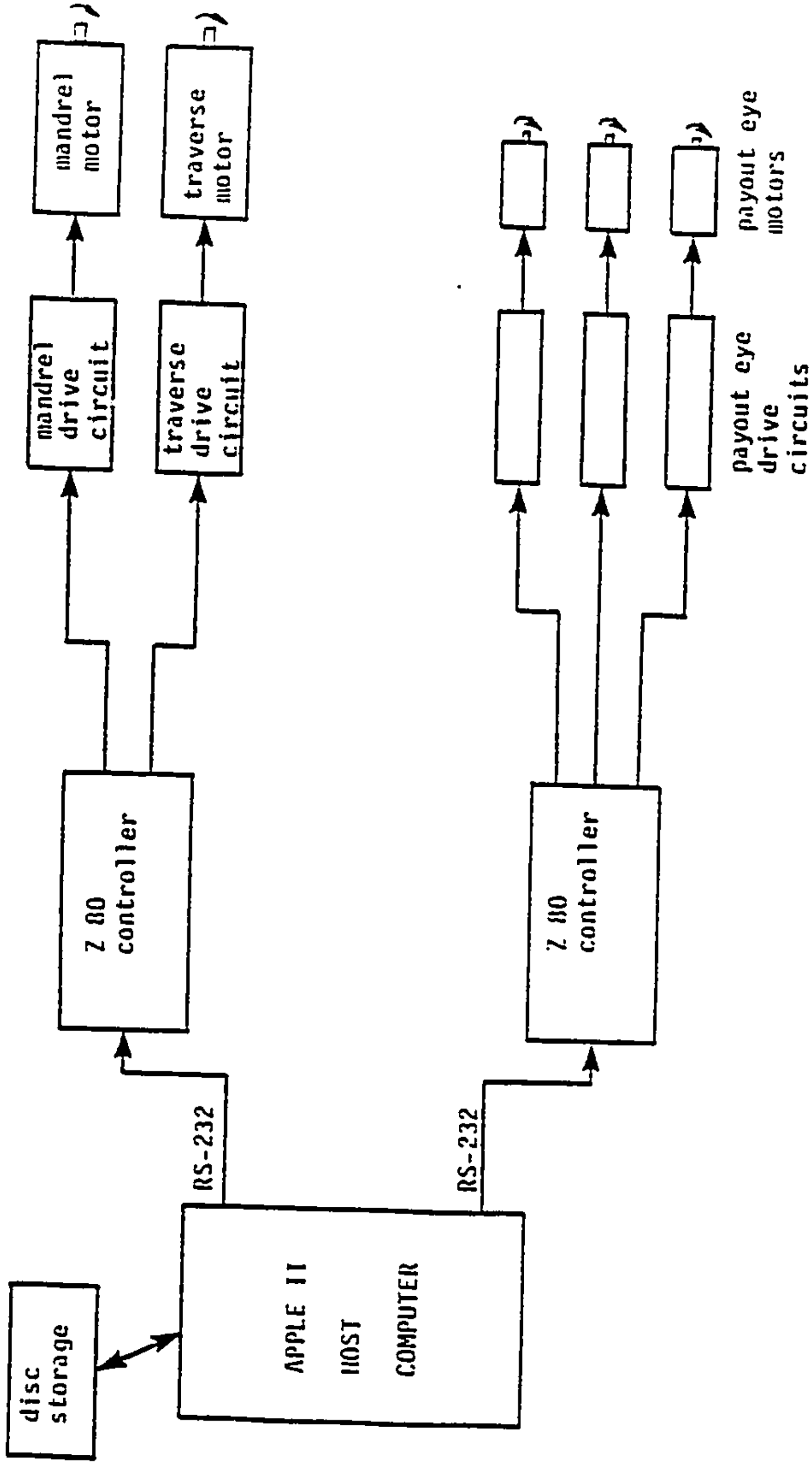

Figure 6–9 Control Hardware

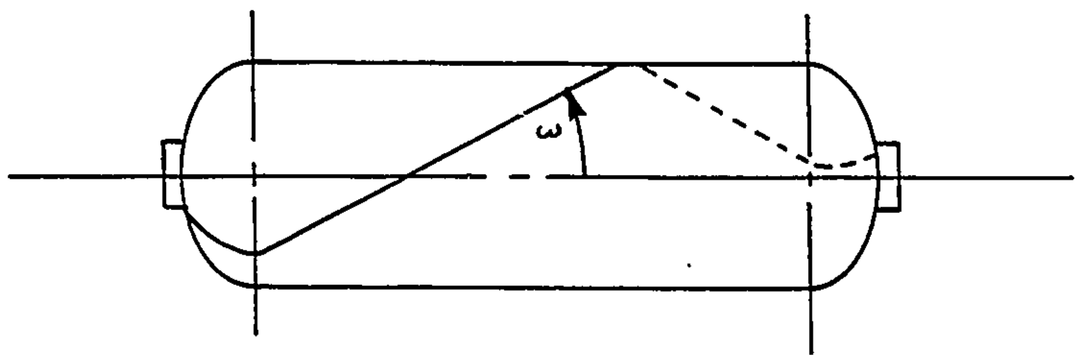

Figure 6–10 Path for Single Circuit

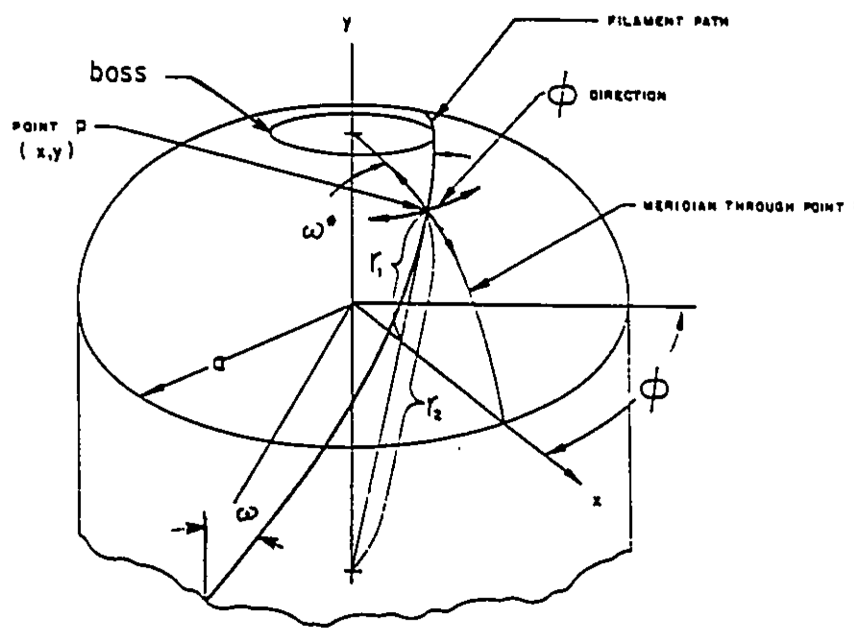

Figure 6–11 Geometry for Geodesic Path (Adapted from [84])

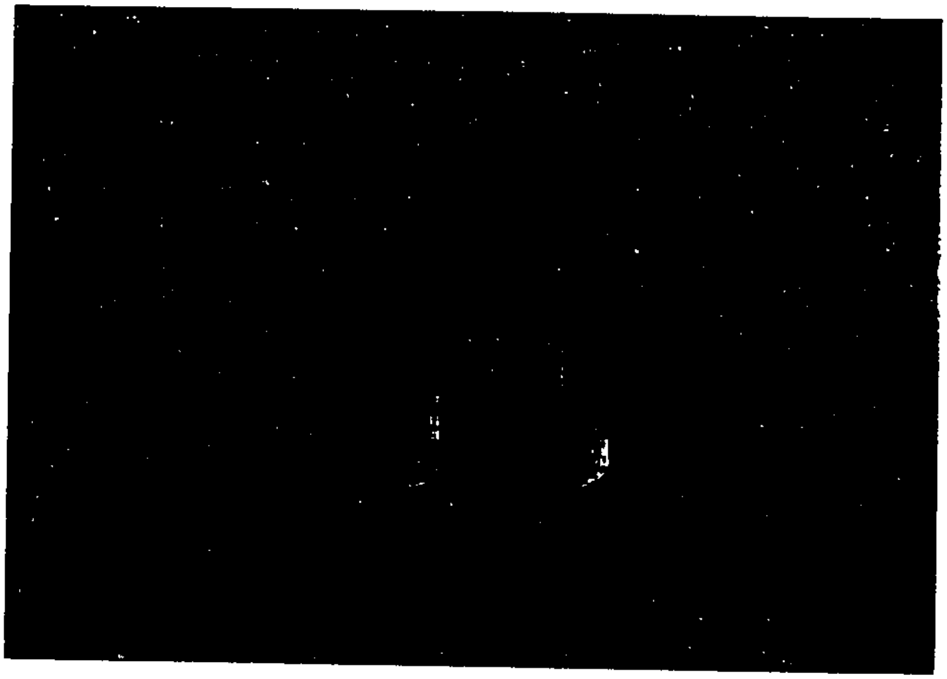

Figure 6–12 Kevlar 49/Epoxy Pressure Vessels

Figure 6–13 E/XA–S/Epoxy Pressure Vessels

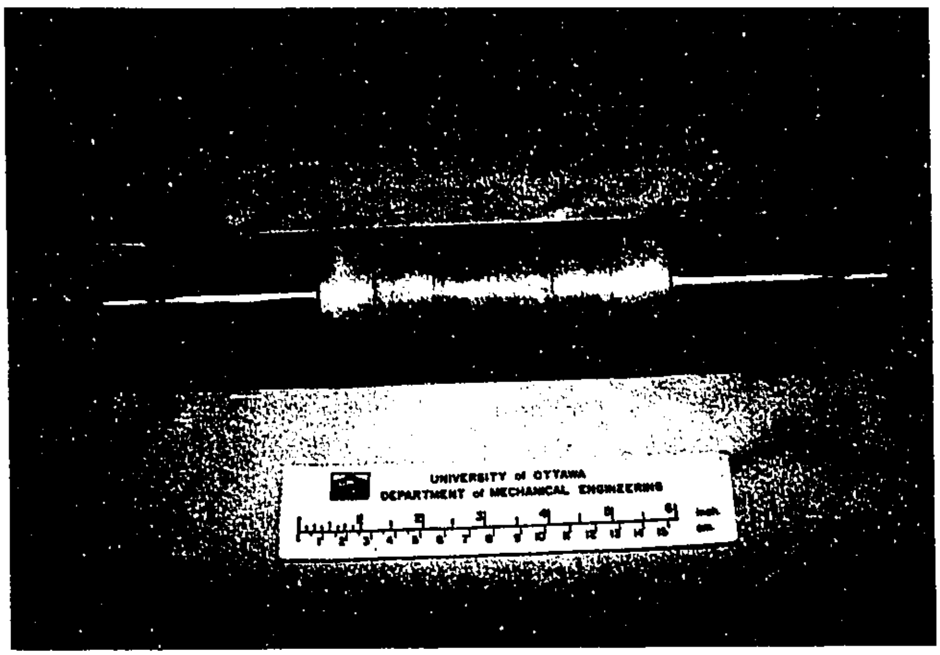

Figure 6–14 Pinned Mandrel Assembly

Figure 6–15 Continuous Uni–Angular Lamina in Tubular Form

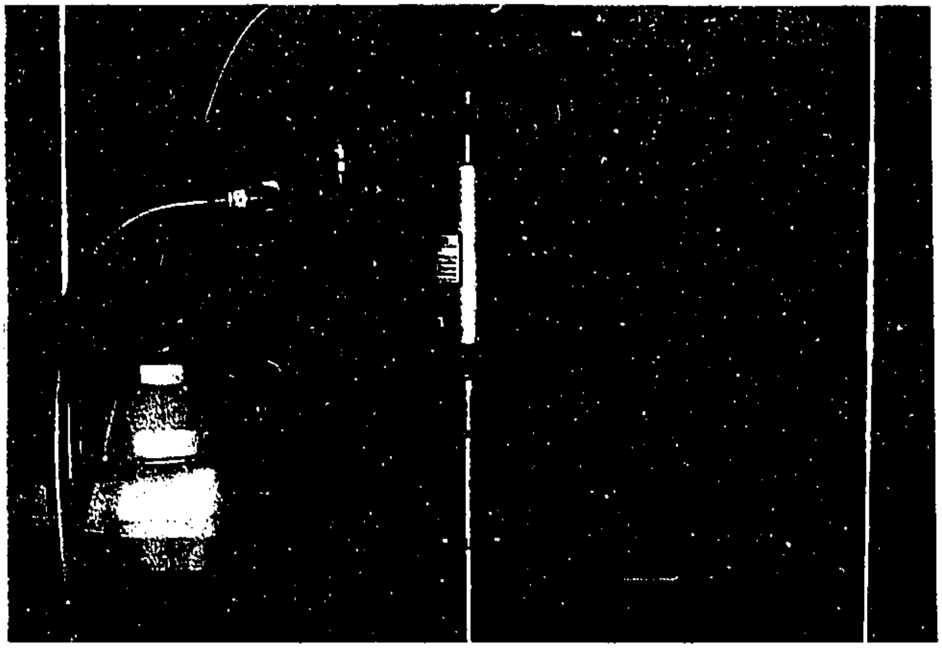

Figure 6–16 Pressure Pump Apparatus

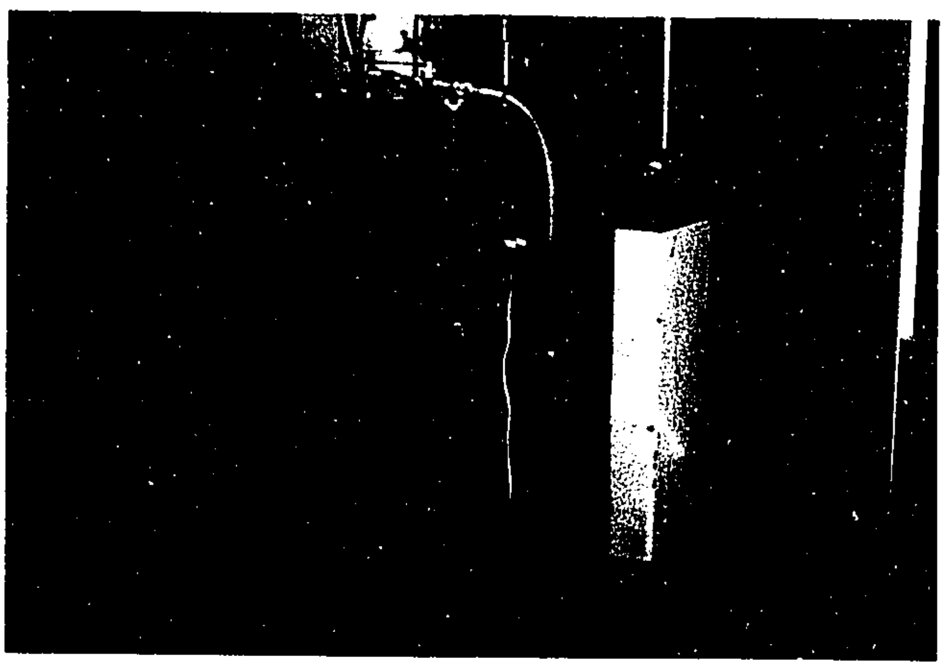

Figure 6–17 Blast Containment Facility

Chapter 7

CONCLUSIONS

7.1 Accomplishments

In this research, a refined shell theory has been presented which allows the calculation of the stresses and strains in a thick orthotropic cylinder. The loading has been assumed to be axisymmetric. The material properties in principle were allowed to vary through the thickness of the cylinder and along the axis of the cylinder.

The basic approach was that the shell deformations u_r, u_θ, and u_z were represented as a power series of arbitrary order in a non–dimensional radial variable. When substituted into the small deformation strain definitions, the cylinder strains were represented as a power series.

The stress equilibrium equations were put in resultant form by multiplying each term by the non–dimensional radial variable raised to an arbitrary power and integrated through the thickness of the cylinder. This generated a set of coupled ordinary differential equations in a generalized stress resultant (when axisymmetric loading was assumed).

The generalized stress resultant equilibrium equations were converted to a system of ordinary differential equations in the deformation coefficients through the use of a generalized Hooke's law and the introduction of a generalized material stiffness. A subsequent transformation of this system to the mid-plane coordinate system enhanced the convergence of the power series. This resulting system of equations, when solved subject to the axial boundary conditions (the radial boundary conditions were specified during the equation development) gave the deformation coefficients, hence the solution to the problem.

Immense problems were encountered in the solution of the system for arbitrary material properties. The matrices defining the system of equations were exceedingly stiff, indicating quickly decaying exponential terms.

A solution was reached for three practical situations however, all for cylinders with material properties constant along their length. Firstly, the solution for a cylinder of infinite length subject to pressure, torque, and axial loads was found. This was compared to existing thin and thick shell solutions for similar loadings and found to be exceedingly accurate. Secondly, a thick cylinder hinged at one end was solved. The cylinder was semi-infinite in length. This was compared to existing solutions. Thirdly, the solution for a thick cylinder rigidly clamped at one end was found. This was also compared to existing thin-wall solutions.

No where in the literature was a specific thick-wall solution available. The solution eigenvalues were compared for an existing thick isotropic cylinder solution.

In an attempt to verify the thick–walled solution, a procedure to fabricate and pressurize a thick orthotropic tubular specimen was developed. The measured surface strains will be compared to a multi–term series solution.

In summary, the postulates of Chapter 1 that addressed the lack of efficiencies in thick–walled composite pressure vessels, namely

(1) imprecise fiber placement

(2) approximate analytical techniques

(3) transverse properties of a composite

have each been addressed. This, in principle, allows future developers to improve vessel weight efficiencies through the use of the tools developed here.

In the development, application, and verification of the refined shell theory, several new pieces of information or research have been uncovered. The major accomplishments are:

(1) realization that expressing the deformations as a power series in the radial coordinate results in a system of equations that can be extended to any arbitrary degree.

(2) derivation of the second order differential equation set for the deformation coefficients, equation (3–21).

(3) introduction of the mid–plane shift, equation (3–24) and re–expressing of the second order set at the cylinder midplane, equation (3–25).

(4) solution of the shell theory when the material properties vary radially but are constant axially through the use of generalized eigenfunctions.

(5) the solution for the infinite cylinder as a power series. This was numerically implemented.

(6) the development of a user friendly routine for the elasticity solution of a thick orthotropic cylinder of infinite extent, subject to axisymmetric loadings.

(7) the solution for a semi-infinite cylinder hinged at the origin – numerically implemented as Case II.

(8) the solution for a semi-infinite cylinder clamped at the origin – numerically implemented as Case III.

(9) the development of a five axis numerically controlled filament winder.

(10) the development procedure for a thick-wall uni-angular continuous fiber tubular specimen.

In addition, several aspects of a less major nature were accomplished. These include:

(11) definition of the generalized stress resultant, equation (3-12).

(12) derivation of the complete axisymmetric generalized stress resultant equations (3-13).

(13) definition of the generalized stiffness matrix, equation (3-18).

(14) general expression for the strains as a power series, equation (3–26).

(15) an examination of the three series truncation schemes.

(16) a general statement relating the stress resultants to the deformation boundary conditions.

(17) development of the generalized stress resultant equations using the principle of minimum complementary energy, equations (3–28) to (3–35).

(18) the expression for the generalized stiffness matrix for a layered composite, equation (4–17).

(19) the occurrence of three eigenvalue groups.

(20) the realization that a particular solution to the general system of ordinary differential equations was the solution to the cylinder of infinite length.

(21) the development of a 70 MPa pressure pumping apparatus useful for a variety of pressure loading situations.

(22) the development of a blast containment facility for safely bursting specimens at ultra-high pressures.

7.2 Future Directions

Two extensions to the existing theory are in partial state of completion by the author. These are:

(1) the extension of the theory for an infinite cylinder to include non-axisymmetric loadings. This is being accomplished by writing angular variations as a complex fourier series. The equations have been developed, but not solved for any specific case.

(2) the extension of the theory to include arbitrary shells of revolution subject to axisymmetric load (orthotropic materials). Again, the equations have been developed, but not tested against any specific examples.

Several extensions to the experimental program are possible. These include:

(1) fabrication and testing of a complete family of uni-angular specimens to check the effect of wind angle and thickness variations.

(2) fabrication and testing of thick multi-angular specimens.

(3) testing of specimens in non-pressure modes, such as axial load and torque. This would be generalized to include multi-loading situations.

(4) fabrication and testing of other composite materials, such as Kevlar or glass reinforced composites.

BIBLIOGRAPHY

1. Dr. B. Jones, *"Analysis of Laminated Composite Materials"*, Short Course presented October 15, 1980, San Francisco, California

2. R.M. Jones, *"Mechanics of Composite Materials"*, Scripta Book Company, Washington, D.C., 1975

3. ASME *"Section X, Fiberglass Reinforced Plastic Pressure Vessels"*, American Society of Mechanical Engineering, New York, 1986

4. Edgar E. Morris, *"Commercial Filament Wound Pressure Vessels for Military and Aerospace Applications"*, SAE Paper #811093, Presented at the Aerospace Congress and Exposition, Anaheim, California, October 5-8, 1981

5. R.L. Grover, S. Ayler *"Development of Thick-Walled Composite Pressure Vessels for Ultra-High Internal Pressures"*, AIAA Paper 81-0584 (1981)

6. T.R. Guess, *"Thick–Wall Kevlar 49/Epoxy Pressure Vessels"*, 29th National SAMPE Symposium, April 3–5, 1984, Reco, Nevada. pp 1007–1021

7. R. Molho, R. Landes, *"Development of Thick–Walled Filament Would High Pressure Containers"*; Aerojet–General Corporation Technical Report AFML–TR–68–126, May 1968, pp. 157

8. F.P. Gerstle Jr., M. Moss, *"Thick Walled Spherical Composite Pressure Vessels"* Composites in Pressure Vessels and Piping, PVP–PB–021, presented at the Energy Technology Conference, Houston, Texas, September 18–23, 1977, pp. 69–87

9. R.F. Foral, *"Composite Spherical Pressure Vessels with Hardening Metal Liners"*, Journal of Pressure Vessel Technology, Trans. of ASME, Vol. 10 L. (August, 1979)

10. F.P. Gerstle, Jr., *"Analysis of Filament Reinforced Spherical Pressure Vessels"*, ASTM STP 466, pp. 604–631

11. R.E. Sherrer, *"Filament–Wound Cylinders with Axial Symmetric Loads"*, Journal of Composite Materials, Vol. I (1967) pp. 344–355

12. M. Moss, *"Filament Reinforced Cylindrical Pressure Vessels: Analysis and Numerical Evaluation"*, Sandia Laboratories Report Number SAND-77-0403, March 1977, pp. 19

13. R.R. Rizzo, A.A. Vicario, *"A Finite Element Analysis of Laminated Anisotropic Tubes"*, Journal of Composite Materials, Vol. 4 (July 1970) pp. 344-359

14. J.N. Reddy, *"Finite Element Modeling of Layered, Anisotropic Composite Plates and Shells: A Review of Recent Research"*, Shock and Vibration Digest, Vol. 13, No. 12, pp. 3-12

15. T.R. Guess, *"Biaxial Testing Composite Cylinders: Experimental-Theoretical Comparison"*, Composites July (1980) pp. 139-148

16. B. Spencer, D. Hull, *"Effect of Winding Angle on the Failure of Filament Wound Pipe"*, Composites, October (1978) pp. 263-271

17. P.D. Soden, D. Leadbetter, P.R. Griggs, G.C. Eckold, *"The Strength of Filament Wound Composite Under Biaxial Loading"*, Composites, October (1979), pp. 247-250

18. M. Uemura, H. Fukunaga, *"Burst Strength of Filament-Wound Cylinder Subject to Internal Pressure"*, Composite Materials, Proceedings of the Japan-U.S. Conference, Tokyo, 1981 pp. 418-427

19. R.H. Marloff, *"Failure Analysis of Filament Wound Graphite/Epoxy Cylinder Under Biaxial Loading"*, SAMPE Quarterly Vol. 17, No. 1 (October 1985) pp. 40–45

20. T.R. Guess, C.B. Haizlip, Jr., *"End–Grip Configuration for Axial Loading of Composite Tubes"*, Experimental Mechanics, January 1980, pp. 31–36

21. J.M. Whitney, G.C. Grimes, P.H. Francis, *"Effect of End Attachment on the Strength of Fiber – Reinforced Composite Cylinders"*, Experimental Mechanics, May 1973, pp. 185–192

22. S.R. Swanson, A.P. Christoforov, G.E. Colvin, Jr., *"Biaxial Testing of Fiber Composites Using Tubular Specimens"*, Experimental Mechanics, September 1988, pp. 238–243

23. R.B. Pipes, J.M. Whitney, *"Analysis of the Axisotropic Cylinder of Finite Length"*, Fiber Science and Technology, (1979) pp. 327–339

24. R.F. Lark, *"Recent Advances in Lightweight Filament–Wound Composite Pressure Vessel Technology"*, Composites in Pressure Vessels and Piping – The Energy Technology Conference, Houston, Texas, September 1979, ASME Report No. PVP–PB–021 pp. 17–49

25. W.W. Schmidt, *"Development of High Efficiency Space Shuttle Tankage"*, Brunswick Corporation, Defense Division, Lincoln, Ne., JANNAF 1975 Propulsion Meeting, Anaheim, Ca., September 1975

26. M.A. Hamstad, T.T. Chino, R.G. Patterson, *"Fatigue Performance of Metal-lined Graphic/Epoxy Pressure Vessels"*, Composites, Vol. 6, (November 1975), pp. 249-253

27. R.L. Glover, R.F. Foral, W.D. Humphrey, *"Development of Kevlar 49/Epoxy Spherical Vessels for Ultra-High Internal Pressures"*, 12th National SAMPE Technical Conference, October 1980, pp. 870-881

28. E.E. Morris, N.P. Patterson, R.C. Landes, R. Gordon, *"Composite Pressure Vessels for Aerospace and Commercial Applications"*, Composites in Pressure Vessels and Piping - The Energy Technology Conference, Houston, Texas, September 1977, ASME Paper No. PVP-PB-021

29. R. Gordon, *"Composite Cylinders for CNG Storage"*, SPI 36th Annual Conference, Washington, D.C., 1980 Paper No. 22-E

30. A.L. Rabenstein, *"Introduction to Ordinary Differential Equations"*, Academic Press Inc. New York, 1966

31. C.W. Bert, *"Analysis of Shells"*, Composite Materials–Structural Design and Analysis Vol. 7 Part 1, L. Broutman and R. Krock Editors, Pub. by Academic Press, (1975)

32. A.E.H. Love, *"On the Small Free Vibration and Deformation of the Elastic Shells"*, Philosophical Trans. of the Royal Society (London) Sero A, Vol. 179A, No. 17 (1888) pp. 491–546

33. L.H. Donnell, *"Stability of Thin Walled Tubes in Torsion"*, NACA Report 479 (1933)

34. S.B. Dong, K.S. Pister, K. Taylor *"On the Theory of Laminated Axisotropic Plates and Shells"*, Journal of Aerospace Science, Vol. 29 (1962), pp. 969–975

35. J.M. Whitney, *"On the Use of Shell for Determining Stresses in Composite Cylinders"*, Journal of Composite Materials Vol. 5 (July 1971), pp. 340–353

36. S.T. Gulati, F. Essenberg, *"Effects of Axisotropy in Axisymmetric Cylindrical Shells"*, Journal of applied Mechanics, Trans. of the ASME, Vol. 34 (Sept. 1967), pp. 659–666

37. J.M. Whitney, J.C. Halpin, *"Analysis of Laminated Anisotropic Tubes Under Combined Loading"*, Journal of Composite Materials, Vol. 2, No. 3 (July 1968) pp. 360–367

38. J.A. Zukas, J.R. Vinson, *"Laminated Transversely Isotropic Cylindrical Shells"*, Journal of Applied Mechanics, Trans. of the ASME Vol. 38 (June 1971) pp. 400–407

39. S.B. Dong, F,K.W. Tso, *"On a Laminated Orthotropic Shell Theory Including Transverse Shear Deformation"*, Journal of Applied Mechanics, Trans. of the ASME, Vol. 39 (December 1972) pp. 1091–1097

40. J.M. Whitney, C.T. Sun, *"A Refined Theory for Laminated Anisotropic, Cylindrical Shells"*, ASME Paper No. 74–APM–B

41. A.T. Vasilenko, G.P. Golub, Y.A. Grigorenko, *"Precise Determination of the State of Stress in Variable–Stiffness Multi–layer Orthotropic Shells"*, Soviet Applied Mechanics Vol. 12, No. 2, pp. 136–141

42. C.F. Liu, J.H. Reddy, *"On a Third–Order Shear Deformation Theory for Laminated Composite Shells"*, Proceedings of the International Symposium on Composite Materials and Structures, Beijing, China, June 10–13, 1986

43. O.E. Widera, G.H. Wu, *"A Boundary Layer Theory for the End Problem of a Circular Cylinder"*, Journal of Engineering Mathematics, Vol. 2, No. 4 (October 1968) pp. 343–353

44. O.E. Widera, S.W. Chung, *"Derivation of Various Non–Homogeneous Anisotropic Shell Theories Applicable in Pressure Vessel Design"*, Nuclear Engineering and Design, Vol. 31 (1974) pp. 405–426

45. O.E. Widera, S.W. Chung, *"Applicability of Various Non–Homogeneous Anisotropic Shell Theories in Pressure Vessel Design"*, Paper No. G117, Second International Conference on Structural Mechanics in Reactor Technology, Berlin, Germany, September 10–14, 1973

46. G.E.O. Widera, M.O.W. Johnson, D.L. Logan, *"An Asymptotic Analysis of the Layered Tube"*, Mechanics Today Vol. 5 (1980) pp. 543–560

47. G.E.O. Widera, D.L. Logan *"Refined Theories for Non–Homogeneous Anisotropic Cylindrical Shells"*, Journal of Engineering Mechanics Division, ASCE Vol. 106 No. EM6, (December 1980) Paper No. 15933, pp. 1053–1074

48. I. Yu. Khoma, *"Some Problems of the Theory of Anisotropic Shells of Varying Thickness"*, Soviet Applied Mechanics, Vol. 10 No. 3, pp. 243–249

49. V.E. Chepiga, *"Refined Theory of Multi-layer Shells"*, Soviet Applied Mechanics, Vol. 12 No. 11, pp. 1127–1136

50. J.R. Vinson, *"Methods of Analysis for Very Thick Walled Cylindrical Shells"*, Naval Engineering Laboratory Technical Report CR 73.002, March 29, 1972

51. J.R. Vinson, *"Methods of Analysis for Very Thick Walled Cylindrical Shells"*, Journal of Engineering for Industry, Trans. of the ASME, (Feb. 1975), pp. 175–199

52. A.I. Soler, *"Higher Order Theories for Structural Analysis Utilizing Legendre Polynomial Expansion"*, Journal of Applied Mechanics, Trans. of the ASME, Vol. 91, No. 4, (December 1969), pp. 757–762

53. Shun Cheng, *"On an Accurate Theory for Circular Cylindrical Shells"*, Journal of Applied Mechanics, Trans. of the ASME, (June 1973), pp. 582–588

54. Shun Cheng, F.B. He, *"Theory of Orthotropic and Composite Cylindrical Shells, Accurate and Simple Fourth Order Governing Equations"*, Journal of Applied Mechanics, Trans. of the ASME Vol. 51 (December 1984), pp. 736–744

55. S. Li, X. Wong, *"Elasticity Solution for Interlaminar Stresses in a Cross-Ply Laminated Circular Cylindrical Shell"*, Proceedings of the International Symposium on Composite Materials and Structures, Beijing, China, June 10-13, 1986

56. N.A. Bazarenko, I.I. Vorovich, *"Analysis of the Three-Dimensional States of Stress and Strain of Circular Cylindrical Shells. Construction of Refined Applied Theories"*. PPM Vol. 33 No. 3 (1969) pp. 495-510

57. A.E.H. Love, *"A Treatise on the Mathematical Theory of Elasticity"*, Dover Publications 1944

58. A.S. Saada, *"Elasticity Theory and Application"*, Pergamon Press Inc., 1974

59. Ya. M. Grigorenko, A.T. Vasilenko, N.D. Pankratova, *"Computation of the Stressed State of Thick Walled Inhomogeneous Anisotropic Shells"*, Prikladnaya Mekhanika, Vol. 10, No. 5 (May 1974), pp. 86-93

60. C.W. Bert, *"Structural Theory for Laminated Anisotropic Shells"*, Journal of Composite Materials, Vol. 1 (1967) p. 414

61. E.M. Wu, K.H. Lo, R.M. Christensen, *"Stress Analysis and Strength Characterization of Thick Composite Laminates"*, Army Materials and Mechanics Research Center Report No. AMMRC TR-79-29, May 1979

62. R.W. Little, *"Elasticity"*, Prentice Hall Inc. 1973

63. R.M. Christensen, *"Mechanics of Composite Materials"*. John Wiley and Sons, 1979

64. S. Mirza Class notes from *"Elasticity"* a graduate course, 1983

65. A.P. Boresi, K.P. Chong *"Elasticity in Engineering Mechanics"*, Elsevier Pub., New York, 1987

66. S. Timoshenko, S. Woinowsky-Kreiger, *"Theory of Plates and Shells"*, McGraw Hill Book Co., 1959

67. H.B. Keller, *"Numerical Methods for Two-Point Boundary-Value Problems"*, Blaisdel Publishing Company (1968)

68. L.C. Kaufman, *"The L Z Algorithm to solve the Generalized Eigenvalue Problem"*, SIAM Journal of Numerical Analysis Vol. 11 (October 1974) pp. 997-1023

69. L. Kaufman, *"Algorithm 496. The L Z Algorithm to Solve Generalized Eigenvalue Problem for Complex Matrices"*, Collected Algorithms from ACM; ACM Transactions on Mathematical Software, Vol. 1 No. 3 (September 1975) pp. 271–281

70. N.J. Pagano, J.M. Whitney, *"Geometric Design of Composite Cylindrical Characterization Specimens"*, Journal of Composite Materials, Vol. 4 (July 1970) pp. 360–378

71. J.D. Lambert, *"Computational Methods for Ordinary Differential Equations"*, John Wiley and Sons, 1973

72. E.P. Popov, *"Mechanics of Materials"*, Prentice–Hall Inc., 1952

73. A. Roy, S. Tsai, *"Pressure Vessels"*, Composites Design Ed. S. Tsai, T. Massard, I. Susuki, Publ. Think Composites, Dayton, Ohio, 1987

74. M. Munro, D. Lindstrom, *"Development of a Method of Design and Manufacture of Composite Material Containers for Ultra–High Pressure Applications"*, Annual Report (1985–1986) DND/DSS Contract No. 85B83–00175 p. 107, 1985 (Classified)

75. M.B. Munro, A. Miyase, R.C. Flannagan, D. Lindstrom, D. Bouchard, C. Aleong, J. Wong, *"Advanced Materials and Manufacturing Studies for Fiber Composite Flywheels"*, Technical Report No. VOME-FP-8304-1, National Research Council of Canada, Contract No. OSU80-00043, 1983

76. M.B. Munro, A. Miyase, *"Basic Material Studies for Fiber Composite Flywheels"*, Report Number UOME-FP-8302-1, NRC/DSS Contract No. OSU80-00043. Department of Mechanical Engineering, University of Ottawa, January 1983, p. 112

77. M. Munro, D. Lindstrom, *"Development of Method of Design and Manufacture of Composite Material Containers for Ultra-High Pressure Applications"*, Annual Report (1983-1984), DND/DSS Contract No. 8SB83-00175, p. 75, 1984 (Classified)

78. M. Munro, D. Lindstrom, *"Development of Method of Design and Manufacture of Composite Material Containers for Ultra-High Pressure Applications"*, Annual Report (1983-1984), DND/DSS Contract No. 8SB83-00175, p. 107, 1986 (Classified)

79. J.S. Hansen, C.P. Bowers, *"An Analysis of Compression Induced Failures of Composite Laminates"*, Failure Processes in Fibre Composites, Proceedings of the Canadian Fracture Conference

CFC-12, May 3-4, 1984

80. L. Librescu, *"Elastostatics and Kinetics of Anisotropic and Heterogeneous Shell-Type Structure"*, Noordoff Publishers, 1975

81. L. Librescu, *"Some Results Concerning the Refined Theory of Elastic Multi-layered Shells Part I"*, Rev. Room Sci. Techn. Vol. 20 (1975) pp. 93-105

82. L. Librescu, *"Some Results Concerning the Refined Theory of Elastic Multi-layered Shells Part II"*, Rev. Room Sci. Techn. Vol. 20 (1975) pp. 471-480

83. A.F. Falhmy, *"Thickness Properties of Laminate Fiber Composites"*, U.S. Army Research Office Report No. AD AOSS 54, April 1978, 12 pp.

84. G. Lubin, *"Handbook of Composites"*, Van Nostrand Reinhold, N.Y., 1982

85. J.T. Hofditz, *"Structural Design Considerations for Fibrous Glass Pressure Vessels"*, Modern Plastics, April 1964, pp. 127-146

Appendix A

MATERIAL DATA BASE

COMPONENT	TYPE/MANUFACTURER
resin	Epon 825 / Shell Oil Co.
hardener fiber	Ancamine 1482 / Pacific Anchor Chemicals
fiber	E/XAS Carbon 12k Hysol/Grafil
	Kevlar 49 Dupont Type 968
	S2 Glass Owens Corning Type 449AA

Resin and hardener preheated at 60° C for 1 hour prior to mixing. Components mixed with propeller type mixer for 1-2 minutes. Resin bath preheated to 50° C.

Table A-1 Material Used to Manufacture Composite Specimens

Appendix B

FLOW CHARTS

Case I Infinite Cylinder - Series Solution

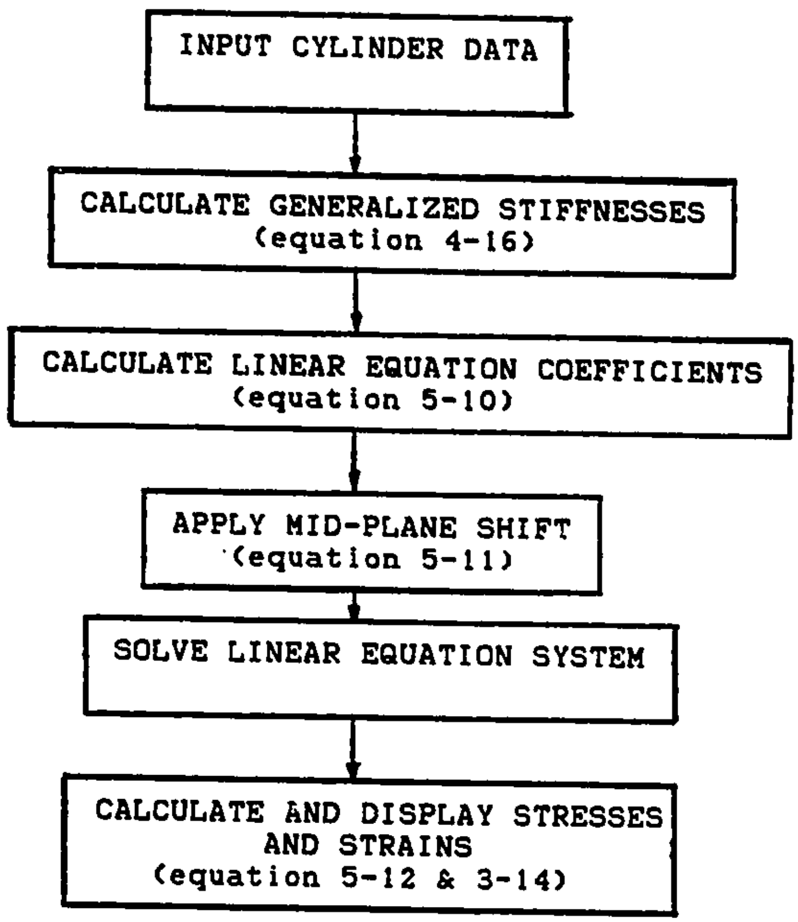

EXACT Infinite Cylinder - Exact Solution

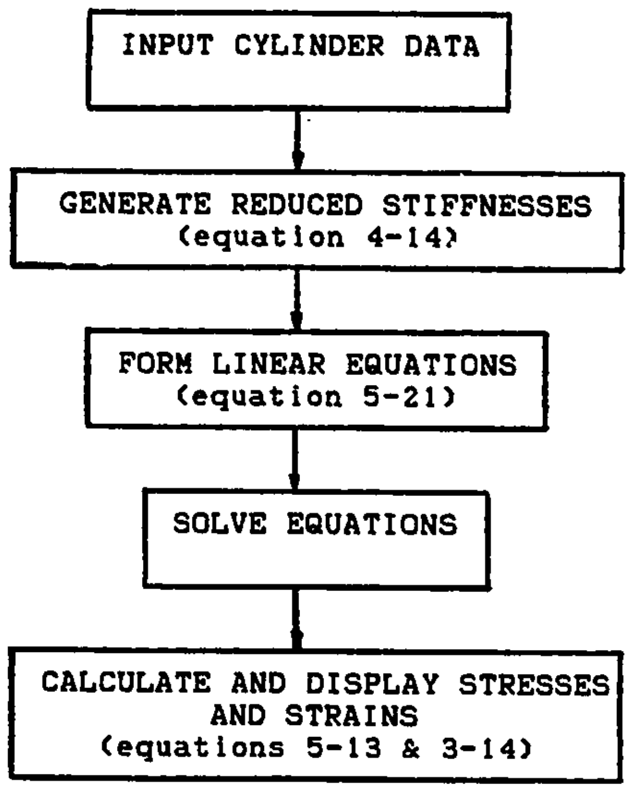

Case II Finite Length Cylinder - Hinged at Origin

INPUT CYLINDER DATA

↓

CALCULATE GENERALIZED STIFFNESSES
(equation 4-16)

↓

CALCULATE EQUATION COEFFICIENTS
(equation 3-20)

↓

APPLY MID-PLANE SHIFT
(equation 3-25)

↓

APPLY LZ ALGORITHM

↓

REMOVE ZERO AND GROWING EIGENVALUES

↓

FORM LINEAR EQUATION SYSTEM
(equation 5-31)

↓

SOLVE LINEAR EQUATION SYSTEM

↓

CALCULATE AND DISPLAY STRESSES
AND STRAINS
(equation 3-26 & 3-14)

Case III Finite Length Cylinder - Rigidly Held at Origin